UNIVERSITÄT ZU LÜBECK

From the Department for Paediatric and Adolescent Medicine

of the University of Lübeck

Director: Prof. Dr. med. Egbert Herting

"Characterisation of gonadal differentiation state in 46,XY individuals with congenital defects of androgen signalling"

Dissertation

for Fulfilment of

Requirements

for the Doctoral Degree

of the University of Lübeck

from the Department of Natural Sciences

Submitted by

Mostafa Ismail Mostafa Alsharkawi

from Egypt

Lübeck 2024

First referee: Prof. Dr. med. Olaf Hiort

Second referee: Prof. Dr. rer. nat. Jens Mittag

Date of oral examination: September 16, 2024

Approved for printing. Lübeck, September 17, 2024

Printed with the support of the German Academic Exchange Service

Contents

List of Publications

Parts of this thesis were published in peer-reviewed journals

Al-Sharkawi M, Calonga-Solis V, Dressler FF, Busch H, Hiort O, Werner R. Persistence of foetal testicular features in patients with defective androgen signalling. Eur J Endocrinol. 2023;188(1).

Publications that are not part of this thesis

Calonga-Solis V, Fabbri-Scallet H, Ott F, Al-Sharkawi M, Kunstner A, Wunsch L, et al. MYRF: A New Regulator of Cardiac and Early Gonadal Development-Insights from Single Cell RNA Sequencing Analysis. J Clin Med. 2022;11(16).

Nazim W, Fateen E, Gouda A, Radwan A, Al-Sharkawi M, Elbaz A. Mass spectrometry for screening of metabolic disorders: 9-year biochemical genetics experience. Journal of The Arab Society for Medical Research. 2023;18(1).

List of Figures

List of Tables

List of Abbreviations

AIS	Androgen insensitivity syndrome
AOI	Area of illumination
AR (also *Ar*)	Androgen receptor
ArKO	Androgen receptor knockout
BTB	Blood-testis barrier
CAIS	Complete androgen insensitivity syndrome
CE	Coelomic epithelium
DCC	Digital count conversion
dpc	Days post-coitum/-conception
DSDs	Disorders (differences) of sex development
DSP	Digital spatial profiler
ECM	Extracellular matrix
FFPE	Formalin fixed, paraffin-embedded
FSH	Follicle -stimulating hormone
GJ	Gap junction
HIER	Heat-induced epitope retrieval
HRP	Horseradish peroxidase
IF	Immunofluorescence
IHC	Immunohistochemistry
LH	luteinising hormone
LMM	Linear mixed-effect model
NGS	Next-generation sequencing
PAIS	Partial androgen insensitivity syndrome
PCR	Ploymerase chain reaction
PGC	Primordial germ cell
PTMC	Peritubular myoid cell
ROI	Region of interest
SCArKO	Sertoli cell-specific androgen receptor knockout
SC	Sertoli cell
scRNA-seq	Single-cell RNA sequencing
SDS-PAGE	SDS-polyacrylamide gel electrophoresis
smFISH	Single molecule fluorescent *in situ* hybridisation
SSC	Spermatogonial stem cell
TJ	Tight junction
TSA	Tyramide signal amplification
UDG	Uracil DNA glycosylase
UMAP	Uniform Manifold Approximation and Projection
wpc	Weeks post-conception
Wt	Wilde-type
WTA	Whole Transcriptome Atlas

Abstract

Congenital defects in androgen synthesis and action in 46,XY individuals result in impaired intrauterine masculinisation despite normal testis determination. Defects of androgen synthesis can occur anywhere along the androgen synthetic pathway, from cholesterol synthesis to peripheral reduction of testosterone to dihydrotestosterone, while defects of androgen action result from resistance to the biological actions of androgens, despite typical male androgen concentrations. Although the testis determination seems to proceed normally in people with the defects of androgen synthesis and action, but show pathological changes. The seminiferous tubules are small and solid, with immature Sertoli cells (SCs) and loss of germ cells (GCs). Leydig cells (LCs) are predominantly affected, showing aplasia or hypoplasia in the defects of androgen synthesis, but hyperplasia in androgen insensitivity syndrome (AIS). In a recent immunohistochemical characterisation of gonadal tissues from a young adult with complete androgen insensitivity syndrome (CAIS), gonadal tissues with SC tumours have been shown to express HSD17B3 in SCs and not in LCs, a pattern of expression that differs from the typical adult human testis and resembles the foetal mouse testis, suggesting an underlying defect of testicular development in defective androgen signalling.

The current study investigated the effect of congenitally defective androgen signalling on the differentiation of the different gonadal somatic cell types in 46,XY children, adolescents and young adults with AIS, caused by androgen receptor loss-of-function variants, and defective androgen synthesis, caused by *CYP17A1* deficiency. Immunohistochemistry (IHC), immunofluorescence (IF), single molecule fluorescent *in situ* hybridisation (smFISH) as well as preliminary data from spatial transcriptomic analysis of formalin-fixed, paraffin-embedded (FFPE) gonadal tissues in children pubertal and young adults with CAIS and PAIS, and a young adult with *CYP17A1* deficiency showed that defective androgen signalling in these conditions is associated with defective differentiation and altered function of all somatic cell types in gonadal tissues. The IHC and smFISH assays show the persistence of *HSD17B3* expression in SCs and lack of its expression in LCs, suggesting defective differentiation of both SCs and LCs in CAIS and *CYP17A1* deficiency. Further characterisation of LC differentiation markers identified two LC populations: a $DLK1^{+}$ foetal/immature and another $INSL3^{+}$ adult/mature LC populations, corroborating the LC differentiation defects and suggesting a possible repopulation of foetal LCs. Additionally, the characterisation of SCs in CAIS and *CYP17A1* deficiency with IF and smFISH revealed disruption of some of the proteins of the blood-testis barrier, including GJA1, CLDN11 and ZO-1, which might contribute to GC loss in these conditions. Furthermore, characterisation of Peritubular myoid cells (PTMCs) in CAIS and *CYP17A1* deficiency shows disruption of expression of adult markers ACTA2 and MYH11, suggesting defective PTMC differentiation.

In partial androgen insensitivity syndrome (PAIS), on the other hand, there was a partial switch of HSD17B3 expression to LCs and normal expression of ACTA2 and MYH11 expression but disruption of CLDN11 expression, suggesting that the partial gain of androgen signalling in this condition might rescue the differentiation of LCs and PTMCs but not SCs.

Further characterisation of gonadal tissues from this condition is needed to get more understanding of GC loss and cancer development and given the rarity of these conditions, archived FFPE gonadal materials might be informative with the recent advances in spatial transcriptomics and proteomics.

Zusammenfassung

Angeborene Defekte in der Androgensynthese und -wirkung bei 46,XY-Personen führen zu einer beeinträchtigten intrauterinen Vermännlichung trotz normaler Hodendetermination. Defekte der Androgensynthese können an jeder Stelle des Androgensynthesewegs auftreten, von der Cholesterinsynthese bis zur peripheren Reduktion von Testosteron zu Dihydrotestosteron, während Defekte der Androgenwirkung aus einer Resistenz gegenüber den biologischen Wirkungen der Androgene resultieren, trotz typisch männlicher Androgenkonzentrationen. Obwohl die Hodendetermination bei den Defekten der Androgensynthese und -wirkung normal zu verlaufen scheint, weisen sie doch einige pathologische Veränderungen auf. Die Hodenkanälchen sind klein und fest, mit unreifen Sertoli-Zellen (SCs) und einem Verlust an Keimzellen (GCs), während die Leydig-Zellen (LCs) überwiegend betroffen sind und bei Defekten der Androgensynthese eine Aplasie oder Hypoplasie, beim Androgeninsensitivitätssyndrom (AIS) jedoch eine Hyperplasie aufweisen. In einer kürzlich durchgeführten immunhistochemischen Charakterisierung von Keimdrüsengewebe eines jungen Erwachsenen mit komplettem Androgeninsensitivitätssyndrom (CAIS) wurde gezeigt, dass Keimdrüsengewebe mit SC-Tumoren HSD17B3 in SCs und nicht in LCs exprimieren, ein Expressionsmuster, das sich vom typischen erwachsenen menschlichen Hoden unterscheidet und dem fötalen Maushoden ähnelt, was auf einen zugrundeliegenden Defekt der Hodenentwicklung durch eine gestörte Androgensignalgebung hindeutet.

In der aktuellen Studie wurde die Auswirkung einer angeborenen Androgensignalstörung auf die Differenzierung der verschiedenen somatischen Zelltypen der Gonaden bei 46,XY-Kindern, Jugendlichen und jungen Erwachsenen mit AIS, verursacht durch Androgenrezeptor-Verlustvarianten, und einer gestörten Androgensynthese, verursacht durch CYP17A1-Mangel, untersucht. Immunhistochemie (IHC), Immunfluoreszenz (IF), Einzelmolekül-Fluoreszenz-in-situ-Hybridisierung (smFISH) sowie vorläufige Daten aus der räumlichen Transkriptomanalyse von in Formalin fixiertem, in Paraffin eingebettetem (FFPE) Gonadengewebe bei pubertären Kindern und jungen Erwachsenen mit CAIS und PAIS, und einem jungen Erwachsenen mit CYP17A1-Mangel zeigten, dass eine fehlerhafte Androgensignalisierung bei diesen Erkrankungen mit einer fehlerhaften Differenzierung und veränderten Funktion aller somatischen Zelltypen im Gonadengewebe einhergeht. Die IHC- und smFISH-Tests zeigen die Persistenz der HSD17B3-Expression in SCs und das Fehlen dieser Expression in LCs, was auf eine gestörte Differenzierung sowohl von SCs als auch von LCs bei CAIS und CYP17A1-Mangel hindeutet. Bei der weiteren Charakterisierung der LC-Differenzierungsmarker wurden zwei LC-Populationen identifiziert: eine DLK1+ fötale/unreife und eine weitere INSL3+ adulte/reife LC-Population, was die LC-Differenzierungsdefekte bestätigt und auf eine mögliche Wiederbesiedlung der fötalen LCs

hinweist. Darüber hinaus ergab die Charakterisierung der SCs bei CAIS und CYP17A1-Mangel mittels IF und smFISH eine Störung einiger Proteine der Blut-Hoden-Schranke, darunter GJA1, CLDN11 und ZO-1, die bei diesen Erkrankungen zum GC-Verlust beitragen könnten. Darüber hinaus zeigt die Charakterisierung der peritubulären myoiden Zellen (PTMCs) bei CAIS und CYP17A1-Mangel eine gestörte Expression der adulten Marker ACTA2 und MYH11, was auf eine gestörte PTMC-Differenzierung hindeutet.

Beim partiellen Androgeninsensitivitätssyndrom (PAIS) hingegen wurde ein teilweiser Wechsel der HSD17B3-Expression zu den LCs und eine normale Expression von ACTA2 und MYH11, aber eine Störung der CLDN11-Expression festgestellt, was darauf hindeutet, dass die teilweise Verstärkung der Androgensignalisierung in diesem Zustand die Differenzierung der LCs und PTMCs, nicht aber der SCs retten könnte.

Eine weitere Charakterisierung von Gonadengewebe aus diesem Zustand ist erforderlich, um ein besseres Verständnis des GC-Verlusts und der Krebsentwicklung zu erlangen. Angesichts der Seltenheit dieser Erkrankungen könnten archivierte FFPE-Gonadenmaterialien mit den jüngsten Fortschritten in der räumlichen Transkriptomik und Proteomik aufschlussreich sein.

1 Introduction

Development of the male reproductive system begins at the foetal stage by the formation of the gonads and is completed by acquiring secondary sexual characteristics and fertility after puberty. Male sex development is a dynamic and complex process that involves the interaction of many genes, proteins, signalling molecules, paracrine and endocrine factors. Male sex determination involves the process by which the bipotential gonad develops into testes, while male sex differentiation refers to the consequent development of male genitalia under the effect of peptide and steroid hormones produced by the developing testis. Male sex determination and differentiation can be divided into three major components: chromosomal, gonadal and anatomic sex. In male sex development, chromosomal sex refers to the presence of the Y chromosome; gonadal sex to presence of the testis; and anatomic sex to presence of male internal and external genitalia.

1.1 Formation of the bipotential gonad

The formation of gonads starts around day 10.0-10.5 post-coitum (dpc) in mouse (1), week 4-5 post-conception (wpc) in human (2, 3), as the intermediate mesoderm bulges into the dorsal aspect of the intraembryonic coelom on each side forming the urogenital ridges. The urogenital ridges further develop into medial genital and lateral mesonephric ridges. The coelomic epithelium (CE) covering the genital ridges proliferates and projects into the underlying mesoderm, and together with cells recruited from the adjacent mesonephric ridge promote further growth of the genital ridges and formation of the bipotential gonads. The formation of the bipotential gonad in mouse is driven by several important transcription factors (Figure 1) including *Wt1*, *Nr5a1*, *Lhx9*, *Cbx2* and *Emx2*, the knockout of which is implicated in gonadal dysgenesis in mice in association with extragonadal defects (1, 4-8). Pathological variants of some of these factors such as *WT1* and *NR5A1* are involved in disorders (differences) of sex development (DSDs) in human, supposedly through their impact on multiple components of gonadal development and function (3).

At this point the gonadal ridges do not show any morphological distinctions between the XX and the XY embryos. Interestingly, the mouse XY genital ridges can be induced to develop into ovaries and the mouse XX genital ridges into testes either by deletion or ectopic expression of pro-testis genes *Sry* and *Sox9*, respectively (1, 9-15), emphasising the concept that the cells forming either the XX or the XY gonadal ridges are equally capable of testicular and ovarian development. The fate of gonadal ridges during normal development is determined by the presence or absence of *Sry* gene, with subsequent activation of different networks of genes that lead to the development of the

gonadal ridge into either a testis or an ovary. The process is so tightly regulated that when one molecular pathway is active, it antagonises the other (1, 16-19).

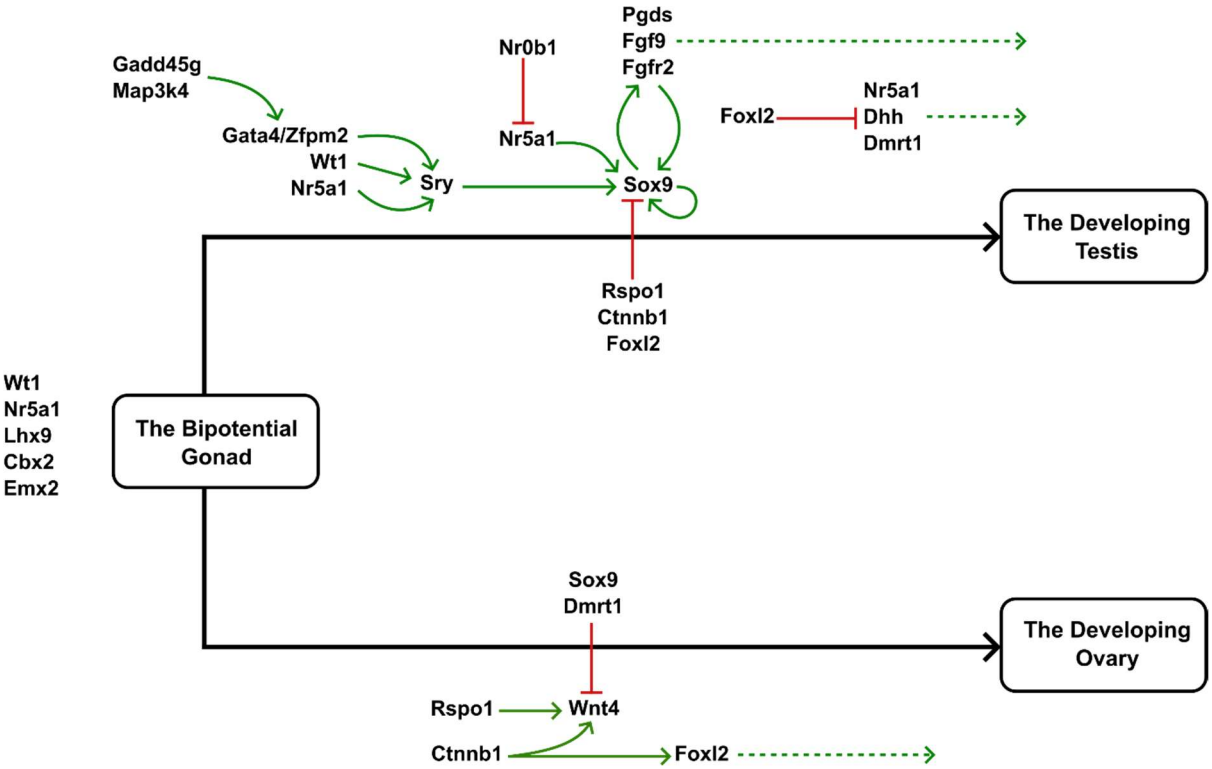

Figure 1. The main gene cascades involved in foetal testis and ovary development.

1.2 Specification of the primordial germ cells (PGCs) and colonisation of the developing gonad

PGCs originate from pluripotent epiblast cells around 6.0-6.5 dpc in mouse (20-22), day 9-16 post-conception in human (23), far away from the genital ridges, and cluster initially close to the evagination of the allantois. Shortly afterwards, PCGs move to the underlying endoderm, become motile and migrate anteriorly along the hindgut into the future genital ridges between 8.0-10.5 dpc in mouse, 4-5 wpc in human, then further migrate along the dorsal mesentery of the hind gut till they reach the genital ridges, whose long narrow structure is believed to facilitate the capturing of migrating PGCs scattered along the hind gut. Once they colonise the genital ridges, PCGs lose their motility and polarised morphology becoming gonocytes (Figure 2).

In mouse, signalling of PGC specification starts by the action of bone morphogenic protein 4 (Bmp4) and Bmp8b from the extraembryonic ectoderm (21, 22), and Bmp2 from visceral endoderm (20), on a subset of epiblast cells to form the founder population of 30-40 PGCs. Bmps act on their receptors and transduce signals via phosphorylation of Smad1, Smad5 and Smad8 that form a transcriptional complex together with Smad4 inducing downstream target genes. Knockout of *Bmps*, *Smad1*, *Smad4* and *Smad5* but not *Smad8* causes severe reduction to total loss of PCGs in mouse (20-22, 24-

27). Bmp4 also activates Wnt3, enhancing the epiblast cells to respond to Wnt signalling activation and inducing another PGC specification transcription factor, Prdm14 (28). The concerted action of Bmp/Smad and Wnt3/β-catenin signalling pathways maintains the expression of *Blimp1* (*Prdm1*) and its target genes together with the expression of *Prdm14* (28). PCG specification fails in *Wnt3* and *Ctnnb1* knockout mice irrespective of Bmp signalling. Blimp1 is a transcription factor the expression of which commits the cells to the germ linage and the knockout of which leads to failure of PGCs specification in mice (28). In addition, Blimp1 induces other PGC specification genes including *Prdm14* and *Tfap2c*, which form a tripartite transcriptional complex with Blimp1 promoting the expression of their target genes (29). *Prdm14* knockout in mice leads to loss of PGCs by 12.5 dpc (30), while *Tfap2c* knockout results in loss of PGC cells possibly through somatic differentiation (31). Blimp1 also induces the expression of *Dnd1*, *Kit* and *Nanos3* which play essential role in development and survival of germ cells (GCs) (29, 32).

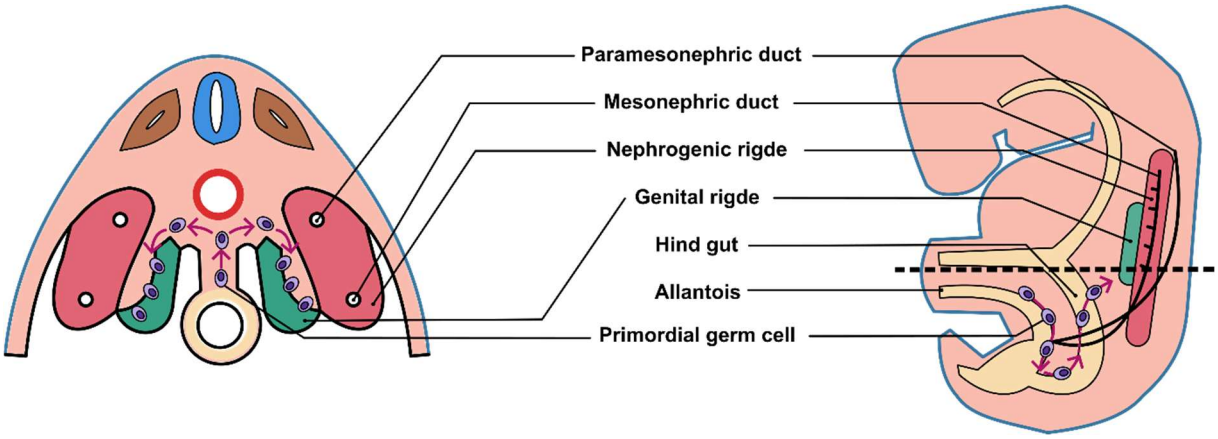

Figure 2. Primordial germ cell migration and colonisation of the developing gonad. Adapted from (33).

The knowledge of specification of PGCs in human is limited because PGC specification is established in pre-gastrulating human embryo, and the molecular events in this embryonal stage is not well characterised (23). However, specification of PGC in human is believed to be driven by BMP and WNT signalling like in mouse. The subsequent PGC development in human is rather well characterised. The number of PGCs in the endoderm of the yolk sac starts between 30-50 at 3 wpc and significantly increases to around 1000 in the following days (23). The pre-migratory PGCs at this stage (around 3-5 wpc) express different markers including TNAP, NANOG, POU5F1, SSEA4 and KIT (34-36).

The molecular factors involved in migration of PGCs are largely unknown in human, but some of them are characterised in mouse, including Cxcl12/Cxcr4, Scf/Kit, Cdh1 and Itgb1. Cxcl12 is a chemokine ligand expressed in the genital ridges and its cognate receptor Cxcr4 on the PGCs. The Cxcl12/Cxcr4 system plays an important role in proper migration of PGCs in the mesenchyme. Knockout of either *Cxcl12* or *Cxcr4* decreases the number of PGCs in the genital ridges and ectopic

Cxcl12 expression causes reorientation and aberrant migration of PGCs (37, 38). Scf/Kit system is another ligand/receptor system that might be involved in proliferation and motility of PGCs (39). Scf is produced and released by somatic cells surrounding the migratory and post-migratory PGCs while its receptor Kit is expressed on PGC surfaces. The Scf/Kit is potentiated by the Wnt5a/Ror2 (40). Cdh1 and Itgb1 are adhesion molecules that contribute to PGC migration, specifically in their exit from the hindgut (41-43). Cdh1 is a cell-cell adhesion molecule the knockout of which leads to aberrant migration and ectopic colonisation of PGCs in mice, while Itgb1 mediates the interaction with the extracellular matrix (ECM) and its knockout leads to impaired colonisation of PGCs in the gonadal ridges (41-43).

1.3 Specification of Sertoli cells (SCs) and formation of testicular cords

Pre-SCs originate CE covering the genital ridge (44) and are first identified after colonising the XY gonad by the expression of sex determining region y (*Sry*) gene (45). In mouse, *Sry*-expressing pre-SCs first appear around 11.0 dpc in the central region of the XY gonad and extend towards the caudal and cranial poles by 11.5 dpc (45, 46). In human, *SRY* is expressed around 5 wpc (47), although the centre-to-periphery pattern of expression is not clearly shown. In either case, the expression of *SRY* is transient (45-47) and drives the differentiation of pre-SCs through the upregulation of *SOX9* (48). For Sry to upregulate *Sox9* expression, it has to reach a threshold expression level within a defined temporal window, as the delay in its expression leads to sex reversal in mouse, possibly by failure of inhibition of the ovary-determining pathway (48, 49). Interestingly, Sry expression is not detectable in all pre-SCs in the developing mouse testis (45), which might be simply explained by the asynchronous expression of Sry in pre-SCs. Another explanation would be that Sry is not an absolute necessity for specification of pre-SCs. In support of the latter proposition is the ability of XY SCs to recruit XX supporting cells into the SC fate in XX-XY chimeras (50), possibly by paracrine prostaglandin D2 signalling (51). In either case, *Sox9* is capable of driving SC differentiation even in the absence of the *Sry* gene, as the ectopic expression of *Sox9* in XX mouse gonad leads them to the testicular fate (13). Shortly after *Sox9* expression, pre-SCs aggregate around GC clusters forming the testicular cords. The mechanism pre-SCs aggregation and organisation in testicular cords is not completely understood, but some factors might be involved, including components of the ECM (52), neurotrophic factors (53) and growth factors (54). For instance, fibroblast growth factor 9 (*Fgf9*) is activated in SCs downstream to *Sry* and Sox9 and increase the number of SCs in the developing gonad by stabilising *Sox9* expression indirectly by repressing pro-ovary genes like *Wnt4* (17, 55). SC fate is not permanent after specification and should constantly maintained. For instance, *Dmrt1* deletion in mouse testis induces *Foxl2* expression in SCs and their reprogramming into granulosa cells (56). Similarly, induced *Foxl2* deletion in the adult mouse ovary leads to upregulation of *Sox9*

and reprograming of granulosa and theca cells into Sertoli-like and Leydig like cells, respectively (57) More importantly, endothelial cells migrating from the adjacent mesonephros play a crucial role in patterning the developing gonad and the organisation of testicular cords (58). Interestingly, the process of testicular cord formation can proceed normally in GC depleted XY gonads, indicating that pre-SC aggregation and organisation around GCs in cord formation is mediated by interaction between SCs with no involvement of GCs in the process (59-62).

At this stage, SCs play crucial role in supporting GCs in the foetal testis. In order for GCs not to proceed into meiosis, SCs produce molecules/factors including Cyp26b1, which catabolises retinoic acid which would signal GCs to precociously enter meiosis (63, 64), and Activin A and transforming growth factor β (Tgfβ), which control GC proliferation and ratio to SCs in foetal testis (65, 66). Postnatally, platelet-derived growth factor and estrogen are also secreted by SCs to enhance their survival (67).

1.4 Specification of peritubular myoid cells (PTMCs)

PTMCs constitute the outer layer of the seminiferous tubules, making direct contact with the basal surfaces of SCs. PTMCs are separated from the seminiferous tubules by the ECM, which is contributed by both PTMCs and SCs. PTMCs form a single layer around the seminiferous tubules in mice and multiple layers in larger mammals, including human, separated by extracellular connective tissue (68). Together with this extracellular connective tissue, PTMCs form the lamina propria that separate the seminiferous tubules form the interstitial tissue and facilitate the transfer of sperms along the tubules through their contractility. PTMCs first emerge in foetal testis shortly after the formation of the testicular cords around 13.5-16.5 dpc in mouse (69, 70) and 12-16 wpc in human (71, 72). Their origin in foetal testis is not completely resolved. They were proposed to originate from the mesonephros adjacent to the developing gonad (73, 74); however, the migrating cells from the mesonephros were shown to contribute to vasculature of the gonad and not to PTMCs (58, 75). They were also proposed to originate either from interstitial cells in the developing gonad or from the CE covering the gonadal ridges (58). Differentiation of PTMCs involves proper signalling form the adjacent SCs in the developing gonad. Desert hedgehog (Dhh) is one of the signalling molecules secreted by pre-SCs shortly after *Sry* expression (76, 77), and is proposed to promote the differentiation of PTMCs and foetal LCs via receptor protein patched homolog 1 (Ptch1) expressed on interstitial cells at the expected time of differentiation of both PTMCs and foetal LCs (78). The knockout of *Dhh* in the developing XY mouse gonad disrupts the development of both PTMCs and foetal Leydig cells (LCs) (78-80), while the ectopic expression of *Dhh* in the developing XX gonad induces foetal LCs but not PTMCs differentiation (81), suggesting that Dhh signalling is not necessary for the initiation of differentiation but for subsequent development of PTMCs. *NR0B1* (*Dax1*)

knockout also disrupts the development of PTMCs and foetal LCs in the developing mouse testis, which suggests that both cell types originate from a common progenitor population (82).

1.5 Specification of foetal Leydig cells (LCs) and establishment of steroidogenic function

Foetal LCs first appear in the interstitial tissue of the developing testis at 12.5 dpc in mouse (83) and around 8 wpc in human (47). The origin(s) of foetal LC progenitors in the foetal testis are not completely resolved, since the evidence depends mainly on the transcriptional differences between the foetal and the adult LCs rather than conclusive lineage tracing studies, leaving the definitive origin(s) of foetal LCs a matter of speculation (1, 84). Several cell populations are proposed to give rise to foetal LC progenitors including migrating neural crest cells, the CE covering the developing gonad and other specialised cells along the border between the developing gonad and the adjacent mesonephros (85). Although neural crest cells can contribute to neuroendocrine cell populations including chromaffin cells in the adrenal medulla, there is no definitive evidence that they could contribute to foetal LCs in the developing gonad. Even though LCs express several neural markers including nestin, Ncam, S-100 and neurofilament protein 200, these neural markers are also expressed in other non-neural cells with no neural crest cell origin. The expression of these neural markers in LCs might reflect their functional contribution to neuroendocrinal system rather than a neural origin (84, 86). The CE covering the genital ridge is believed to contribute to SCs and LCs through epithelial-to-mesenchymal transition. Lineage tracing studies of CE cells in ex vivo mouse gonadal tissue explants shows that CE cells labelled earlier in gonadal development can migrate into the developing testis and reside either in the tubular or the interstitial compartment, while CE cells labelled later in development become restricted only to the interstitial compartment, denoting possible foetal LC fate (44). These observations have been recently corroborated by single-cell RNA sequencing (scRNA seq) analysis of developing mouse and human gonads (47, 87, 88), which show that SCs and LCs in foetal mouse and human testes share a common progenitor cell population that arise from CE. However, these studies do not totally exclude the contribution of mesonephros to the foetal LC progenitor population, since they either investigated a subset of CE cells (88) or excluded the mesonephros from scRNA seq and/or analysis (47). Some evidence suggests an additional progenitor population for foetal LCs that arise along the gonad-mesonephros border and invade the developing gonad in association with vascular endothelial cells during foetal gonad patterning and testicular cord formation (85).

Dhh is one of the most important factors produced by SCs in the developing testis that drive the differentiation of foetal LCs through their action on Ptch1 on foetal LCs and PTMCs (78-81). Another important factor is Nr5a1 (Sf-1) which supports foetal LC differentiation. In mice, *Nr5a1*

haploinsufficiency results in a delay of foetal LC differentiation but complete blockage of adult LC differentiation (76, 89, 90). Notch signalling is also important to set the balance between foetal stem LC renewal and differentiation into foetal LCs. Interestingly, blocking Notch signalling increases the number of LCs in the foetal mouse testis, while its constitutive activation leads to profound LC loss and increase in the undifferentiated mesenchymal progenitors (91). Development of foetal LCs in mice is independent of gonadotropins. In normal mice, the expression of steroidogenic enzymes starts at 13 dpc, long before the production of luteinising hormone (LH) which begins around 17 dpc (92). Moreover, the expression of steroidogenic enzymes in hypogonadal mice is comparable to normal until birth (92). Luteinising hormone receptor (*Lhr*) knockout in mice does not affect testicular testosterone production until the first postnatal day (93). In contrast, inactivating variants of luteinising hormone receptor (*LHCGR*) as well as LH β-subunit (*LHB*) in human negatively impact foetal LC steroidogenesis and foetal masculinisation (94).

Foetal LCs produce androgens necessary for masculinisation of the male foetus. An interesting feature of androgen production in foetal mouse testis is that foetal LCs express all the canonical steroidogenic enzymes necessary for androgen production except 17β-hydroxysteroid dehydrogenase type 3 (*Hsd17b3*), the enzyme responsible for reduction of androstenedione to testosterone, which is expressed in foetal SCs (95, 96). In addition to androgens, foetal LCs also produce insulin like 3 (Insl3), a member of insulin-relaxin family of peptides, which acts on G-protein coupled receptor relaxin/insulin-like family peptide receptor 2 (Rxfp2) expressed in the gubernaculum (97) to induce its thickening and contraction needed for testicular descent as evidenced in knockout models of both genes (98-101).

The fate of foetal LCs in postnatal testis and their relation to development of adult LCs is controversial. The experimental evidence form linage tracing studies of mouse testis suggests that foetal LCs persist in the postnatal and adult mammalian testis, and that their development, unlike adult LCs, is independent of androgen signalling (102, 103). There are three models proposed for LC development (83): the first model proposes that both foetal and adult LCs develop from two distinct progenitor populations. This might be evident from morphological and physiological differences between foetal and adult LCs. As noted shortly above, development of adult but not foetal mouse LCs is dependent on LH (93, 104). In addition, foetal LCs are responsive to adrenocorticotrophic hormone (ATCH) stimulation, while adult LCs are not (105). The second proposes that both foetal and adult LCs develop form a common progenitor population. In support of this proposition, constitutive activation of the hedgehog pathway in mouse testis increases the number of foetal LCs but decreases the numbers of adult LCs in the prepubertal mouse testis (106). What signalling pathways determine the fate of progenitors into either foetal or adult LCs remain questionable (83).

Recently, the scRNA-seq analysis of human testicular tissues from the foetal to the adult stages has shown the foetal LCs as distinct population from the adult LC population, that persist in the normal adult testis and share a common progenitor with adult LCs and PTMCs (107). The third model proposes foetal LCs originate from a foetal LC progenitor population and dedifferentiate in the postnatal testis until puberty, where they redifferentiate to adult LCs. Lineage tracing studies of foetal LCs in mouse testis has shown that some of them dedifferentiate and reside around seminiferous tubules until puberty where they develop into adult LCs (108). More interestingly, the specific disruption of these foetal LCs resulted in a decline in adult LC numbers (108).

Similar to foetal LCs, adult LCs differentiate from their progenitors in response to signalling molecules from SCs like Dhh and Pdgf, since their deletion in mouse results in LC loss (80, 109). But unlike foetal LCs, androgen signalling might be implicated in maintenance of adult LC stem cells, since the reduction of androgen action in foetal mouse testis either by androgen receptor knockout (ArKO) or dibutyl phthalate-induced foetal LC depletion results in reduction of adult LC stem cells and compensated adult LC failure (110).

Testicular growth is rapid during puberty and is mostly due to the expansion of the GC population. This expansion is accompanied by growth of the seminiferous tubular diameter in response to androgens. The expansion of the GC population, or spermatogenesis, is the process of transformation of diploid spermatogonia into haploid spermatozoa (111). It is a complex biological process that involves expansion of spermatogonial stem cell (SSC) population by mitosis, differentiation of SSCs into spermatogonia, division of spermatogonia by meiosis I to form preleptotene, leptotene and zygotene spermatocytes, then meiosis II to produce the haploid round spermatids, which further differentiate into elongated spermatids and then mature spermatozoa that are released into the lumen of the seminiferous tubules in a process known as spermiogenesis (111). The developing GCs are arranged in layers within the seminiferous tubules, and the developmental changes in one layer is in synchrony with those in the other layers, creating a sequence of stages, I-XIV in mouse and rat (111, 112) and I-VI in human (113), with each stage composed of a unique combination of different GCs at different phases of development.

1.6 The blood-testis barrier (BTB)

As spermatogenesis proceeds in the adult seminiferous tubules, GCs traverse the seminiferous epithelium in a tightly regulated process that involves restructuring of the junction between the adjacent SCs as well as the junctions between SCs and GCs at the BTB. The BTB is located close to basal lamina of the seminiferous tubules (Figure 3A), dividing them into a basal and an adluminal compartment, with spermatogonia and preleptotene spermatocytes residing in the basal

compartment and leptotene and zygotene spermatocytes, round and elongated spermatids residing in the adluminal compartment (112). The main purpose of this compartmentalisation is to sequester the meiotic and postmeiotic GCs from the immune system, hence creating an immune privileged microenvironment for completion of spermatogenesis (112). BTB is a dynamic structure so that it breaks ahead of meiotic GCs to allow their movement through the barrier and reseals behind them to keep them protected from the immune system (112). The process of BTB restructuring is tightly regulated that a third intermediate compartment emerges, sealing the leptotene spermatocytes from the basal and the adluminal compartments.

BTB between adjacent SCs is mainly formed by tight junctions (TJs), but other cell junctions contribute to it, including ectoplasmic specialisations, desmosomes and gap junctions (GJs), each serving a different function (Figure 3). For instance, TJs serve as gates, preventing the passage of water, solutes and large molecules through the paracellular space, and as fences, preventing the movement of cell membrane proteins and lipids between apical and basolateral domains, hence creating SC polarity (112). Desmosomes mediate robust cell-cell adhesion. GJs serve as intercellular channels, allowing the diffusion of metabolites, secondary messengers and small molecules between cells.

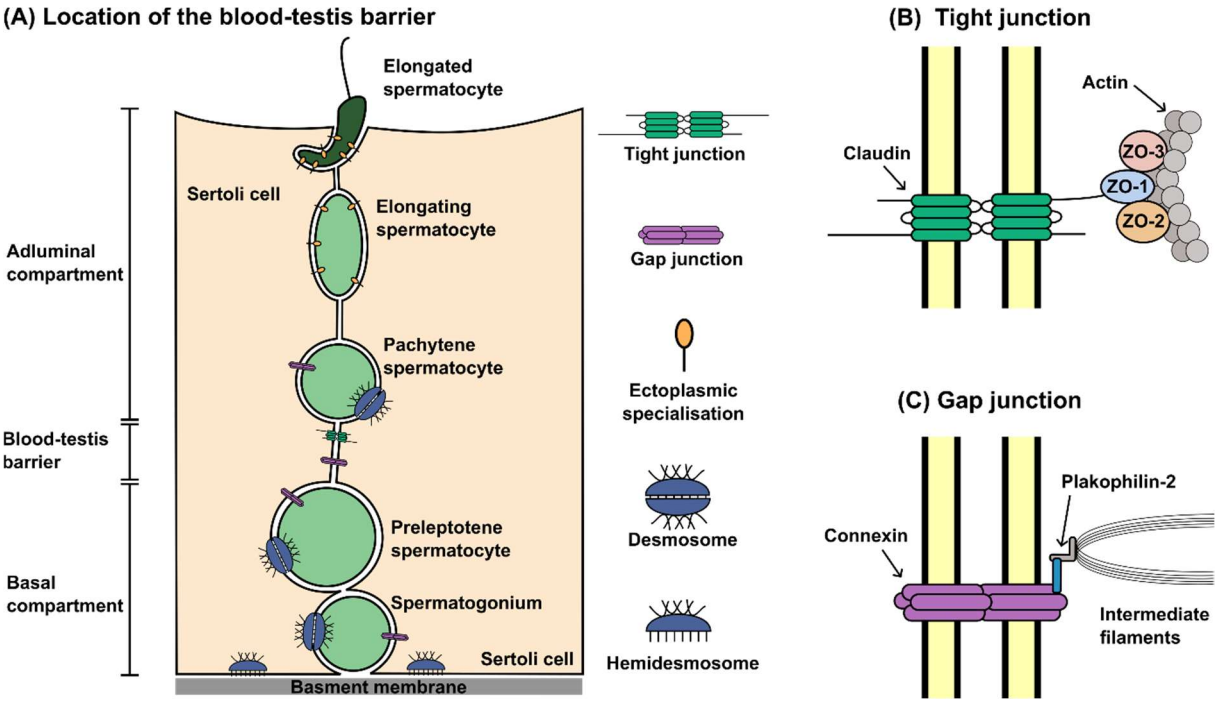

Figure 3. Simplified illustration showing the location of the blood-testis barrier and the main proteins that form it.

Fibrils of TJs are organised around cells in a continuous, anastomosing conformation, creating an impermeable barrier that seals the paracellular spaces (112). Typically, the fibril is composed of an

integral membrane protein in association with scaffolding, signalling and cytoskeletal proteins (Figure 3B and C). The integral membrane proteins that take part in BTB formation include occludin and claudins. Occludin is an integral membrane protein having 4 membrane-spanning domains, two extracellular loops and 2 intracellular segments (114). Occuldin is expressed in mouse and rat testis but not human testis (115). Overexpression of occludin in epithelial cells increases transepithelial electrical resistance, indicating that it confers barrier function to cells (116), while its knockdown disrupts cell polarity (117). Like occludin, claudins can confer barrier function to cells, since the overexpression of *Cldn1* and *Cldn2* induces assembly of TJs in fibroblasts inherently lacking TJs (118). Cldn3 and Cldn11 are expressed in mammalian testis. Cldn3 is detectable in newly formed TJ behind migrating spermatocytes but undetectable ahead of them (119). *Cldn11* knockout leads to disruption of SC polarity and barrier function and consequently to SC detachment and sloughing in conjunction with defective spermatogenesis (120, 121).

The area adjacent to the TJs, the cytoplasmic plaque, is enriched in several scaffolding proteins, whose function is to link the integral membrane proteins of TJ to the cytoskeleton and to recruit signalling molecules for the regulation of TJs (112). Zona occuldens (ZO) proteins are a family of scaffolding proteins that are expressed in mammalian testis at the BTB, acting as adaptors for the attachment of occludins and claudins to the cytoskeleton (Figure 3B) (112). ZO proteins are composed of three **P**ost synaptic density protein, **D**rosophila disc large tumour suppressor, and **Z**onula occludens-1 protein (PDZ) domains, one **S**RC **H**omology 3 (SH3) domain and one **GU**anylate **K**inase (GUK) domain that mediate their interaction with other proteins supporting the TJs. For instance, ZO-1 or tight junction protein 1 (Tjp1) plays a role in the internalisation of the gap junctional plaque by serving as a linker molecule between Gja1 or connexin 43 (Cx43) and actin (122, 123). ZO-1 (Tjp1) promotes the polymerisation of claudins for the assembly of TJs (124).

Regulation of SC junctions at the BTB is mediated by several mechanisms that regulate levels, localisation and interaction between integral membrane, scaffolding and signalling proteins (112, 125). Transcriptional regulation of BTB proteins is mediated by autocrine and paracrine factors, including cytokines and testosterone (125). SCs and GCs produce several cytokines, such as tumour necrosis factor α (TNF-α), transforming growth factor β (TGF-β), interleukins and interferons (125). Binding of cytokines to their receptors recruits adaptor proteins to the receptor/ligand complexes, activating signalling cascades that up- or downregulates transcription (125). For instance, TNF-α downregulates occuldin transcription and translation in rat testis (126, 127). Testosterone, on the other hand, enhances the BTB function (125). SC-specific ArKO leads to downregulation of Cldn3 and increased BTB permeability (128). Cytokines and testosterone can also regulate endocytosis of integral membrane proteins of TJs by accelerating their internalisation within early endosomes (125).

For instance, TGF-β3 and TNF-α induce internalisation of occludin, N-cadherin and junctional adhesion molecule-A (Jam-A) via clathrin-mediated endocytosis (129). More interestingly, TGF-β3 induced ubiguitin-conjugating enzyme E2J1 (Ube2J1), destining the internalised occludin into the protein degradation pathway (130). While testosterone was shown also to induce clatherin-mediated internalisation of occludin, it induced caveolin-1 and Ras-related protein (Rab11), involved in transcytosis and recycling (130). Cytoskeletal remodelling via cytokines can also regulate the BTB (125). Filamentous (F-) actin, a cytoskeletal protein organised in hexagonally packed bundles and linked to TJs, GJs and ectoplasmic specialisations, can be remodelled into a highly branched, less organised structurer under the effect of cytokines. For instance, interleukin-1α (IL-1α) destabilises actin bundles and BTB integrity via mislocalisation of epidermal growth factor receptor pathway substrate 8 (Esp8), a protein involved in actin capping and bundling, from SC surfaces (131, 132).

1.7 46,XY disorders (differences) of sex development (DSDs)

Paediatric disorders (differences) of sex development refers to conditions where the chromosomal, gonadal or anatomic sex is atypical (133). Sex chromosome DSDs involves conditions with differences in the number of sex chromosomes and include Klinefelter syndrome (47,XXY and its variants), Turner syndrome (45,X and its variants), 45,X/46,XY mosaicism and its variants and true chromosome chimerism (46,XY/46,XX) (3). 46,XX DSDs refer to conditions with normal female sex chromosome complement with atypical female sex development and can be categorised into disorders of ovary development, disorders of androgen synthesis and other conditions affecting female sex development. Similarly, 46,XY DSDs refer to conditions with normal male sex chromosome complement with atypical male sex development. They can be categorised into disorders of testis development, disorders of androgen synthesis, disorders of androgen action, and other conditions affecting male sex development. Disorders of testis development encompass a spectrum of phenotypes and presentations. Complete testicular dysgenesis is associated with complete lack of androgenisation of the external genitalia and persistence of Müllerian structures, due to the lack of androgens and anti-müllerian hormones, respectively. In contrast, partial gonadal dysgenesis is associated by partial androgenisation of the external genitalia and rudimentary Müllerian structures. Congenital disorders of androgen synthesis can occur anywhere along the androgen synthetic pathway, from cholesterol synthesis to peripheral reduction of testosterone to dihydrotestosterone, resulting impaired intrauterine masculinisation despite apparently normal testis determination. When the genetic defects affect the early steps of steroidogenesis, which is common for mineralocorticoids, glucocorticoids, and androgens, they cause adrenal insufficiency in conjunction with the failure of androgenisation, as in *STAR*, *CYP11A1*, *HSD3B2* or *CYP17A1* deficiency (134, 135). Conversely, genetic defects in *HSD17B3* or *SRD5A2* affect the final steps of androgen

synthesis and cause androgen deficiency, sparing adrenal function (136, 137). On the other hand, disorders of androgen action result from resistance to the biological actions of androgens, despite typical male androgen concentrations (138-140). This condition is caused by loss-of-function variants affecting the androgen receptor (*AR*) gene and is known as androgen insensitivity syndrome (AIS) (140-143).

The magnitude of the defects in androgen signalling may correlate with the degree of masculinisation of external and internal genitalia in affected individuals. The appearance of the external genitalia may range from a male with hypospadias to a complete female phenotype (144). Müllerian-derived structures are usually absent, resulting in a blind vaginal pouch, and Wolffian-derived structures are usually stabilised but may be missing or hypoplastic (144). Testicular descent is usually hindered, with testes located intraabdominal or inguinal (145-148), but could be palpable in the labio-scrotal folds in a few cases (149). Although testis determination in defects of androgen synthesis and action proceeds apparently in a normal way, little is known about the testicular structure, function, and pathology (134). In defective androgen signalling in general, seminiferous tubules are small and solid, with immature SCs and loss of GCs (145). LCs are predominantly affected, showing aplasia or hypoplasia with an accumulation of lipid droplets in defects of androgen synthesis (145), but hyperplasia in AIS (147). These observations underline the importance of androgen signalling for normal interaction between LCs and SCs to maintain a normal spermatogenesis (134). More interesting is an observation from a recent immunohistochemical characterisation of gonadal tissues from a young adult with complete androgen insensitivity syndrome (CAIS). Gonadal tissues with SC tumour have been shown to express *HSD17B3* in SCs and not in LCs (150), a pattern of expression that differs from the typical adult human testis and resembles an expression pattern observed in the foetal mouse testis (95, 96). This suggests an underlying defect of testicular development in defective androgen signalling.

In this study, the effect of congenital defective androgen signalling on the development and function of gonadal tissues was investigated in archived formalin-fixed, paraffin embedded gonadal tissues from adolescents and young adults with congenital defects of androgen synthesis and action. The expression of several steroidogenic, developmental and differentiation markers of the different somatic cell types was determined at the mRNA level using multiplex fluorescent in situ hybridisation, and at the protein level by immunohistochemistry (IHC) and immunofluorescence (IF). To get some insight of how the developmental defects relate to normal testicular development, publicly available scRNA-seq data from normal human testicular tissues in the foetal, neonatal and adult stages were reanalysed and the expression of different markers was indirectly compared to the expression profiles in gonadal tissues from these conditions. Finally, to further investigate gonadal

differentiation state in these conditions, a preliminary whole transcriptomic analysis was performed to characterise the transcriptomic signature of the main testicular somatic cell types by leveraging the power of spatial whole-transcriptomic analysis.

2 Patients, Materials and Methods

2.1 Patients

To study the effect of androgen signalling on the differentiation of the verious gonadal somatic cell types in human testis, we investigated archived, formalin fixed, paraffin-embedded (FFPE) gonadal tissues from one adolescent and three young adults with complete androgen insensitivity syndrome (CAIS), one young adult patient with *CYP17A1* deficiency, and one prepubertal child and one adolescent with partial androgen insensitivity syndrome (PAIS). The study was conducted according to the Declaration of Helsinki and approved by the ethical committees at the University of Lübeck, Lübeck, Germany and the State University of Campinas, São Paulo, Brazil (Ethical approval numbers 20-038 and CAAE: 97594718.5.0000.5404, respectively). The clinical diagnosis was based on the 46,XY karyotype, the degree of virilisation, hormonal analysis, and confirmation of pathogenic variants by Sanger sequencing. Three normal testicular tissues from 14-, 28- and 31-year-old Caucasians without known comorbidities were provided by Tissue Solution Ltd, a BioIVT company (Glasgow, Scotland) as normal controls. To investigate the effect of defects of androgen synthesis on adult mouse testis, archived FFPE testicular tissues from adult wild-type (Wt) and *Cyp17a1* knockout XY mice (151) were included. Similar to *CYP17A1* deficiency, *Cyp17a1* knockout (KO) XY mice have a female external phenotype, an altered steroid hormone profile including low serum testosterone, are infertile, have small testis with smaller seminiferous tubules that lack spermatogenesis and lack wolffian derivative structures, making it a convenient model to study the effects of androgen synthetic defects on testicular tissue development (151).

Table 1. Summary of the relevant clinical and molecular data of the patients

Patient	Gonad position	Age at gonadectomy (years)	Affected gene	Variant type	Nucleotide change[a]	Amino acid change
Patients with CAIS						
P1	Inguinal	13.7	*AR*	Missense	c.1738T>C	p.(Cys580Arg)
P2	Inguinal	16.6	*AR*	Frameshift	c.549_550del	p.(Ile184Profs*50)
P3	Abdominal	19.6	*AR*	Missense	c.1847G>A	p.(Arg616His)
P4	Abdominal	25.8	*AR*	Frameshift	c.2453del	p.(Pro818Glnfs*5)
Patient with CYP17A1 deficiency						
P5	Inguinal	23.4	*CYP17A1*	Missense	c.287G>A	p.(Arg96Gln)
				Frameshift	c.1435_1438dup	p.(Pro480Hisfs*27)
Patients with PAIS						
P6	Inguinal	6	*AR*	Missense	NA	p.(Leu831Phe)
P7	Inguinal	18	*AR*	Missense	NA	p.(Leu831Phe)

[a]The positions of *AR* and *CYP17A1* variants are described in relation to RefSeq NM_000044.6 and RefSeq NM_000102.4, respectively. CAIS and PAIS are X-chromosomal recessive conditions caused by a hemizygous pathogenic variant in the *AR* gene, while *CYP17A1* deficiency follows an autosomal-recessive inheritance, thus two pathogenic variants (compound heterozygous) are described.
AR, androgen receptor; NA, not available

2.2 Materials

2.2.1 Chemicals and reagents

Following is a list of the chemicals and reagents used in the study.

Table 2. List of chemicals and reagents.

Chemicals and Reagents	Provider	Cat. No.	Country
Acrylamide/Bis solution (37.5:1), 30%	Carl Roth	3029.2	Germany
Ammonium persulfate	Serva	13375	Germany
Ampuwa sterile water	Fresenius Kabi	B230673	Germany
Bromophenol blue	Sigma	B6131	Germany
cOmplete protease inhibitor cocktail	Merk	04693116001	Germany
Dako Liqid DAB+ Substrate Chromogen System	Agilent	GV825	USA
Dako REAL Peroxidase-Blocking Solution	Agilent	S2023	USA
Deoxycholate	Sigma	D6750	Germany
Diethyl pyrocarbonate (DEPC)	Carl Roth	K028.1	Germany
Difco skim milk	BD	232100	Germany
Dithiothreitol (DTT)	Merk	43815	Germany
Dulbecco's Modefied Eagle Medium (DMEM)/F12	Gibco	11320-033	USA
Dulbecco's Balanced Salt Solutiuon (DPBS)	Gibco	14190-094	USA
Ethanol, 99%	ChemSolute	2211.5000	Germany
Ethylenediaminetetraacetic acid (EDTA)	Sigma	E4884	Germany
Eukitt Quick-hardening Mounting Medium	Merk	03989	Germany
Formamide, deionised	Thermo Fisher	AM9342	USA
Formamide, Hi-Di (highly deionised)	Applied Biosystems	4401457	USA
FuGene HD	Promega	E2311	USA
Glycerol, 99%	Sigma	G9012	Germany
Glycine	Merk	357002	Germany
Hemalum solution acid according to Mayer	Carl Roth	T865.1	Germany
Hydrochloric acid	Carl Roth	9277.1	Germany
Methanol, 100%	J T Baker	8045	Netherlands
Normal Goat Serum	Abcam	Ab7481	UK
Normal Rabbit Serum	Vector Laboratories	IS-5000	USA
Potassium chloride	Carl Roth	6781.3	Germany
Potassium phosphate monobasic	Serva	26870	Germany
ProLong Gold Antifade Mountant with DNA Stain DAPI	Invitrogen	P36941	USA
Proteinase K	Thermo Fisher	AM2546	USA
Roti Histol	Carl Roth	6640.1	Germany
Sodium chloride	Sigma	71376	Germany
Sodium dodecyl sulfate (SDS)	Sigma	L4390	Germany
Sodium phosphate dibasic	Carl Roth	4984.2	Germany
SYTO13	Invitrogen	S7575	USA
Tetramethylethylendiamin (TEMED)	Sigma	D8418	Germany
Tris base	Sigma	T1503	Germany
Tri-Sodium Citrate Dihydrate	Merk	71402	Germany
Trypsin-EDTA, 0.05%	Gibco	25300-054	USA
Tween20	Sigma	P2287	Germany

2.2.2 Commercially available kits

Following is a list of the commercially available kits used in the study.

Table 3. List of commercially available kits.

Kits	Provider	Cat. No.	Country
Alexa Fluor 488 Tyramide SuperBoost Kit (Goat anti-Rabbit IgG)	Invitrogen	B40922	USA
Blocking buffer (10% Goat Serum)			
Poly-HRP-conjugated secondary antibody			
Alexa Fluor 488 tyramide reagent			
Reaction buffer			
Reaction Stop Reagent			
Dimethylsulfoxide (DMSO)			
AMPure XP beads	Beckman Coulter	A63880	Germany
BrilliantDye Terminator v3.1 Cycle Sequencing Kit	NimaGen	BRD3-100	Netherlands
RR sequencing premix			
5× sequencing buffer			
pGEM control			
-21 M13 primer			
GeoMx RNA Slide Prep Kit containing:	Nanostring	121300313	USA
Buffer S			
Buffer W			
Buffer R			
GeoMx Whole Transcriptome Atlas (WTA) Human RNA Probes for NGS	Nanostring	121401102	USA
RNAscope™ Intro Pack for Multiplex Fluorescent Reagent Kit v2 containing:	Advanced Cell Diagnostics / Bio-Techne	323285	USA
RNAscope 10× Target Retrieval		322000	
RNAscope 50× Wash Buffer		310091	
RNAscope Hydrogen Peroxide		322381	
RNAscope Multiplex FL v2 AMP 1		323110	
RNAscope Multiplex FL v2 AMP 2		323110	
RNAscope Multiplex FL v2 AMP 3		323110	
RNAscope Multiplex FL v2 HRP-C1		323110	
RNAscope Multiplex FL v2 HRP-C2		323110	
RNAscope Multiplex FL v2 HRP-C3		323110	
RNAscope Multiplex FL v2 HRP blocker		323110	
RNAscope Protease Plus		322381	
RNAscope TSA Buffer Pack		322809	
TSA Vivid Fluorophore 520		323271	
TSA Vivid Fluorophore 570		323272	
TSA Vivid Fluorophore 650		323273	
Vectastain ABC-HRP Kit	Vector Laboratories	PK-4001	USA
Blocking Serum (Normal Goat Serum)			
Biotinylated Secondary Goat Anti-Rabbit Antibody			
Reagent A (Avidin, ABC)			
Reagent B (Biotinylated HRP, ABC)			
Western Lightning Plus ECL	Perkin Elmer	NEL103001EA	USA
Enhanced luminol Reagent Plus			
Oxidizing Reagent Plus			

2.2.3 Consumables

Following is a list of the consumables used in the study.

Table 4. List of consumables.

Consumables	Provider	Cat. No.	Country
6-well culture plates	Greiner Bio-One	657160	Germany
75-cm^2 culture flasks	Sarstedt	83.3911.002	Germany
Aluminum foil	Various	Various	Germany
Cell Scraper, Med, 2-POS Blade	Sarstedt	83.3951	Germany
CellStar Tubes, 50 mL	Greiner Bio-One	227261	Germany
CellStar Tubes, 15 mL	Greiner Bio-One	188271	Germany
Coplin jars	Various	Various	Germany
Cover Slips 24 × 50 mm	Fisher Scientific	15737592	Germany
Dako Hydrophobic Barrier Pen (for IHC)	Agilent Dako	S2002	USA
SafeSeal SurPhob Filter tips (DNase/RNase free) for 10-1,000 µL	BioZym	Various	Germany
Forceps (for slide handling)	Various	Various	Germany
Gel Blotting Papers Whatman 3MM, thickness 0.34 mm	Whatman	3030917	UK
ImmEdge Hydrophobic Barrier Pen (For RNAscope)	Vector Laboratory	H-4000	USA
Kimtech Science Precision Wipes	Kimberly-Clark Professional	05511	UK
Microcentrifuge tubes (DNase/RNase free) 1.5-2 mL	Eppendorf	Various	Germany
NucleoSEQ	Macherey-Nagel	740523.250	Germany
Immobilon-P transfer membranes	Merk	IPVH00010	Germany
Qiashredder homogenizer	Qiagen	79654	
RNase Away	Thermo Fischer	7002PK	USA
Series 3 Adhesive Microscope Slides	Trajan Scientific and Medical	473042491	Australia

2.2.4 Devices and equipment

Following is a list of the devices and equipment used in the study.

Table 5. List of devices and equipment.

Devices and equipment	Provider	Country
3130 DNA Genetic Analyzer	Applied Biosystems	USA
2100 Bioanalyzer Instrument	Agilent	USA
ACD EZ-Batch Slide Holder (20 slide capacity)	ACD/Bio-Techne	USA
Airflow Controller	Waldner	Germany
Baking Oven	Memmert	Germany
Balance	Sartorius	Germany
Biophotometer Plus	Eppendorf	Germany
Cooling Centrifuge 5804R	Eppendorf	Germany
Galaxy 170 S CO_2 incubator	Eppendorf	Germany
Gel Documentation System	Vilber	Germany
GeoMx Digital Spatial Profiler	Nanostring	USA
Heidolph Unimax 1010 Orbital Shaker	Heidolph Instruments	Germany
Hund Laboratory Microscope Wilovert Standard PH 40	Helmut Hund	Germany
HybEZ II Hybridization System	ACD/Bio-Techne	USA

Table 5. List of devices and equipment (cont.)

Devices and equipment	Provider	Country
HybEZ Humidity Control Tray (with lid)	ACD/Bio-Techne	USA
IKAMAG RCT magnetic stirrer	Kern	Germany
Mastercycler nexus - PCR Thermocycler	Eppendorf	Germany
Mini Protean 3 Cell vertical electrophoresis	BioRad	USA
Neubauer haemocytometer	Paul Marienfeld	Germany
NovaSeq platform	Illumina	USA
Pipettes for 5–1,000 µL	Eppendorf	Germany
PowerPac 300	BioRad	USA
Qubit Fluorometer	Invitrogen	USA
S20 SevenEasy pH meter	Mettler Toledo	Germany
Thermomixer 5436	Eppendorf	Germany
Vortex-Genie 2	Scientific Industries	USA
Water bath	Gesellschaft Fuer Labortec	Germany
Zeiss AxioVert 200M	Carl Zeiss	Germany

2.2.5 Preparations of buffers

Following is a list of the buffers used in the study with their respective compostions.

Table 6. List of buffer recipes.

Buffer	pH	Component	Concentration
Citrate buffer	6.0	Na citrate	10 mM
		Tween 20	0.05% (v/v)
Lysis buffer C	7.4	Tris	40 mM
		EDTA	1 mM
		Glycerol	10% (v/v)
Lysis buffer A (components dissolved in lysis buffer C)		Deoxycholate	5% (w/v)
		SDS	0.8% (w/v)
		Triton X-100	1% (v/v)
Lysis buffer A, working		cOmplete Protease inhibitor cocktail	One tablet
		Lysis buffer A	7 mL
Laemmli loading buffer, 2×	6.8	Tris	100 mM
		SDS	4% (w/v)
		Glycerol	20% (v/v)
		Bromophenol blue	0.2% (w/v)
		Dithiothreitol (DTT)	10 mM
Neutral buffered formalin (NBF) stop buffer		Tris	100 mM
		Glycine	100 mM
Phosphate buffered saline (PBS), 10×	6.8	NaCl	1.73 M
		KCl	27 mM
		Na_2HPO_2	100 mM
		KH_2PO_4	18 mM
PBS-T, 1× (prepared in 1× PBS)		Tween 20	1% (v/v)
SDS-gel running buffer, 10×		Tris	250 mM
		Glycine	1.92 M
		SDS	1% (w/v)

Table 6. List of buffer recipes (cont.)

Buffer	pH	Component	Concentration
Saline sodium citrate (SSC) buffer, 20×	7.0	NaCl	3 M
		Na citrate	300 mM
Transfer buffer, 10×		Tris	165 mM
		Glycine	150 mM
Wester blotting transfer buffer, 1×		Transfer buffer, 10×	100 mL
		Deionised H_2O	700 mL
		Methanol	200 mL
Tris-EDTA (TE) buffer, 10×	9.0	Tris-HCl	100 mM
		EDTA	10 mM

2.3 Methods

2.3.1 Sanger sequencing

To confirm the sequences of the cDNA clones used for the transfection experiments, Sanger sequencing was performed using BrilliantDye Terminator v3.1 Cycle Sequencing Kit according to the manufacturer's instructions. The kit components including BrilliantDye and the 5× sequencing buffer were thawed and kept on ice protected from light in addition to the DNA templets (Table 7) and primers (Table 8).

Table 7. cDNA clones used in the study.

Gene	Organism	Vector	Tag	Provider	Cat. No.
Cyp17a1	Mouse	PCMV6KN	free	OriGene	MC205573-OR
CYP17A1	Human	pCMV-SPORT6	free	BioCat	BC062997-TCH1003-GVO-TRI
Hsd17b3	Mouse	pCMV6-Entry	Myc-DDK	OriGene	MR224793-OR
HSD17B3	Human	pCMV-SPORT6	free	BioCat	BC034281-TCH1003-GVO-TRI

Table 8. List of primers used to confirm the sequences of cDNA clones.

Primer	Sequence	Template
mCyp17a1_897_fwd	5′-TGG-GGC-AGG-CAT-AGA-GAC-ACC-T-3′	mouse *Cyp17a1* in pCMV6-Kan/Neo
mCyp17a1_566_fwd	5′-ACA-AGG-ATC-CGA-TAC-TGA-CTA-CCA-3′	
mHsd17b3_666_fwd	5′-GAC-CCC-TTA-TTC-TAT-TTC-AAC-C-3′	mouse *Hsd17b3* in pCMV6-Entry
HSD17B3_200_fwd	5′-AGC-TAG-CAA-AAC-GTG-GAC-TCA-AT-3′	human HSD17B3 in pCMV-SPORT6
HSD17B3_486_fwd	5′-TTT-TAG-TCA-ACA-ATG-TCG-GAA-T-3′	
HSD17B3_652_fwd	5′-GCA-AAA-GAA-GTC-ATC-ATC-CAG-GTG-3′	

For the standard sequencing reaction (20 µL), the reaction components were added in 500 µL microcentrifuge tubes as in the following example (Table 9):

Table 9. Components of a single sequencing reaction.

Reaction component	Volume (µL)
Ampuwa® sterile water	13.5
5× sequencing buffer	3.5
DNA template (0.5 µg)	1.0
primer (20 pmol/µL)	1.0
BrilliantDye	1.0
Total volume (µL)	**20.0**

The reaction mixtures were briefly swirled and centrifuged then placed in the Mastercycler nexus thermal cycler, and the cycle sequencing was performed under the following conditions (Table 10):

Table 10. Thermal cycler conditions for the sequencing reaction.

		25 cycles			
Parameter	**Incubate**	**Denature**	**Anneal**	**Extend**	**Hold**
Temperature	96°C	98°C	60°C	50°C	10°C
Time (mm:ss)	03:00	00:10	01:30	01:30	until ready to purify

To remove salts, unincorporated dye terminators and dNTPs from sequencing products, the sequencing reactions were cleaned-up using NucleoSEQ columns First, the columns were centrifuged at 750 × *g* for 30 sec to collect the dry gel matrix on the bottom of the cartridge then hydrated with 600 µL Ampuwa sterile water, vortexed to remove air bubbles and left for 30 min. The bottom plugs were then removed and the columns were placed in collection tubes and centrifuged at 750 ×g for 5 min to collect and discard the excess liquid. The hydrated columns were placed in new collection Eppendorf tubes, and the sequencing reactions were carefully loaded on the centre of the gel resin and then eluted by centrifugation at 750 × *g* for 5 min. The purified sequencing reactions were denatured by incubation with one volume Hi-Di Formamide at 95°C for 2 min and then subjected to capillary electrophoresis in 3130 DNA Genetic Analyzer for sequencing (Applied Biosystems).

2.3.2 HEK-293 and HeLa cell line culture

HEK-293 and HeLa cell vials were thawed in 37°C water bath for 1 min, decontaminated with 70% ethanol, rapidly transferred to 15-mL tubes containing prewarmed Dulbecco's Modified Eagle Medium (DMEM)/F-12 containing 10% foetal bovine serum without antibiotics, then centrifuged at 300 × *g* for 3 min. The supernatant was discarded and the cells were resuspended in fresh prewarmed culture medium, transferred to 75-cm^2 culture flasks and incubated in the 37°C Galaxy 170 S CO_2 incubator with ~95% relative humidity and 5% CO_2. The culture medium was changed as needed till 80-90% confluency before passaging. The culture medium was aspirated cautiously and the cells in culture flasks were rinsed twice with Dulbecco's Balanced Salt Solution (DPBS), then incubated with 3 mL of prewarmed Trypsin-EDTA solution in the 37°C incubator for 3 min. After complete detachment, Trypsin-EDTA in culture flasks was inactivated by 10 mL DMEM/F-12, and the cell

suspensions were transferred to 50 mL tubes, centrifuged at 300 × *g* for 3 min, the supernatant was discarded, and cells were resuspended in fresh prewarmed culture medium and transferred to 75-cm^2 culture flasks and incubated as before. At 80-90% confluency, the cells were harvested with trypsinisation as described above, counted using Neubauer haemocytometer and subcultured in 6-well plates at seeding cell densities 450,000 and 350,000 cells/well for HEK-293 and HeLa cells, respectively, for subsequent transfection.

2.3.3 FuGene HD transient transfection

Transfection experiments were performed using FuGene HD according to the manufacturer's instructions. The transfection complex was prepared by adding FuGene HD reagent and the DNA clones at a ratio of 3:1 (µl/µg) directly to serum free DMEM, so that the final concentration of the DNA was 20 ng/µL, and the mixture was swirled immediately then left for 15 min at RT. At ~80% confluent cells were either transfected by sprinkling transfection mixture containing either of the DNA clones (2 µg per well) or left without transfection as negative controls. The plates were then agitated gently on Heidolph Unimax 1010 Orbital Shaker and returned to the incubator.

2.3.4 Cell lysis and protein extraction

One day after transfection, the culture medium was removed by aspiration, and the cells were washed twice with ice cold 1× PBS. The cells were lysed with 300 µL lysis buffer per well for 6-well plate, rapidly scraped with cell scraper and rapidly transferred to 1.5-mL Eppendorf tubes on ice. To homogenise cell lysates, the lysates were centrifugated at 14,000 × g for 1 min at 4°C, then loaded on the inner wall of Qiashredder homogenizer and centrifuge again at 13,000 × g for 1 min at 4°C. The homogenised lysates were quick-frozen at -20°C till further analysis by western blotting.

2.3.5 SDS-polyacrylamide gel preparation and pouring

The Mini-Protean glass plates (with 1.5 mm spacer) were assembled according to the manufacturer's instructions. 10% resolving gels were prepared by mixing the following components (Table 11):

Table 11. Preparation of two resolving 10% polyacrylamide gel casts

Component	Volume
Deionised water	4.0 mL
30% acrylamide/bis solution	3.3 mL
1.5 M Tris, pH 8.8	2.5 mL
10% SDS	100 µL
10% ammonium persulfate	100 µL
TEMED	4 µL

After addition of tetramethylethylenediamine (TEMED), the mixture was swirled and poured immediately in gap between the glass plates, leaving around 1 cm for the staking gels. The acrylamide solutions were overlayed with 99% ethanol and placed in vertical position at RT to

polymerise. After polymerisation of resolving gels, the stacking gels were prepared by mixing the following components (Table 12):

Table 12. Preparation of two stacking polyacrylamide gel casts

Component	Volume
Deionised water	3.4 mL
30% acrylamide/bis solution	0.83 mL
1 M Tris, pH 6.8	0.63 mL
10% SDS	50 µL
10% ammonium persulfate	50 µL
TEMED	5 µL

The overlay was poured off, the gel tops were washed with deionised water, and the remaining water was drained using the edges of Gel Blotting Papers Whatman 3MM Again, after addition of TEMED, the mixture was swirled and poured immediately onto the surface of the polymerised resolving gels, clean Teflon combes were inserted into the stacking gels, and the gels were placed in vertical position at RT to polymerise.

2.3.6 Sample preparation for SDS-Polyacrylamide gel electrophoresis (SDS-PAGE)

One volume of 2× Laemmli buffer containing 10 mM dithiothreitol was added to one volume of sample, and the samples, along with the protein marker, were vortexed and heated at 95°C for 3 min to denature the proteins.

2.3.7 SDS-polyacrylamide gel electrophoresis (SDS-PAGE)

The Mini Protean 3 Cell was assembled according to the manufacturer's instructions. The inner chamber was filled with 1× SDS-gel running buffer, ensuring that there was no leakage to the outer chamber, and that the wells are filled with the buffer. The outer chamber was filled with 1× running buffer, and samples and the protein marker were loaded in the assigned wells and separated in SDS-PAGE at constant voltage of 100 V for 80 min. After the electrophoretic separation, a gel knife was inserted between the glass plates of the cassette at the notched ("well") side to remove the top plate and, then used to cut and discard the staking gel. The gel with separated proteins was immersed in transfer buffer to equilibrate for 10 min before blotting.

2.3.8 Western blotting

PVDF membranes were activated in 100% methanol for 15 sec, then equilibrated in 1× transfer buffer for 5 min along with filter papers. A gel sandwich is constructed for wet transfer in order from anode to cathode (fiber pad, filter paper, PVDF membrane, gel, filter paper, fibre pad), ensuring the removal of air bubbles for even transfer of proteins. The apparatus was assembled according to the manufacturer's instruction, the frozen cooling unit was added and the tank was filled with 1× transfer buffer. The proteins were transferred to the PVDF membranes at a constant voltage of 100 V for 80

min. After complete transfer, the PVDF membranes were blocked in 5% skim milk (Table 2) in 1× PBS with agitation for one hour then incubated with the primary antibodies (Table 13) diluted in 5% skim milk in 1× PBS-T at 4°C overnight. The day after, the membranes were washed in wash buffer 1× PBS-T 5 times with agitation, 5 min each, then incubated with secondary antibodies (Table 13) diluted in 5% skim milk in 1× PBS-T at RT for 1 hour. The membranes were washed in 1× PBS-T 5 times with agitation, 5 min each, then incubated with enhanced chemiluminescent substrate working solution for one minute. Excess substrate was drained and the membranes were wrapped in sheet protectors, ensuring the removal of air bubbles, and the signals were detected on Chemiluminescent Imaging system. For reprobing the membranes without stripping, the membranes were blocked with 5% skim milk in 1× PBS for one hour at RT then reprobed with the primary and secondary antibodies as described above.

Table 13. Antibodies used in western blots.

Antibodies	Conjugate	Host Species	Dilution	Provider	Cat. No.
CYP17A1	non	Rabbit	1:1000	ProteinTech	14447-1-AP
HSD17B3	non	Rabbit	1:1000	ProteinTech	13415-1-AP
ß-actin	non	Rabbit	1:1000	Sigma	A2066
GAPDH	non	Rabbit	1:2500	abcam	ab9485
Goat anti-rabbit secondary antibodies	HRP	Rabbit	1:2000	Abcam	A6721

2.3.9 Immunohistochemical and Immunofluorescent Assays

Five-µm FFPE tissue sections were deparaffinised and hydrated, and then incubated in 10 mM citrate buffer, 0.05% Tween 20, pH 6.0 at 99°C for 30 min for heat-induced epitope retrieval (HIER). Endogenous peroxidase in the tissues was blocked with Dako REAL Peroxidase-Blocking Solution. Thereafter, and the tissue sections were then blocked with serum, and incubated with the primary antibodies (Table 14). In immunohistochemical assays, chromogenic signal amplification and development was performed using VectaStain ABC-HRP Kit (Table 3) according to manufacturer's instruction. The tissue sections were incubated with biotinylated secondary antibodies (Table 14), washed, then incubated with avidin-bitotin-horseradish peroxidase (HRP) complex (ABC-HRP), washed again, and then incubated with Dako DAB+ chromogenic substrate for chromogenic signal development. The tissue sections were then washed, counterstained with Mayer's Haematoxylin, dehydrated and mounted with Eukitt™ Quick-hardening mounting medium.

In immunofluorescence assays, detection of abundant proteins in tissue sections is achieved by incubation with fluorophore-conjugated primary antibodies (Table 14). Otherwise, secondary antibodies were used for protein detection, conjugated with either fluorophores or HRP (Table 14) with subsequent tyramide signal amplification (TSA) for signal development. TSA and fluorescent signal development were achieved using Tyramide SuperBoost™ Kit with Alexa Fluor 488-conjugated

Tyramide according to the manufacturer's instructions. After incubation with the HRP-conjugated secondary antibodies, the tissue sections were washed three times in 1×PBS for 10 min each, incubated with Alexa Fluor 488-conjugated tyramide working solution for 10 min, and then the reaction was stopped with stopping buffer. The tissue sections were then washed again three times in 1×PBS for 10 min each, counterstained and mounted with ProLong Gold Antifade Mountant with DNA Stain DAPI.

Table 14. Antibodies used in immunohistochemistry and immunofluorescent assays.

Antibodies	Conjugate	Host Species	Dilution	Provider	Cat. No.
Steroidogenic markers					
CYP17A1	non	Rabbit	1:500	ProteinTech	14447-1-AP
HSD17B3	non	Rabbit	1:100	ProteinTech	13415-1-AP
AKR1C3 (HSD17B5)	non	Goat	1:160	Novus	NB-100-1940
CYP21A2	non	Rabbit	1:200	Sigma	HAP048979
Sertoli cell markers					
SOX9	non	Rabbit	1:1000	Sigma	AB5535
Germ cell markers					
DDX4	non	Rabbit	1:200	Abcam	ab13840
Leydig cell development markers					
DLK1	non	Rabbit	1:400	Abcam	ab21682
INSL3	non	Rabbit	1:100	Sigma	HPA028615
Blood-testis barrier markers					
CLDN11	non	Rabbit	1:50	Sigma	HPA013166
GJA1 (CX43)	non	Rabbit	1:50	Sigma	HPA035097
TJP1 (ZO-1)	non	Rabbit	1:1000	ProteinTech	21773-1-AP
Peritubular myoid cell markers					
ACTA2	Alexa Fluor 594	Mouse	1:20	Bio-Techne	IC1420T
MYH11	non	Rabbit	1:500	Sigma	HPA015310
Secondary antibodies					
FITC goat anti rabbit	FITC	Goat	1:200	Sigma	F2765
Cy3 goat anti mouse	Cy3	Goat	1:200	Sigma	A10521
Alexa Fluor 647 goat anti rabbit	Alexa Fluor 647	Goat	1:500	Sigma	A21244
Biotinylated goat anti rabbit	Biotin	Goat	1:200	VectorLabs	BA-1000-1.5
Biotinylated rabbit anti goat	Biotin	Rabbit	1:200	VectorLabs	BA-5000-1.5

2.3.10 Single molecule Fluorescent In Situ Hybridisation (smFISH) Assays

The RNA fluorescent *in situ* hybridisation assays were performed using RNAscope Intro Pack for Multiplex Fluorescent Reagent Kit v2 (Table 3) according to the manufacturer's instructions (152). Figure 4 briefly shows how the RNAscope technology works. Five µm FFPE tissue sections were baked at 60°C for 1 hour, deparaffinised three times in Roti Histol for 5 min each, dehydrated two times in 99% ethanol for 5 min each and dried in a baking oven at 60°C for 5 min. Endogenous peroxidase was blocked by incubation with hydrogen peroxide (Table 3) for 10 min. Antigens were retrieved by HIER in 1× RNAscope retrieval buffer at 99°C for 30 min and RNA targets were exposed by RNAscope Proteinase Plus digestion at 40°C for 15 min. The tissue sections were incubated with 1× RNAscope target probes (Table 15) in HybEZ II

Hybridization System (Table 5) at 40°C for 2 hours, washed twice in 1× RNAscope wash buffer (Table 3) for two min each, then preserved in 5× SSC overnight at RT. The day after, signal amplification was achieved by sequential incubations of preamplifier, amplifier and HRP-conjugated label probes at 40°C for 30 min, with two-times wash steps in 1× RNAscope wash buffer for two min each after each incubation. Fluorescent signal was developed by incubation with TSA Vivid Fluorophores (Tables 3 and 16) at 40°C for 30 min, with subsequent washes in 1× RNAscope wash buffer and HRP blocking with RNAscope HRP Blocker at 40°C for 15 min.

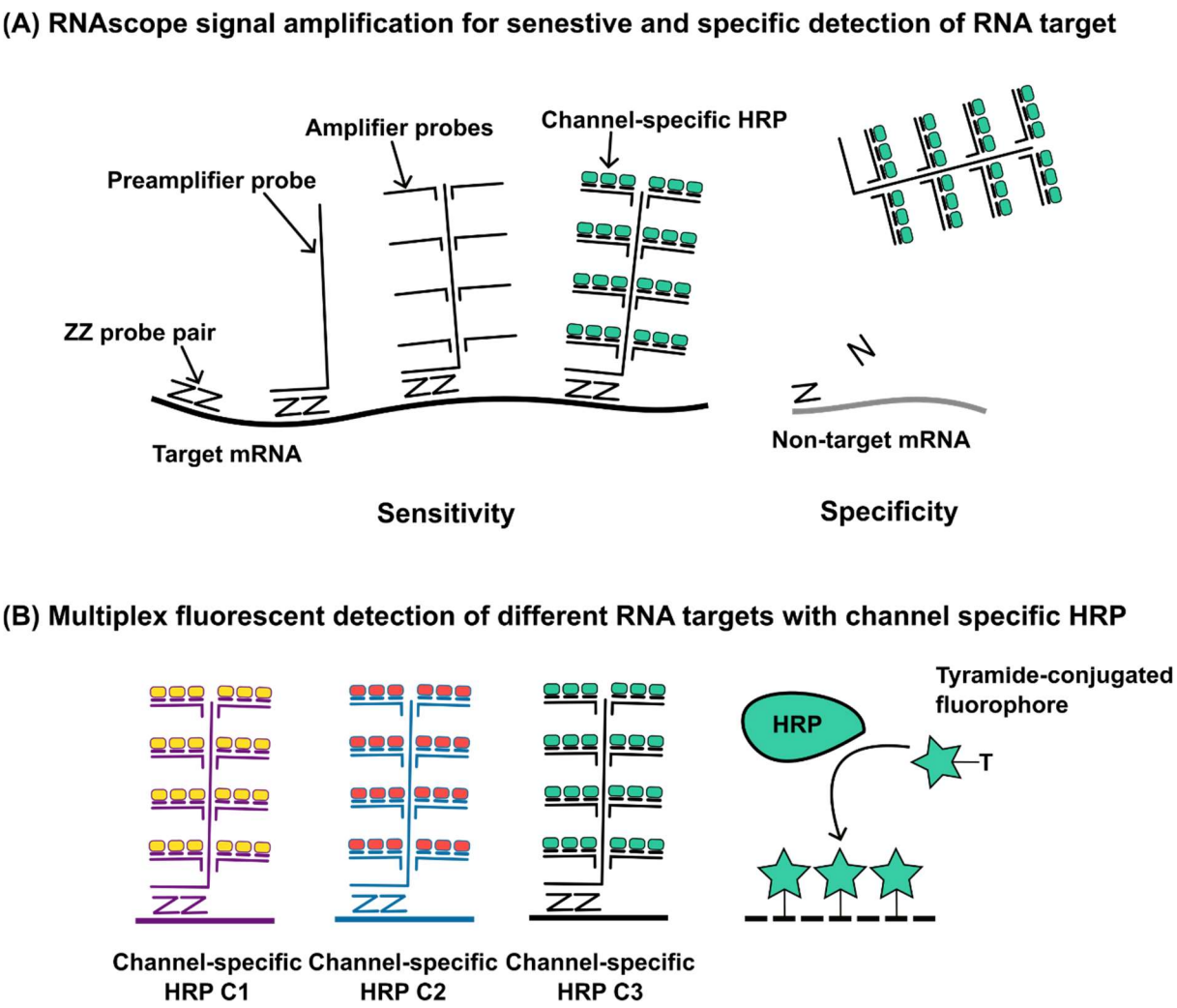

Figure 4. Schematic representation of RNAsope signal amplification. (A) RNAscope signal amplification for sensitive and specific detection of RNA targets. A set of approximately 20 ZZ probe pairs hybridises contiguously to complementary sequences on the target mRNA. Only a ZZ probe pair specifically binds to a preamplifier to insure specific detection of the target mRNA. The ZZ probe pairs are detected by sequential hybridisation of preamplifier, amplifier and channel specific HRP to yield up to 8000 labels for each target mRNA insuring sensitive detection. Nonspecific detection of the target probes is unlikely since a head to tail annealed ZZ probe pair is necessary to stabilise the amplification tree, insuring specific detection. (B) Multiplex fluorescent detection of different RNA targets with channel-specific HRP. Following the building of the amplification tree the first HRP C1 is added followed by incubation with one tyramide-conjugated fluorophore which precipitates around the target mRNA. For detection of the second mRNA target, the HRP C1 is inactivated, the second HRP C2 is added, then incubated with a different tyramide-conjugated fluorophore, and so on.

Table 15. RNAscope target probes.

Target Probe	Target Species	Target Region (bp)	No. of Pairs	Conc.	Provider	Cat. No.
Hs-HSD17B3[a]	Human	190 - 1130	20	1×	Advanced Cell Diagnostics / Bio-Techne	467661
Hs-CYP17A1-C3[b]	Human	332 - 1250	20	50×		467251-C3
Hs-CLDN11[a]	Human	2 - 1538	20	1×		525671
Hs-INSL3-C3 [b]	Human	2 - 750	17	50×		1060371-C3
Hs-DLK1 [a]	Human	200 - 1542	22	1×		529961
Mm-Hsd17b3-No-XHs[a]	Mouse	2 - 1274	17	1×		516601

[a] C1 target probes are supplied as 1× solution.

[b] C3 target probes are supplied as 50× solution that can be diluted in prob diluent buffer in single fluorescent assays or in 1× C1 target probes in multiplex fluorescent assays.

Multiplex fluorescent *in situ* hybridization assays were developed by different sets of target probes, each detected by corresponding sets of preamplifiers, amplifiers and HRP-conjugated label probes. Each set of target probes along with the corresponding preamplifiers, amplifiers and target probes are referred to as channel probe and is assigned a number: C1, C2 or C3. In our multiplex fluorescent *in situ* hybridisation assays, C1 and C3 probe channels were used to detect RNA targets in tissue sections. C3 target probes were diluted in the target probes of the C1 probe channel, and the target probe mixture was hybridised to RNA targets in tissue sections under the previously specified conditions. Fluorescent signal development was achieved sequentially firstly for C1 channel. After detection with TSA fluorophores, HRP-C1 was blocked, the tissue sections were incubated with HRP-labelled C3-probes and detected with a different TSA Vivid fluorophore (Table 16). The tissue sections were washed, blocked again with RNAscope HRP Blocker, counterstained and mounted with ProLong Gold Antifade Mountant with DNA Stain DAPI.

Table 16. TSA Vivid Fluorophores

Fluorophore	Dilution	Excitation [nm]	Emission [nm]
TSA Vivid Fluorophore 520	1:1000	488	520
TSA Vivid Fluorophore 570	1:1500	555	570
TSA Vivid Fluorophore 650	1:1000	654	668

The fluorophores are diluted in TSA buffer

In combined fluorescent *in situ* hybridization / immunofluorescent assays, the RNAscope fluorescent assay is developed first followed by immunofluorescent assay as described in section 2.3.9 starting at serum blocking.

2.3.11 Reanalysis of publicly available scRNA-seq data

To determine the proportion of cells expressing HSD17B3 and AKR1C3, publicly available scRNA-Seq data from 20 human testicular tissue samples (Supplementary materials, Table 19), obtained from the embryonal to adult stages through 10× Genomics platform (107, 153, 154), were reanalysed. The raw sequences were processed and aligned to the human reference cDNA GRCh38 using fastp

(v0.22.0) (155), Kallisto (v0.46.1), and BUStools (v0.39.3) (156). The downstream filtering and analyses were performed with the R package Seurat v4.1.1 (157). Genes were retained if they were expressed in at least three cells, and the cells were retained if they expressed between 500 and 9000 genes, with <25% of mitochondrial genes, and <40 000 mRNA molecules detected. Gene counts in each cell were normalised by total cell expression using the NormalizeData function, with log-transformation and a scale factor of 10000. Samples were integrated using FindIntegrationAnchors and IntegrateData functions. Cells were clustered with a shared nearest neighbour modularity optimisation, and cell populations were classified using the same marker genes as in the original (107, 153, 154) and other publications (158, 159). The average expression levels of HSD17B3 and AKR1C3 between all cells of LCs and SCs clusters were calculated with the function AverageExpression of Seurat using the default parameters. The percentage of LCs and SCs was also estimated relative to the total number of cells present in each individual. Plots were generated using ggplot2 v3.3.6 (160) and ggprism v1.0.3 (161) packages from R v4.1.2 (162).

2.3.12 GeoMx Digital Spatial Analysis of RNA

The GeoMx digital spatial profiler (DSP) is one of the recent technologies that allow spatially resolved transcriptomic profiling of tissue sections by combining standard immunofluorescent techniques with digital barcoding (Figure 5A). It quantifies the abundance of RNAs by counting unique indexing oligos assigned to each RNA target. These indexing oligos are covalently attached to a mRNA hybridisation probes with a UV-photocleavable linker (Figure 5B). The assay starts by deparaffinisation and hydration of the FFPE sections followed by HEIR, then mild proteinase K digestion to expose the RNA targets followed by a post-fix to preserve the tissue morphology. The tissue sections are then hybridised to RNA probes that target more than 18,000 protein coding genes then washed to remove off target probes and stained for up to three protein or RNA targets in addition to nuclear stains to identify the tissue morphology. The slides are then loaded on the GeoMx DSP and scanned to produce a high-resolution, full image of the tissue sections, which are used to guide the ROIs selection. The selected ROIs can be of any shape thanks to the programmable digital micromirror device (DMD) (Figure 5C), which projects UV light precisely to illuminate the ROIs and release the photocleavable oligos (163). Next generation sequencing (NGS) libraries are prepared from the collected photocleaved oligos for generation of NGS readouts that are further processed in bioinformatic pipelines to generate NGS digital counts. Those are further filtered by quality control then normalised to give matrix of expression values of genes in the ROIs.

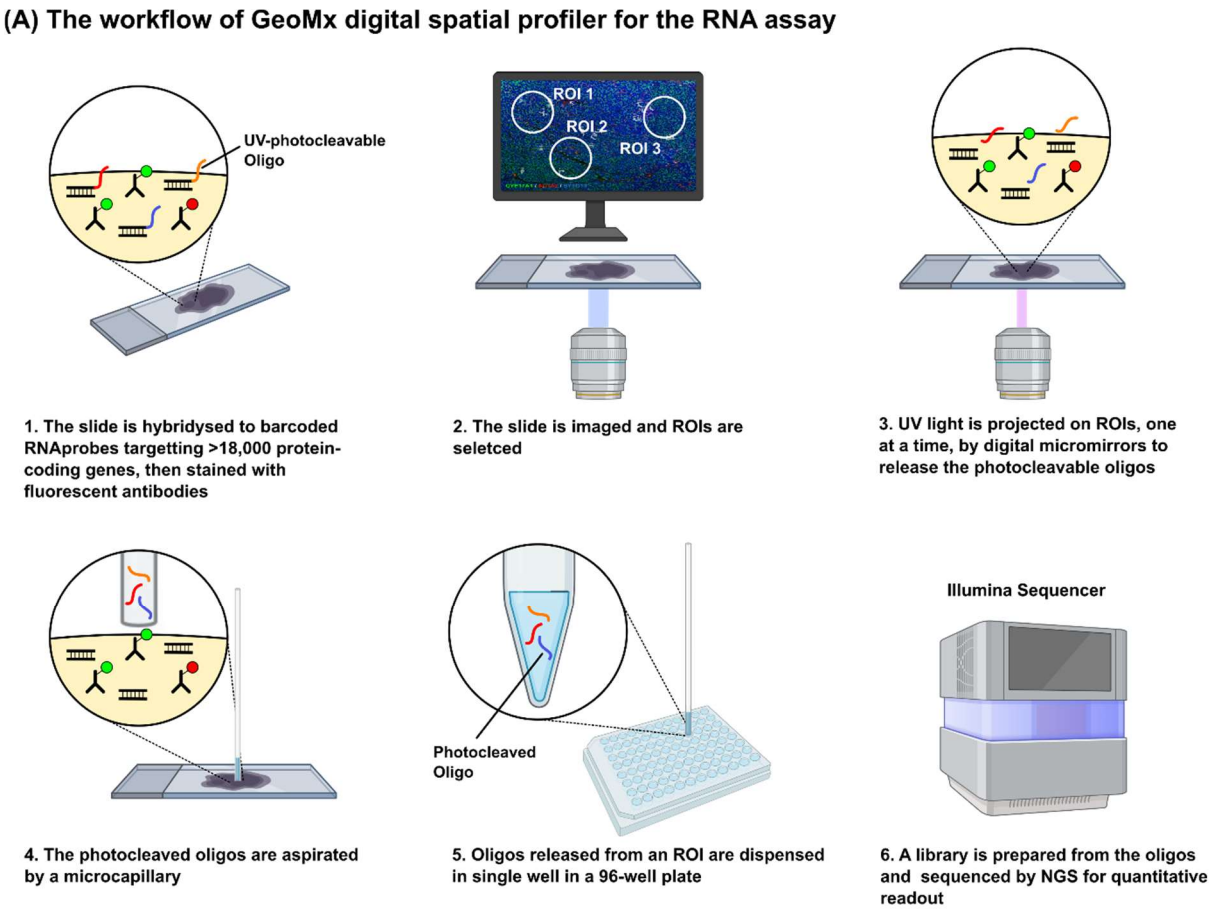

Figure 5. Overview of the GeoMx Digital Spatial Profiler RNA assay. (A) The workflow of the GeoMx DSP RNA assay. (B) The GeoMx target RNA probe. The indexed oligo contains a readout tag sequence identifier (RTS ID) to identify the biological target and a unique molecular identifier (UMI) to enable the removal of duplicates introduced by the PCR reaction. The sequencing primer reads (SPR) 1 and 2 enable the hybridisation of the oligos to the sequencing primers with the i7 and i5 indexing sequences. (C) Illumination of ROIs by the digital micromirror chip. The digital micromirror device (DMD) is composed of around one million of micromirrors each 1 μm^2 which are programmable to allow for the precise illumination of ROIs. Created with BioRender.

2.3.12.1 Manual Slide Preparation for RNA Analysis

The slides were prepared for spatially resolved, whole transcriptome analysis using the GeoMx DSP instrument according to the manufacturer's instructions (164). A five-µm FFPE tissue section from P1 was backed at 60°C for 1 hour, deparaffinised three times in Roti Histol (Table 2) for 5 min each, rehydrated two times in 99% ethanol for 5 min each, one time in 95% ethanol for 5 min and one time in 1× PBS, and then subjected to HIER in 1× Tris-EDTA buffer (pH 9.0) at 99°C for 30 min, then washed in 1× PBS for 5 min. The RNA targets in the tissue section were exposed by incubation with Proteinase K (Thermo Fisher) in 1× PBS at a concentration of 1 µg/mL at 37°C for 15 min. To preserve the tissue morphology after Proteinase K digestion, the tissue section was fixed in 10% neutral buffered formalin (NBF) for 5 min, then the post-fix reaction was stopped by two washes in NBF stop buffer (0.1 M Tris, 0.1 M glycine) for 5 min each, then one time in 1× PBS for 5 min. The tissue section was hybridised with Whole Transcriptome Atlas (WTA) probe mixture (containing more than 18,000 different UV-cleavable oligonucleotide probes) diluted in puffer R (Nanostring) at 37°C overnight. The next day, the off-target probes were removed by two stringent washes in 50% deionised formamide in 2× SSC at 37°C for 25 min each, followed by two additional washes in 2× SSC for 2 min each at RT. To identify the tissue morphology with IF for subsequent selection of regions of interest (ROIs), the tissue section was blocked with buffer W (Nanostring) for 30 min at RT. The section was then incubated with primary antibodies (Alexa Fluor 594 conjugated mouse anti ACTA2 and unconjugated rabbit anti CYP17A1) mixed with the nucleic acid stain SYTO13 and diluted in buffer W (Nanostring) for 1 h at RT. Unbound antibodies and excess SYTO13 were removed by one wash in 2× SSC for one min, then additional four incubations in 2× SSC for three min each. A secondary antibody incubation step using the Alexa Fluor 647 goat anti rabbit antibodies (Table 14) was performed to detect the unconjugated CYP17A1 antibodies followed by another wash step in 2× SSC. The tissue section was then transferred in 2× SSC to be loaded on the GeoMx digital spatial profiler (DSP) for spatially resolving target probes hybridised to target RNAs in the tissue section.

2.3.12.2 Selection of ROIs and collection of target probes on GeoMx DSP

Scanning of tissue section, selection of ROIs and collection of target probes was performed on the GeoMx DSP using GeoMx DSP software v3.1 according to the manufacturer's instructions (165). The tissue sections were scanned in each fluorophore channel at the appropriate exposure time to generate a full image with overlayed fluorescent signals, and hence visually identify the morphology of the tissues. Assuming that cells with same identity and same expression profile of morphology markers have the same transcriptomic signature, we have created ROIs to illuminate areas comprising either Leydig or Sertoli cells (Figure 6). The ROIs were selected in accordance with the criteria recommended by the manufacturer (Table 18). After selection of ROIs, a data collection run

was started to collect the target probes sequentially from each ROI in a corresponding well in the collection plate.

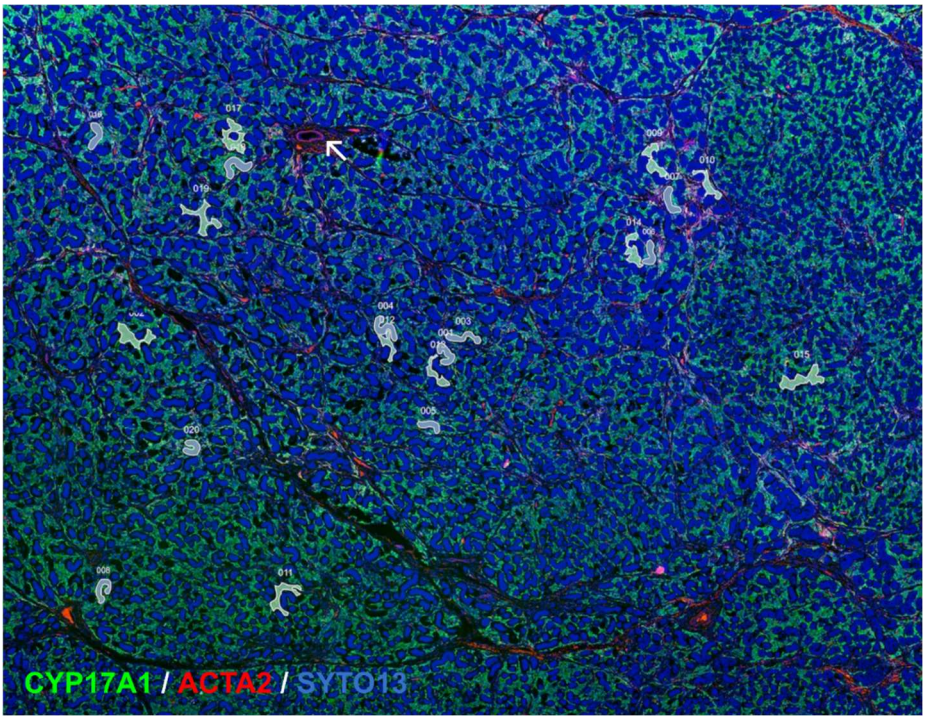

Figure 6. Distribution of the ROIs selected in a gonadal tissue from a 13.7-year-old patient with CAIS (P1) for spatially resolved whole transcriptome analysis with GeoMx DSP. LCs were targeted with antibodies labelling CYP17A1 (green) and PTMCs were targeted with antibodies labelling ACTA2 (red), while the nuclei were counterstained with SYTO13 (blue). Unexpectedly, ACTA2 was expressed only in myoepithelial cells around blood vessels (open arrow) and not in PTMCs around the seminiferous tubules. Selection of ROIs comprising either LCs or SCs was based on the presence or absence of CYP17A1 expression, respectively. The morphology markers in the image are given pseudo-colours for easy visual identification.

2.3.12.3 Next-generation sequencing (NGS) readouts of photocleaved DNA oligos

The NGS library preparation and sequencing was performed according to manufacturer's instructions (166). After collection, photocleaved DNA oligos from each ROI were indexed with Illumina's i5×i7 dual-indexing primers and then decontaminated from carryover products by incubation with uracil DNA glycosylase (UDG) and amplified in a PCR in a Thermocycler under the conditions specified in Table 17. The PCR products were pooled and purified in two rounds with magnetic AMPure XP beads (Beckman Coulter). Each round of purification consists of pelleting the beads on a magnetic stand, discarding the supernatant, washing twice with 80% ethanol, pelleting the beads, discarding the supernatant, drying the beads then resuspending them in elution buffer and transferring the supernatant containing the sequencing library into a new tube for the second round of purification. The quality of the sequencing library was assessed by capillary electrophoresis in 2100 Bioanalyzer Instrument (Agilent) and the concentration was quantified by Qubit Fluorometer (Invitrogen). The libraries were paired-end sequenced on the NovaSeq platform (Illumina) and demultiplexed on the instrument to produce one pair of FASTQ files per ROI. The raw sequencing

reads were processed using TrimGalore for removing the adaptor sequences and Paired-End Read Merger for merging the overlapping pair-end reads, then aligned to analyte barcodes using Bowtie. To generate NGS digital counts from the processed reads, PCR-introduced duplicates were removed using UMI-tools. The generated Digital Count Conversion (DCC) files were uploaded into R for data processing using the GeomxTools open software package.

Table 17. Thermal cycler conditions for the PCR

Step	Temp	Time (mm:ss)	No. of cycles
UDG incubation	37°C	30:00	1×
UDG deactivation	50°C	10:00	1×
Initial denaturation	95°C	03:00	1×
Denaturation	95°C	00:15	18×
Annealing	65°C	01:00	
Extension	68°C	00:30	
Final extension	68°C	05:00	1×
Hold	4°C	until pooling and AMPure cleanup	1×

UDG, uracil DNA glycosylase

2.3.12.4 Data Analysis

The analysis of the NGS readouts was performed according to the manufacturer's instructions (167). To determine the overall quality of data, some of the basic metrics collected from the run were compared to the expected range of values. ROIs with a minimum of 1000 raw reads, 80% trimmed reads, 80% aligned reads, 50% sequencing saturation were retained for further analysis. To exclude global outlier probes for genes that are detected by multiple target probes, probes having 10% or less average counts across all ROIs and probes failing Grubb's outlier test in 20% or more of the ROIs were filtered out. For high confidence detection of gene expression, the limit of quantification (LOQ) was set to two, and ROIs with less than 10% of their genes showing expression above this LOQ were filtered out. Similarly, genes expressed in less than 5% of ROIs were filtered out. For subsequent statistical analysis, the probe counts were normalised with Quartile 3 (Q3) Normalisation method using the normalisation function from NanoStringNCTools. To investigate how related the different ROIs with SCs or LCs are, uniform manifold approximation and projection dimension reduction analysis (UMAP) was performed using the umap package. ROIs which cluster apart from each other were further subjected to differential gene expression using the linear mixed-effect model (LMM).

Table 18. Features of ROIs selected for whole transcriptome profiling by GeoMx DSP

ROI	Profiled cell type	Surface area (μm^2)	Number of cells	Total number of aligned reads
001	Sertoli cell	13751	193	36579720
002	Leydig cell	22416	163	28625259
003	Sertoli cell	13551	184	27222081
004	Sertoli cell	17019	239	27218868
005	Sertoli cell	9977	140	11690454
006	Sertoli cell	11761	175	29761802
007	Sertoli cell	13743	175	31881339
008	Sertoli cell	12727	146	20835738
009	Leydig cell	12918	111	22316390
010	Leydig cell	10045	112	7971312
011	Leydig cell	11954	111	8476835
012	Leydig cell	17108	126	28306285
013	Leydig cell	28055	216	45215466
014	Leydig cell	13758	183	28463446
015	Leydig cell	23899	158	33816451
016	Sertoli cell	18796	258	34455348
017	Leydig cell	22950	180	28079228
018	Sertoli cell	12145	160	10718693
019	Leydig cell	13751	193	36579720
020	Sertoli cell	22416	163	28625259

3 Results

3.1 Validation of CYP17A1 and HSD17B3 antibodies for detection of the corresponding proteins from human and mouse

Detection of mouse Hsd17b3 protein in immunohistochemistry assays is challenging due to the lack of specific antibodies. Specific detection of mouse Hsd17b3 protein in previous immunohistochemistry and immunofluorescence studies was achieved either by antibodies produced in house (95, 102, 168) or commercially by Santa Cruz (169) which were discontinued. To predict whether the CYP17A1 (ProteinTech, 1447-1-AP) and HSD17B3 (13415-1-AP) antibodies, being raised in rabbit against fusion proteins containing amino acid sequences identical to the corresponding human proteins, would also detect the corresponding mouse proteins, the sequences of these fusion proteins were aligned to the corresponding mouse proteins. The mouse Cyp17a1 protein shared only 65% identity with the epitope while Hsd17b3 shared 87% identity with the epitope (Figure 7A and B), suggesting that the chances are not heigh to detect the mouse Cyp17a1 and Hsd17b3 proteins with these antibodies. To further validate the specificity of CYP17A1 and HSD17B3 antibodies in detecting the corresponding proteins from human and mouse, HEK-293 and HeLa cell lines were cultured and either transfected with human *CYP17A1*, mouse *Cyp17a1*, human *HSD17B3* or mouse *Hsd17b3* cDNAs, or left without transfection as a negative control. After 24 hours, the cells were then lysed, and the extracted proteins were blotted on PVDF membranes and probed with either CYP17A1 (ProteinTech, 14447-1-AP) or HSD17B3 (ProteinTech, 13415-1-AP) antibodies. The CYP17A1 antibodies detected clear bands at ~50 kD corresponding to the recombinant human and mouse CYP17A1 proteins in both transfected HEK-293 and HeLa cells, while no bands are seen in the non-transfected cells (Figure 7C), indicating that the CYP17A1 antibodies can specifically detect both the human and the mouse proteins in western blots and that they have the potential to detect them in immunohistochemistry assays. On the other hand, the HSD17B3 blot show clear bands in HEK-293 and HeLa cells only transfected with the human protein at ~25 kD, while no bands were seen either in cells transfected with the mouse Hsd17b3 cDNA or in the non-transfected cells (Figure 7D, middle panel). To exclude the possibility that the mouse Hsd17b3 protein was not detectable in cells transfected with the mouse cDNA because the transfection did not succeed in these cells, the membrane was reprobed with Myc-tag antibodies (Cell Signalling, 2272S), making use of the Myc-tag at the C-terminus of the mouse protein. The Myc-tag antibodies could detect the mouse Hsd17b3 protein in transfected HEK-293 and HeLa cells at ~34 kD (Figure 7D, lower panel), indicating that the HSD17B3 antibodies are non-specific for detection of the Hsd17b3 mouse protein in western blot, and most probably will not detect the mouse protein in immunohistochemistry assays. Therefore, an alternative method should be used for detection of Hsd17b3 expression in FFPE mouse testicular tissues.

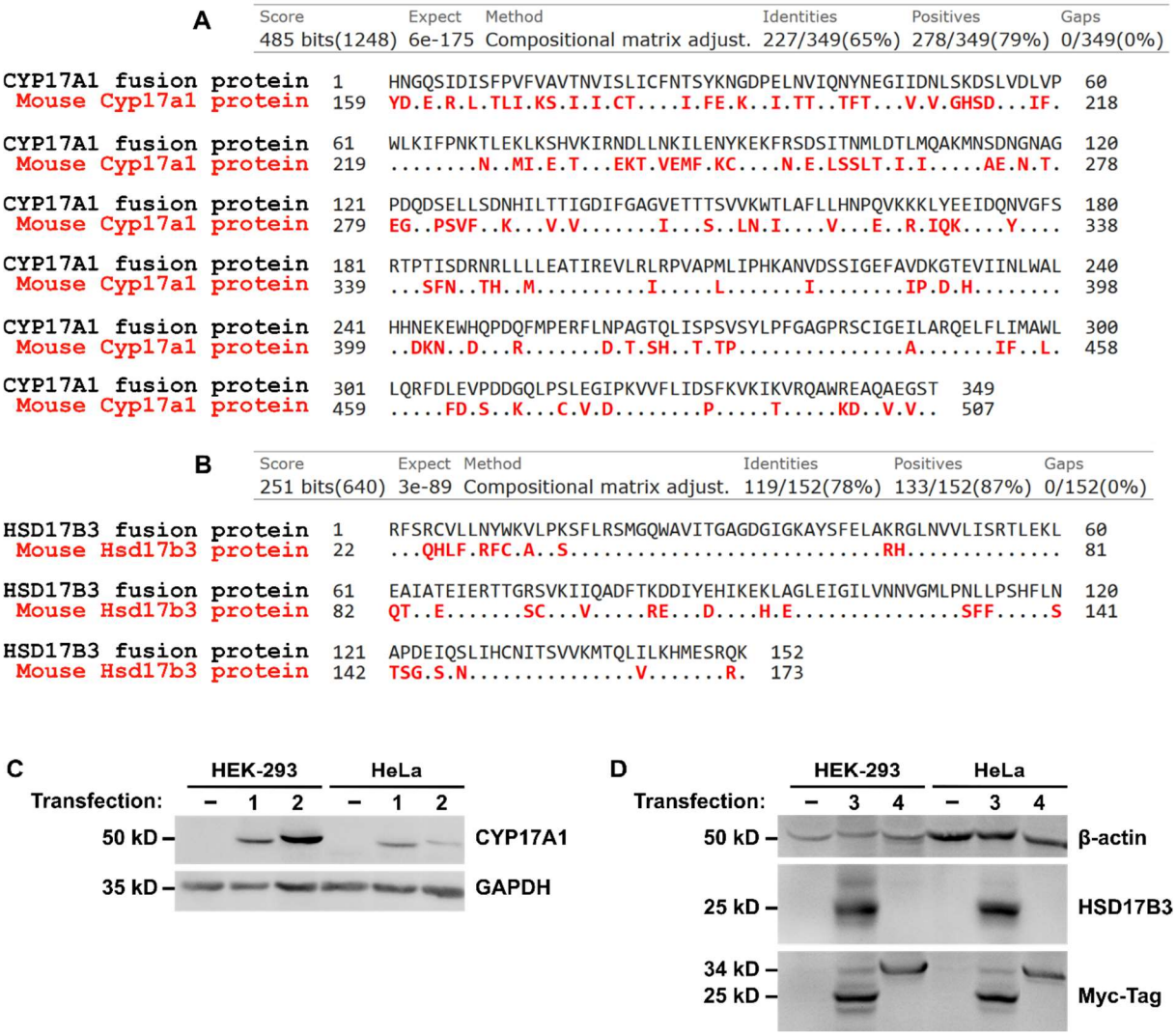

Figure 7. Validation of specificity of (A) CYP17A1 and (B) HSD17B3 antibodies in detecting the corresponding proteins from human and mouse. Panels A and B show alignment of amino acid sequences of the epitope used to generate the CYP17A1 and HSD17B3 antibodies against the corresponding mouse proteins. The epitopes are given black font and the mouse proteins are given red font. The matching amino acids are represented as black dots while the mismatching amino acids are named as one-letter abbreviations and given red font. Panels C and D show the specificity of both antibodies in detecting the corresponding proteins form human and mouse in Western blots. HEK-293 and HeLa cells were cultured in 6-well plates and transfected with either (1) human CYP17A1, (2) mouse Cyp17a, (3) human HSD17B3 or (4) mouse Hsd17b3 cDNAs at 80% confluency, then lysed and harvested one day after. Non-transfected cells were used as a negative control. The proteins in cell lysates were purified and subjected to western blotting. Panel C shows protein bands at ~50 kD corresponding to the human and mouse proteins in transfected cells and no detectable bands in the non-transfected cells after detection with CYP17A1 antibodies (ProteinTech, 14447-1-AP). Panel D shows protein bands at ~25 kD corresponding to the protein only in cells transfected with the human cDNA after detection with HSD17B3 antibodies (ProteinTech, 13415-1-AP), but neither in cells transfected with mouse cDNA nor in non-transfected cells. Reprobing the membrane with Myc-Tag antibodies (Cell Signalling, 2272S) could detect the Myc-tagged Hsd17b3 mouse protein, excluding the possibility of failed transfection or Hsd17b3 protein expression. GAPDH and β-actin house-keeping proteins were used in CYP17A1 and HSD17B3 blots, respectively, to insure equal loading of samples.

3.2 HSD17B3 is exclusively expressed in SCs in gonadal tissues from adolescents and young adults with CAIS and patients with *CYP17A1* deficiency

In foetal mouse testis, androgen synthesis is a concerted action of both LCs and SCs. Foetal LCs express all steroidogenic enzymes needed for testosterone synthesis except *Hsd17b3*, which is expressed in foetal SCs (95, 96, 102), making the latter the site of reduction of androstenedione to testosterone in foetal mouse testis. In adult mouse testis, however, LCs express *Hsd17b3*, and hence are capable of reduction of androstenedione to testosterone. In a recent case report, a gonadal tissue from a young adult patient with CAIS was shown to express HSD17B3 in SCs and not in LCs in a SC tumour and the adjacent tissue (150), a pattern of expression that resembles the foetal mouse testis and suggests that differentiation of both LCs and SCs in gonadal tissues from CAIS patients might be defective. To test whether this foetal pattern of HSD17B3 persists in gonadal tissues from pubertal and young adult patients with congenital defects of androgen signalling, gonadal tissue sections from pubertal and young adult patients with CAIS (P1-P4) and a young adult patient with CYP17A1 deficiency (P5) were immunostained for HSD17B3 and compared to normal control testicular tissue. In the normal control testicular tissue, HSD17B3 was strongly expressed in LCs and less in seminiferous tubules (Figure 8A, Supplementary materials Figure 29A), whereas HSD17B3 was exclusively expressed in seminiferous tubules in all CAIS gonadal tissues (Figure 8B, Supplementary materials Figure 29B-D), and not in hyperplastic LCs in the interstitium, identified by CYP17A1 expression (Figure 8E, Supplementary materials Figure 29F-H). The HSD17B3-expressing cells in these seminiferous tubules are SCs and not GCs, because the seminiferous tubules in CAIS gonadal tissue highly expressed SC marker SOX9 (Figure 8K, Supplementary materials Figure 29J-L) but did not express GC marker DDX4 (Figure 8N, Supplementary materials Figure 29N-P). Similarly, HSD17B3 was expressed exclusively in seminiferous tubules and not in interstitial tissue in gonad the young adult patient with *CYP17A1* deficiency (Figure 8C). This patient harbours the pathogenic compound heterozygous *CYP17A1* mutation p.(Arg96Gln)/p.(Pro480Hisfs*27) and the LCs in the interstitial tissue in this gonad weakly expressed CYP17A1 (Figure 8F) but strongly expressed the adult LC marker INSL3 expression (Figure 8I). the HSD17B3-expressing cells in this gonadal tissue are SCs because they expressed SOX9 (Figure 8L) but did not express DDX4 (Figure 8O).

In all gonadal tissues except for the oldest (25.8-year-old), there were small regions where the seminiferous tubules had some residual, $DDX4^+$ GCs (Figure 9A and B, Supplementary materials Figure 30A-F). The adjacent SCs in these tubules, identified by SOX9 expression (Figure 9C, Supplementary materials Figure 30G-I), expressed HSD17B3 (Figure 9D, Supplementary materials Figure 30J-L), while the neighbouring LCs, identified by CYP17A1 expression (Figure 9E, Supplementary materials Figure 30M and N), did not express HSD17B3 (Figure 9D, Supplementary materials Figure 30J-L).

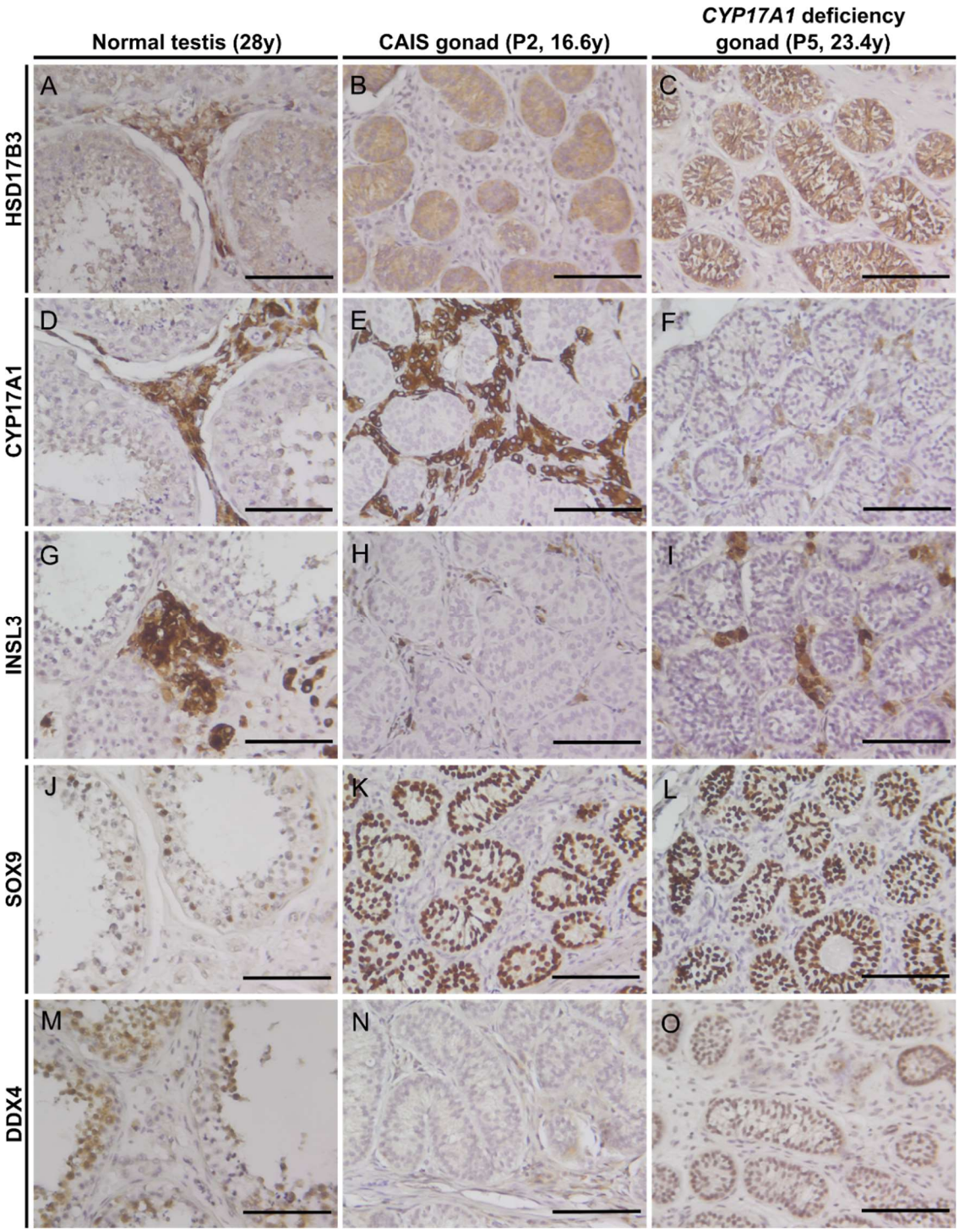

Figure 8. HSD17B3, CYP17A1, INSL3, SOX9 and DDX4 protein expression in testicular tissue from a 28-year-old control compared with a gonadal tissue from a 16.6-year-old patient with CAIS (P2) and a 23.4-year-old patient with CYP17A1 deficiency (P5). HSD17B3 is expressed in the interstitial tissue and, to a lesser extent, in the seminiferous tubules in normal adult testicular tissues (A), but only in the seminiferous tubules in CAIS gonadal tissue (B) or CYP17A1-deficient tissue (C). LCs in the interstitial tissues were identified by the expression of CYP17A1 in normal adult testis (D) and showed typical Leydig cell hyperplasia in CAIS gonad (E) and only faint staining in CYP17A1-deficient tissue (F). INSL3 was used as a second Leydig cell marker (G-I). Cells in the seminiferous tubules of the control adult testis express both SOX9 (J) and DDX4 (M), but cells in the seminiferous tubules of the CAIS or CYP17A1-deficient gonad express only SOX9 (K, L), and are mostly devoid of germ cells and do not express DDX4 (N, O). Scale bar, 100 µm. Reproduced from (170) according to the terms of the creative Commons Attribution-NonComercial License (https://creativecommons.org/ licenses/by-nc/4.0/).

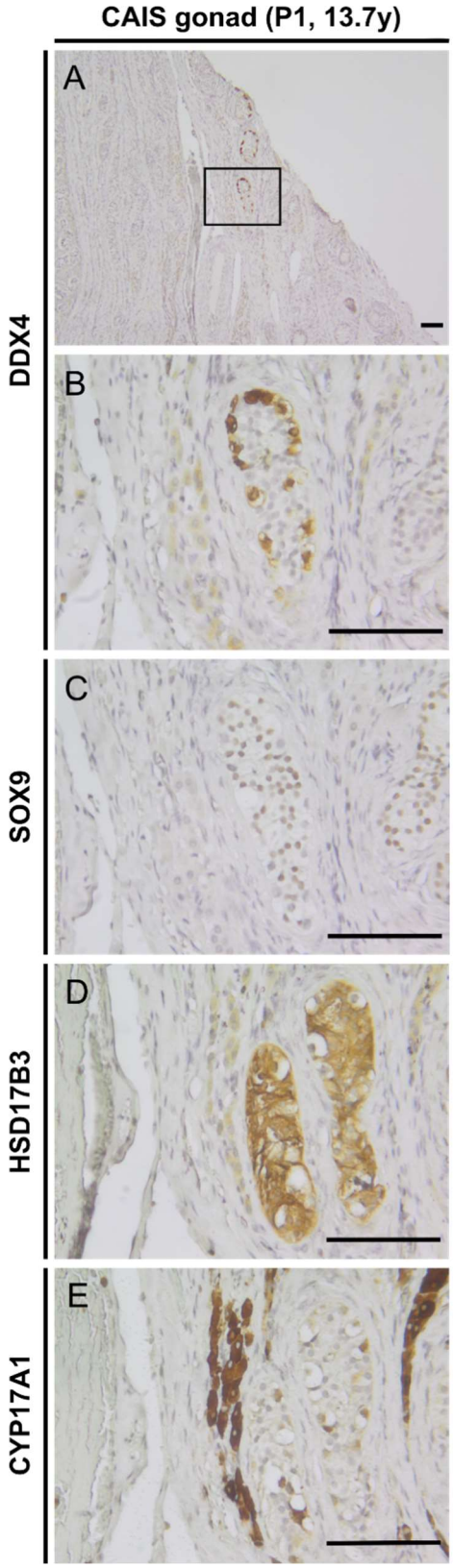

Figure 9. DDX4, SOX9, HSD17B3, and CYP17A1 protein expression in gonadal tissue from a 13.7-year-old patient with CAIS (P1) in a region containing residual germ cells. At some regions in the CAIS gonad residual germ cell containing tubules could be detected. These germ cells are positive for DDX4 (A, B). Like in tubules without germ cells, Sertoli cells within these tubules identified by SOX9 are also positive for HSD17B3 (C, D), while adjacent Leydig cells strongly express CYP17A1 (E). Scale bar, 100 µm. Reproduced from (170) according to the terms of the creative Commons Attribution-NonComercial License (https://creativecommons.org/ licenses/by-nc/4.0/).

To confirm HSD17B3 expression pattern in CAIS gonadal tissues, *HSD17B3* and *CYP17A1* mRNAs were detected in gonadal tissue from the pubertal CAIS patient (P1) with fluorescent *in situ* hybridisation. Similar to the protein distribution of HSD17B3 described above in CAIS gonadal tissues, *HSD17B3* mRNA was expressed exclusively in the seminiferous tubules (Figure 10D and E) and not in LCs identified by *CYP17A1* mRNA expression (Figure 10D and F). In contrast, in the normal control testis, *HSD17B3* mRNA is strongly expressed in LCs (Figure 10A and B). Collectively, the results show the maintained foetal pattern of HSD17B3 expression in pubertal and adult patients with defective androgen signalling (170).

3.3 *Hsd17b3* mRNA is expressed in SCs in adult *Cyp17a1 KO* mouse testis

As shown in section 3.1, the gonadal tissue of the young adult with *CYP17A1* deficiency shows exclusive expression of HSD17B3 in SCs and not in LCs, a feature of foetal mouse testis, suggesting that the lack of androgen synthesis in this condition is associated with defect of SC and LC differentiation. It was interesting to investigate whether the lack of androgens would produce the same effect in mouse testis. Therefore, *Hsd17b3* expression was investigated in adult *Cyp17a1* KO compared to wild-type (Wt) mouse testis. Since specific antibodies against mouse Hsd17b3 protein are not readily available (see section 3.1), the expression of *Hsd17b3* mRNA was evaluated instead by smFISH. In adult Wt mouse testis, *Hsd17b3* was highly expressed in LCs with no detectable *Hsd17b3* mRNA in the seminiferous tubules (Figure 11A and B). In contrast, *Hsd17b3* mRNA was mainly expressed in seminiferous tubules in the adult *Cyp17a1* KO mouse testis and much less in LCs (Figure 11C and D), suggesting that the lack of testosterone in the *Cyp17a1* KO mouse testis also leads to persistence of the previously described foetal pattern of *Hsd17b3* expression in mouse testis (95, 96) and emphasising a similar role of androgens in SC and LC development in mouse and human testis.

3.4 HSD17B3 expression switches from SCs in prepubertal PAIS gonadal tissues to LCs in young adult PAIS gonadal tissues

To further investigate whether the switch of HSD17B3 expression from SCs to LCs is dependent on androgen signalling, gonadal tissue sections from a prepubertal and a pubertal patient with PAIS were stained for HSD17B3 protein. HSD17B3 was expressed in seminiferous tubules of gonadal tissue from a prepubertal patient with PAIS (Figure 12B) and not in peritubular LCs, identified by CYP17A1 expression (Figure 12E). In gonadal tissue from a pubertal patient with PAIS, HSD17B3 was expressed in some LC nodules and to a lesser extent in SCs (closed arrow in Figure 12C and Figure 13C), comparable to the testicular tissue from the young adult control (Figure 12A). However, some LCs in the pubertal PAIS gonadal tissue did not express HSD17B3 including a large LC nodule (Figure 13B). Interestingly, SCs in the seminiferous tubules adjacent to this LC nodule strongly expressed HSD17B3 (closed arrows in Figure 13B). Taken together, the results suggest that PAIS gonadal tissues maintain the foetal pattern of

HSD17B3 before puberty and that the partial gain of androgen signalling during puberty might partially induce the switch of HSD17B3 expression from SCs to LCs, rescuing LC and SC maturation to some extent.

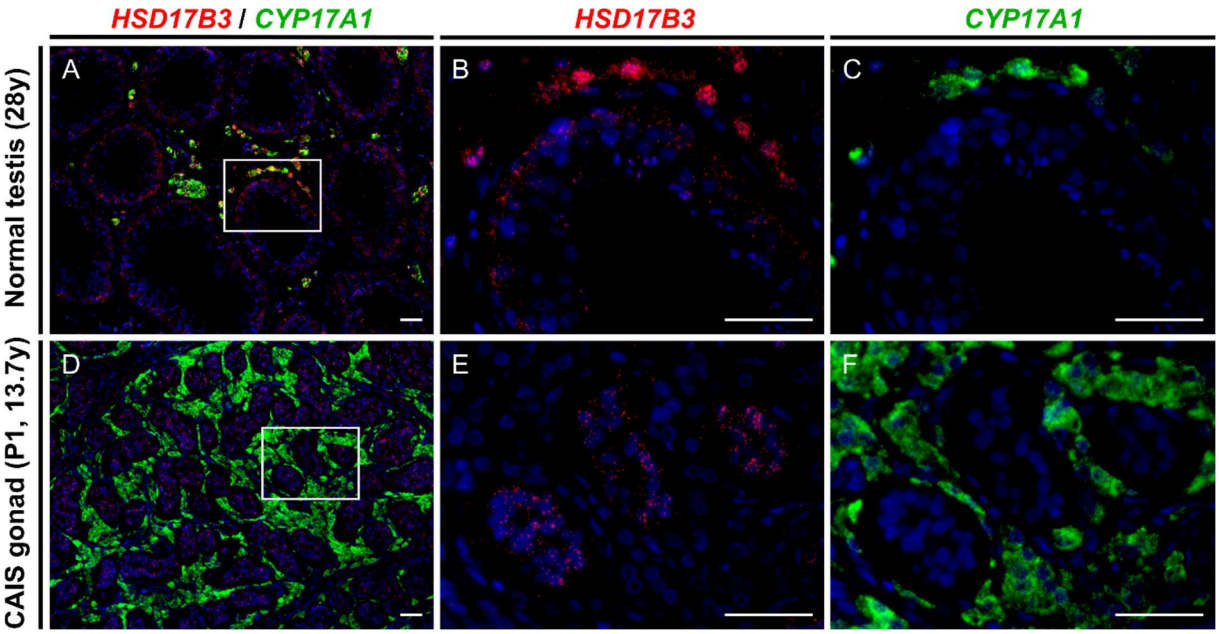

Figure 10. *HSD17B3* and *CYP17A1* mRNA expression in testicular tissue from a 28-year-old control compared to gonadal tissue from a 13.7-year-old patient with CAIS (P1). *HSD17B3* is expressed in Leydig cells in the interstitial tissue and, to a lesser extent, in the seminiferous tubules in normal adult testicular tissues (A and B), but only in the seminiferous tubules in CAIS gonadal tissue (D and E). Leydig cells are identified in both tissues by their expression of *CYP17A1*, and show the typical hyperplasia known for CAIS gonadal tissues. Scale bar, 50 µm.

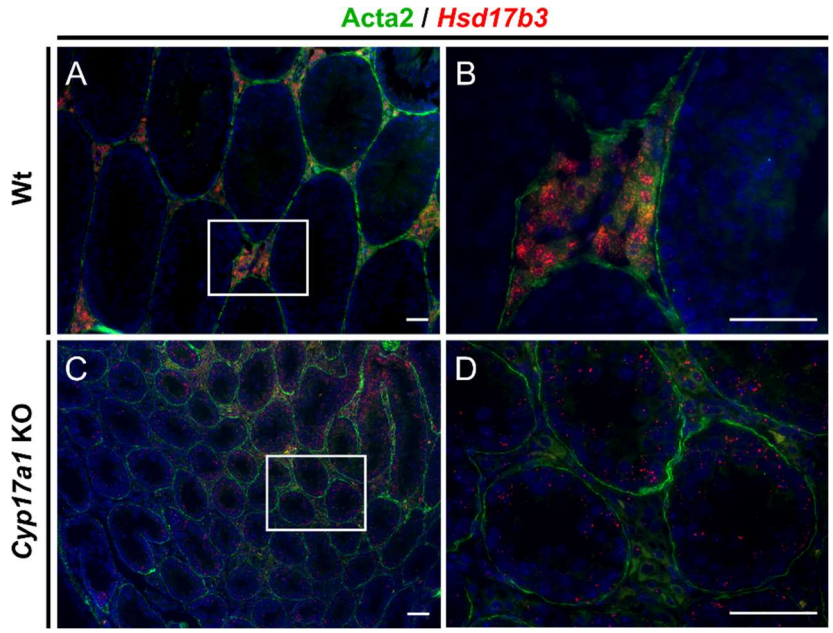

Figure 11. HSD17B3 mRNA and Acta2 protein expression in wild-type mouse testicular tissue compared to Cyp17a1 knockout mouse testicular tissue. *HSD17B3* mRNA is expressed in Leydig cells in the interstitial tissue of the wt adult mouse testis (A and B), but only in the seminiferous tubules in the *Cyp17a1* knockout mouse testis (C and D). Acta2 protein is expressed in PTMCs surrounding the seminiferous tubules in both the Wt and the *Cyp17a1* knockout mouse testes, allowing the visual discrimination of the tubular and the interstitial compartments in both tissues. Wt; wild-type, KO; knockout. Scale bar, 50 µm.

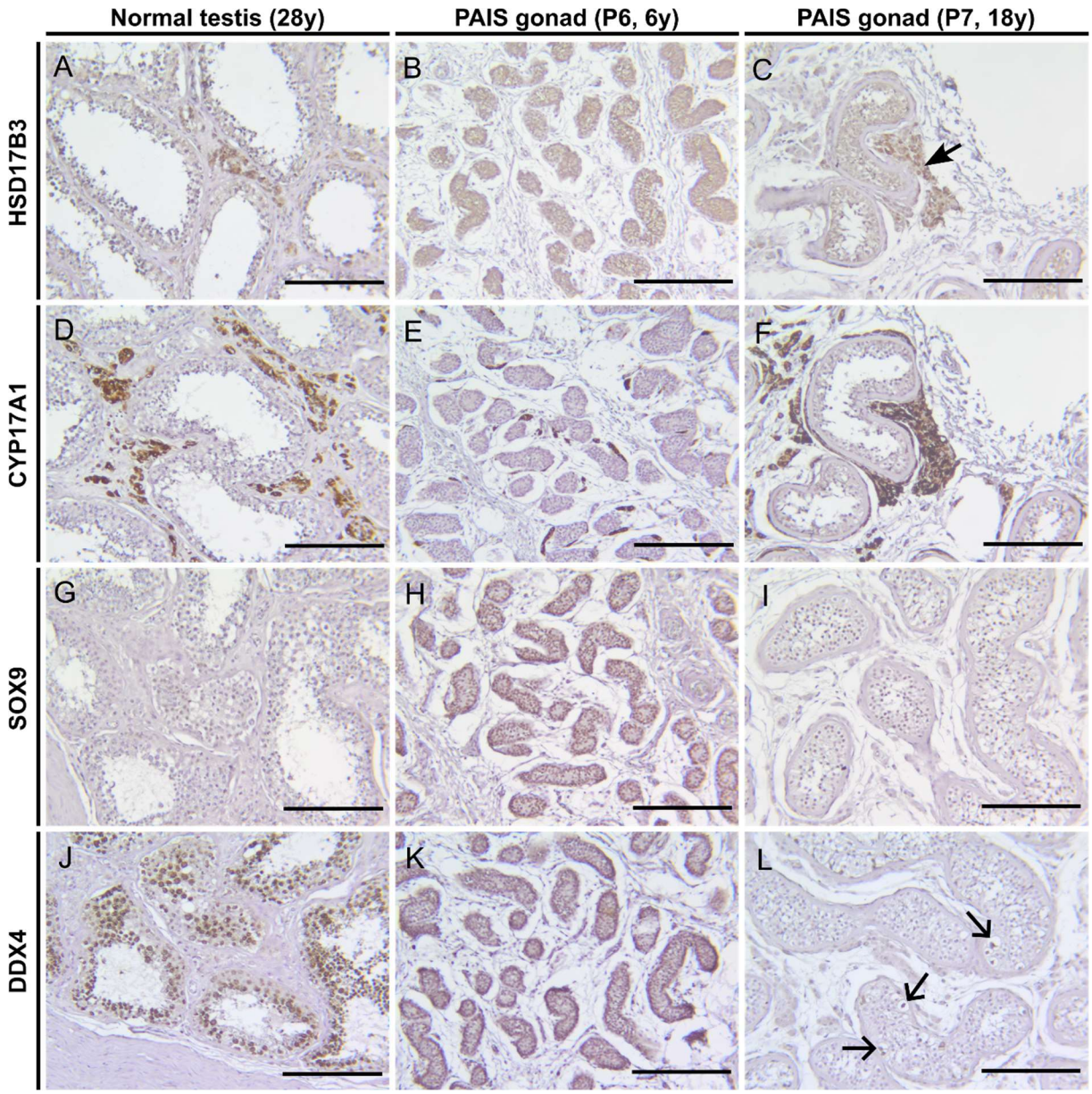

Figure 12. HSD17B3, CYP17A1, SOX9 and DDX4 protein expression in testicular tissue from a 28-year-old control compared to gonadal tissues from a 5-year-old (P6) and 15-year-old (P7) PAIS patients. HSD17B3 is expressed in the interstitial tissue and, to a lesser extent, in the seminiferous tubules in the normal adult testicular tissue (A) but only in the seminiferous tubules in the prepubertal patient with PAIS (B), and not in CYP17A1-expressing LCs residing around the seminiferous tubules (E). In contrast, HSD17B3 is expressed in LC nodule in the young adult with PAIS (closed arrow in C). The different cells in the seminiferous tubules in testicular tissue from the adult normal control express SOX9 (G) and DDX4 (J). In contrast, most of the cells in the seminiferous tubules in gonadal tissues from the prepubertal and the young adult patients with PAIS express SOX9 (H and I) and few spermatogonial cells express DDX4 (open arrows in L). Scale bar, 200 µm.

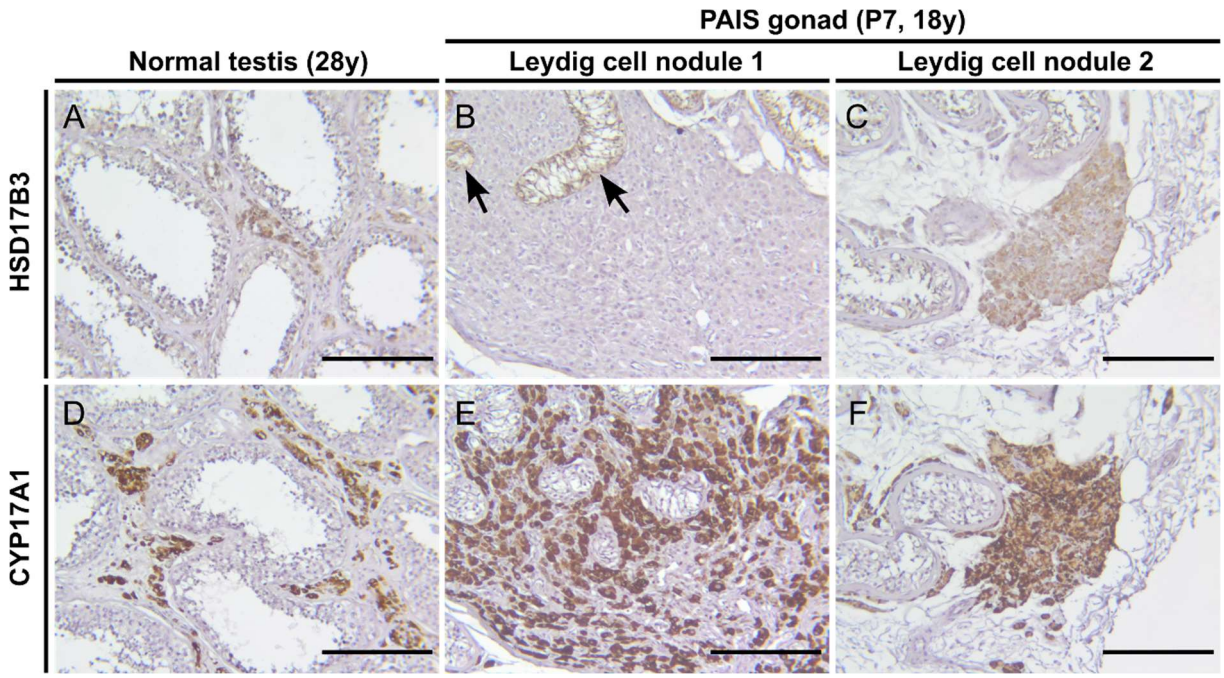

Figure 13. Partial rescue of LC and SC differentiation in PAIS. HSD17B3 and CYP17A1 protein expression in two Leydig cell nodules in gonadal tissue from an 18-year-old patient with PAIS (P7) compared to testicular tissue from a 28-year-old control. HSD17B3 is expressed in Leydig cells in the interstitial tissue and, to a lesser extent, in the seminiferous tubules in normal adult testicular tissues (A). HSD17B3 is not expressed in a large Leydig cell nodule in the interstitial tissue in the pubertal PAIS gonad (B). Like in CAIS, it is expressed in the nearby seminiferous tubules (arrows in B). Another smaller Leydig cell nodule resembles the normal control and expresses HSD17B3, but not in the nearby seminiferous tubules (C). CYP17A1 labels Leydig cells in normal adult testicular tissue (D) and in the pubertal PAIS gonadal tissue (E and F). Scale bar, 200 µm.

3.5 AKR1C3 is expressed in LCs in gonadal tissues from adolescents and adults with CAIS

Post-pubertal individuals with CAIS show normal or even elevated testosterone compared to normal male controls, despite any signs of virilisation. The exclusive expression of HSD17B3 in SCs in CAIS gonadal tissues raises the question whether reduction of androstenedione takes place solely in SCs or could be contributed by LCs. AKR1C3, also known as HSD17B5, is an isoenzyme of HSD17B3 that can reduce androstenedione to testosterone (171), and is expressed in normal adult LCs. The expression of AKR1C3 has been reported in LCs in gonadal tissue from a 46,XY pubertal patient with HSD17B3 deficiency and was proposed as possible source of testosterone production in this patient (136). To investigate whether LCs can contribute in reduction of androstenedione to testosterone in gonadal tissues from patients with CAIS, gonadal tissue sections from pubertal and young adult patients with CAIS were stained for AKR1C3 protein. AKR1C3 was expressed in LCs in control testicular tissues (Figure 14E and Supplementary materials Figures 31I and 32E) and in hyperplastic LCs in gonadal tissues from all CAIS patients (Figure 14F and Supplementary materials Figure 31J-L). The same pattern was also observed in *CYP17A1* deficiency (Supplementary materials Figure 32). This expression pattern suggests that LCs, lacking HSD17B3 expression, might still contribute to testicular testosterone production by reduction of androstenedione to testosterone by expressing AKR1C3 (170).

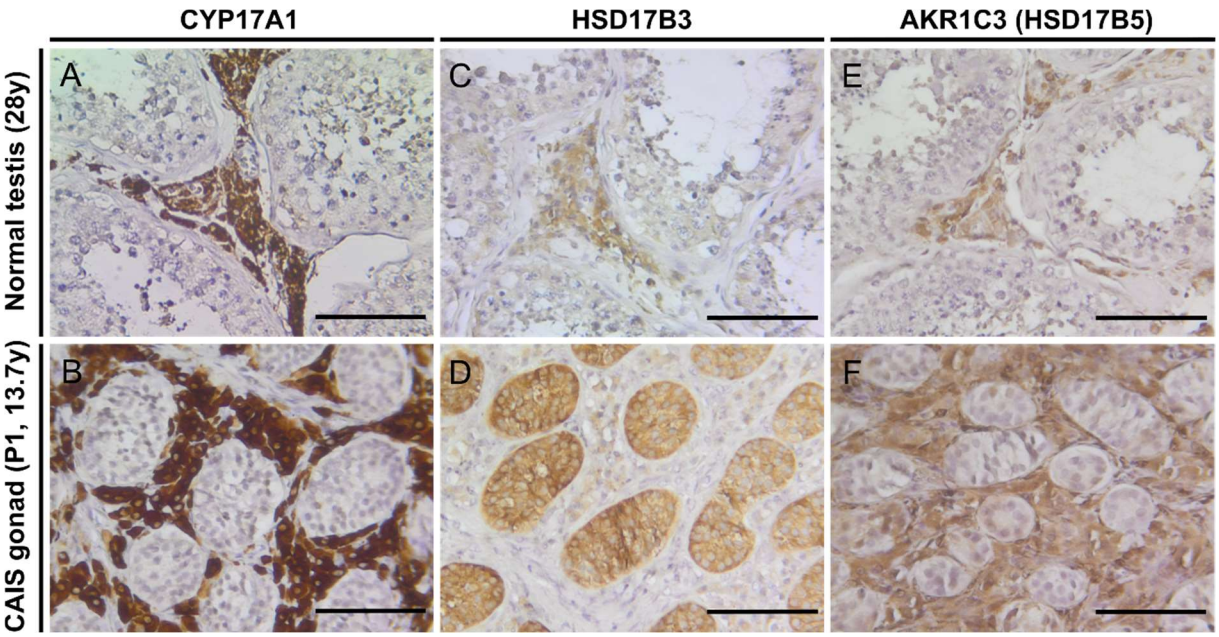

Figure 14. AKR1C3 (HSD17B5), HSD17B3 and CYP17A1 protein expression in gonadal tissue from a 13.7-year-old patient with CAIS (P1) compared to testicular tissue from a 28-year-old control. CYP17A1 expression identifies Leydig cells in both normal adult testicular tissue (A) and CAIS gonadal tissue (B). HSD17B3 is expressed mainly in Leydig cells and to a lesser extent in seminiferous tubules in normal adult testicular tissue (C), but exclusively in seminiferous tubules in CAIS gonadal tissue (D). AKR1C3 is expressed in Leydig cells in both normal adult testicular tissue (E) and CAIS gonadal tissue (F). Scale bar, 100 µm. Adapted from (6) according to the terms of the creative Commons Attribution-NonComercial License (https://creativecommons.org/ licenses/by-nc/4.0/).

3.6 HSD17B3 is expressed in human foetal (and neonatal) SCs while its isoenzyme AKR1C3 is expressed mainly in adult LCs

It was interesting to investigate whether the pattern of HSD17B3 expression shown previously in gonadal tissues from pubertal and young adult patients with CAIS and *CYP17A1* deficiency is also present in normal foetal human testis. Publicly available scRNA-seq data from human testicular tissues acquired at different developmental stages from foetal to adult (Supplementary materials Table 19) were reanalysed to estimate relative expression levels of HSD17B3 in SCs and LCs. *HSD17B3* expression starts in SCs in the embryonal and foetal stages and then declines gradually until birth, rises again at mini-puberty, then decreases and stays low through adulthood (Figure 15A). In contrast, *HSD17B3* is barely expressed in LCs in the embryonal and foetal stages, but its expression starts in LCs at mini-puberty and through puberty, still relatively lower than in SCs (Figure 15A). In adulthood, *HSD17B3* expression in LCs is low, although relatively higher than SCs (Figure 15A). The expression of *AKR1C3* in LCs, on the other hand, starts low in the embryonal and foetal stages and remains so in the prepubertal stage, then rises through puberty and adulthood (Figure 15B). The change in LC percentages in samples from foetal, neonatal, pubertal and adult stages captures the triphasic nature of LC proliferation during development (Figure 15C), and highlights their role during male sex development, either by providing testosterone precursors during foetal (and mini-pubertal) stages or by directly synthesising testosterone during the pubertal and adult stages (170).

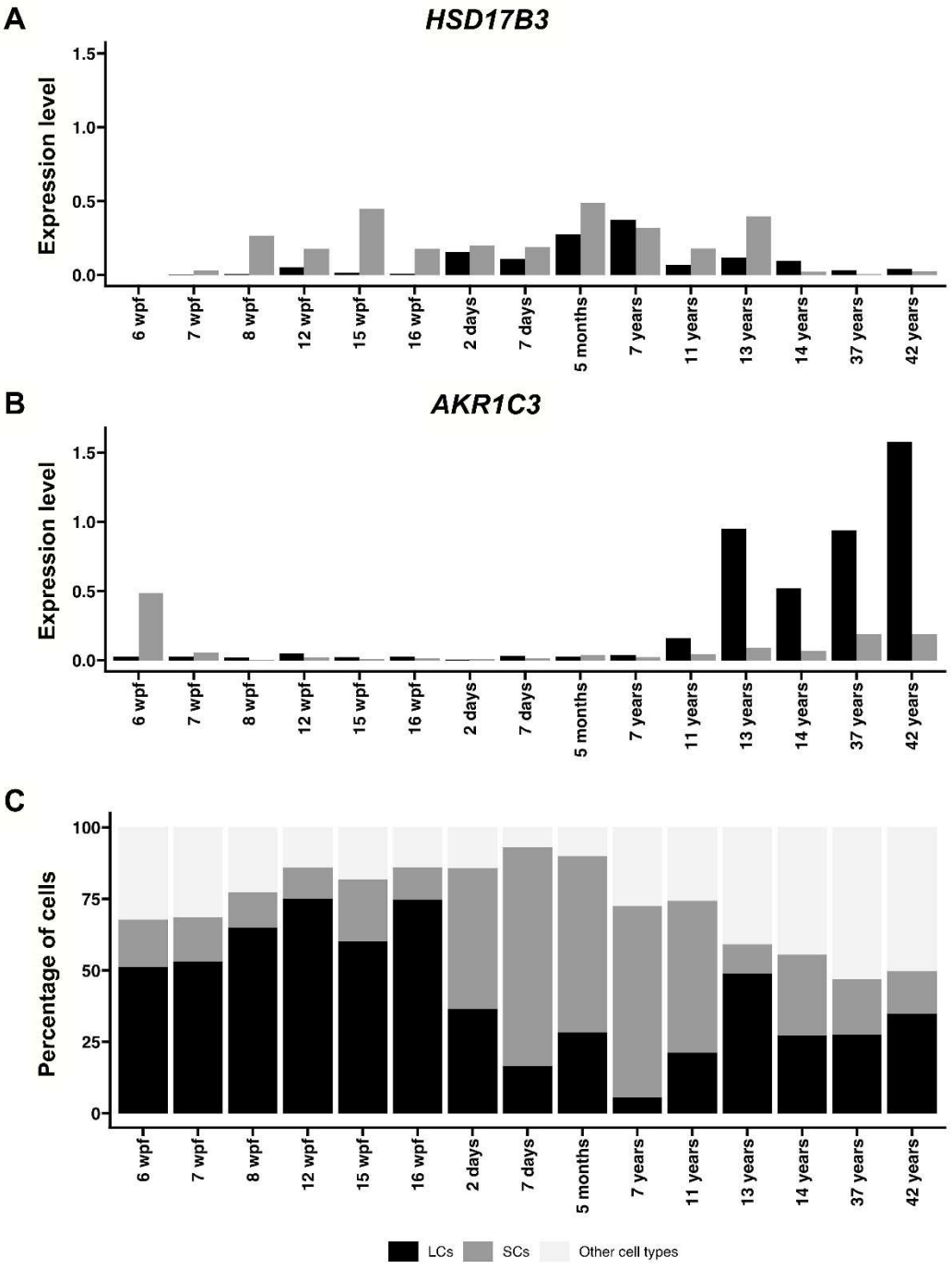

Figure 15. Reanalysis of publicly available single-cell RNA sequencing data from testicular tissues collected from embryonal, foetal, neonatal, prepubertal, pubertal and adult stages.
(A) Bar plot comparing the average expression of *HSD17B3* in Leydig cells versus Sertoli cells in normal testicular tissue samples collected at different developmental stages. (B) Bar plot comparing the average expression of *AKR1C3* (*HSD17B5*) in Leydig cells versus Sertoli cells in the same samples. (C) Bar plot comparing the cellular composition of these testicular tissues. The average expression values and cell percentages represented in the blots are extracted from publicly available single-cell RNA sequencing data from the studies listed in Table S1. LC, Leydig cell; SC, Sertoli cells. Reproduced from (170) according to the terms of the Creative Commons Attribution-NonComercial License (https://creativecommons.org/ licenses/by-nc/4.0/).

3.7 DLK1 and INSL3 are expressed in subsets of LCs in CAIS and *CYP17A1*-deficiency gonadal tissues

The persistence of foetal expression pattern of HSD17B3 in gonadal tissues from pubertal and young adult patients with CAIS and *CYP17A1* deficiency suggests that LCs in these gonadal tissues might represent repopulation of foetal LCs or persistence of immature adult LCs. In adult *Ar* gene knockout mouse testis, adult LCs develop but lack *Hsd17b3* expression, and hence considered immature adult LCs (102, 172). To our knowledge, no specific markers can differentiate foetal from adult LCs. Some markers of LC development have been proposed, though. DLK1 is expressed in LCs in human foetal testis but only in progenitor and immature LCs in adult human testis, and is expressed inversely proportional to INSL3 (173). To assess LC differentiation in gonadal tissues from patients with congenital defective androgen signalling, gonadal tissue sections from pubertal and young adult patients with CAIS and *CYP17A1* deficiency were stained for DLK1 and INSL3 protein. In control testicular tissue, LC showed high INSL3 expression and low DLK1 expression (Figure 16A and B and Supplementary materials Figures 33A and B and 34A and B). DLK1 was expressed in subsets of LCs in gonadal tissues from CAIS patients (Figure 16D and Supplementary materials Figure 33C and E). INSL3 expression varied among gonadal tissues, with strong expression in gonadal tissue from pubertal CAIS patient P1(Supplementary materials Figure 34D), moderate expression in gonadal tissues from young adult CAIS patients (P2 an P3) (Supplementary materials Figure 33D and Figure 16C) and no expression in gonadal tissue from oldest CAIS patient P4 (Supplementary materials Figure 33F).

Although it was difficult to confirm that DLK1 and INSL3 were expressed in different subsets of LCs, few LC aggregations (LC nodules) in gonadal tissues from CAIS P1 and P3 overexpressed DLK1 (Supplementary materials Figure 34E and Figure 16F) but barely expressed INSL3 (Supplementary materials Figure 34F and Figure 16E), supporting the proposition that $DLK1^{+}$ and $INSL3^{+}$ LCs are different populations of LCs (170). It was difficult to show the mutual exclusive pattern of DLK1 and INSL3 in gonadal tissue from the young adult with *CYP17A1* deficiency (Supplementary materials Figure 335G and H), though.

Therefore, the expression of *DLK1* and *INSL3* mRNAs was further investigated in CAIS gonadal tissues by smFISH. Most of LCs in the control testicular tissue co expressed *DLK1* and *INSL3* mRNAs (Figure 17A-C). In contrast, most LCs in the interstitial tissue of the CAIS gonad exclusively expressed *DLK1*, some exclusively expressed *INSL3* and very few co-expressed both markers (Figure 17D-F), while LCs in the LC nodule exclusively expressed *DLK1* (Figure 17G and H) with no detectable expression of INSL3 (Figure 17G and I). This expression pattern corroborates the protein expression patterns shown above and gives further support to the proposition that $DLK1^{+}$ and $INSL3^{+}$ LCs represent different differentiation stages.

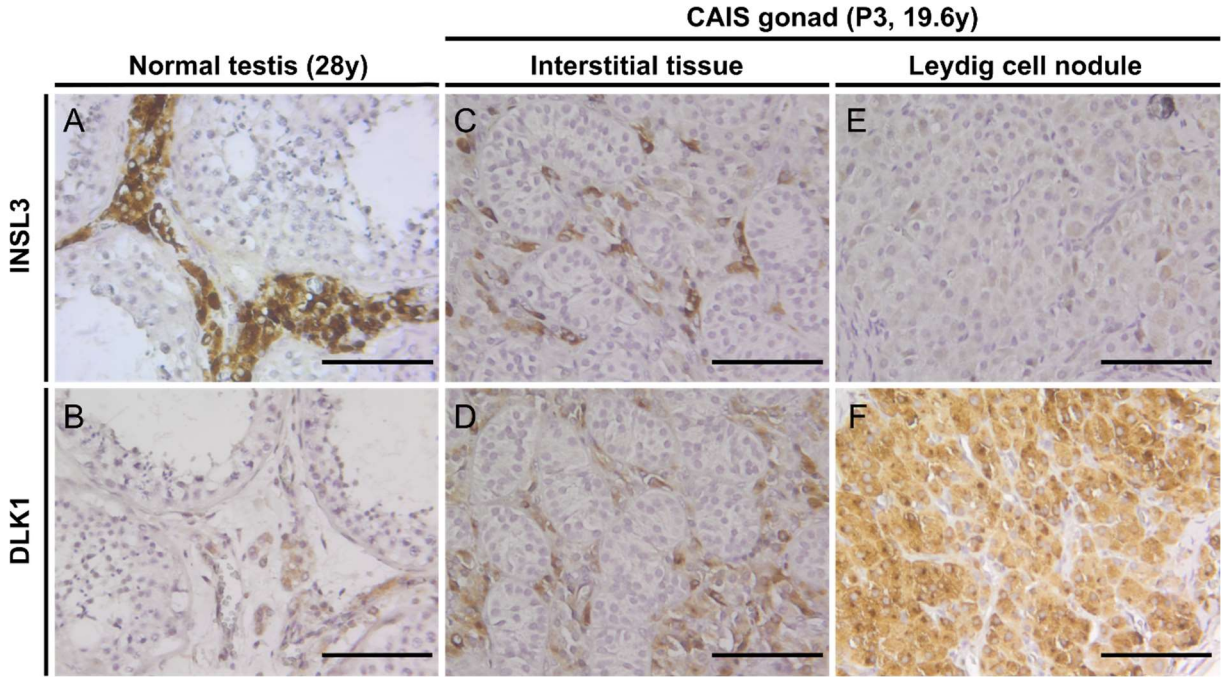

Figure 16. INSL3 versus DLK1 protein expression in gonadal tissue from a 19.6-year-old patient with CAIS (P3) compared to normal testicular tissue from a 28-year-old control. INSL3 is expressed in most of Leydig cells in the normal adult testicular tissue (A) while DLK1 is expressed in some of them (B). INSL3 and DLK1 are expressed in subsets of Leydig cells in the young adult CAIS gonadal tissue (C and D). A Leydig cell nodule in the CAIS gonadal tissue barely express INSL3 (E) but highly express DLK1 (F). Scale bar, 100 µm. Reproduced from (170) according to the terms of the creative Commons Attribution-NonComercial License (https://creativecommons.org/ licenses/by-nc/4.0/).

3.8 HSD17B3^{+} nodules express *DLK1* and *INSL3*, while HSD17B3^{-} nodule express only *DLK1* in the young adult PAIS gonadal tissue

As shown above, two LC nodules were seen in the young adult PAIS gonadal tissue: one that expressed HSD17B3 like mature/adult LCs and another that did not express HSD17B3 like immature/foetal LCs. To examine differentiation state of LCs in both of the LC nodules, the mRNA expression of mature/adult LC marker *INSL3* and the immature/foetal LC marker *DLK1* was investigated using *in situ* hybridisation. Like LCs in the adult control testicular tissue, the HSD17B3^{+} LC nodule 2 strongly expressed *INSL3* mRNA and moderately expressed *DLK1* mRNA (Figure 18G-I). In contrast, the HSD17B3^{-} LC nodule 1 highly expressed *DLK1* mRNA and did not express *INSL3* mRNA (Figure18D-F) like LC nodules observed in CAIS gonadal tissues of P1 and P3. The results suggest that the partial rescue of response to androgenic stimulation the young adult PAIS gonadal tissue could advance the differentiation of some LCs but not the others, that there is a threshold for testicular androgenic stimulation needed to drive the differentiation of LCs, and that other local factors possibly act in concert with androgen signalling for proper differentiation of LCs in human testis.

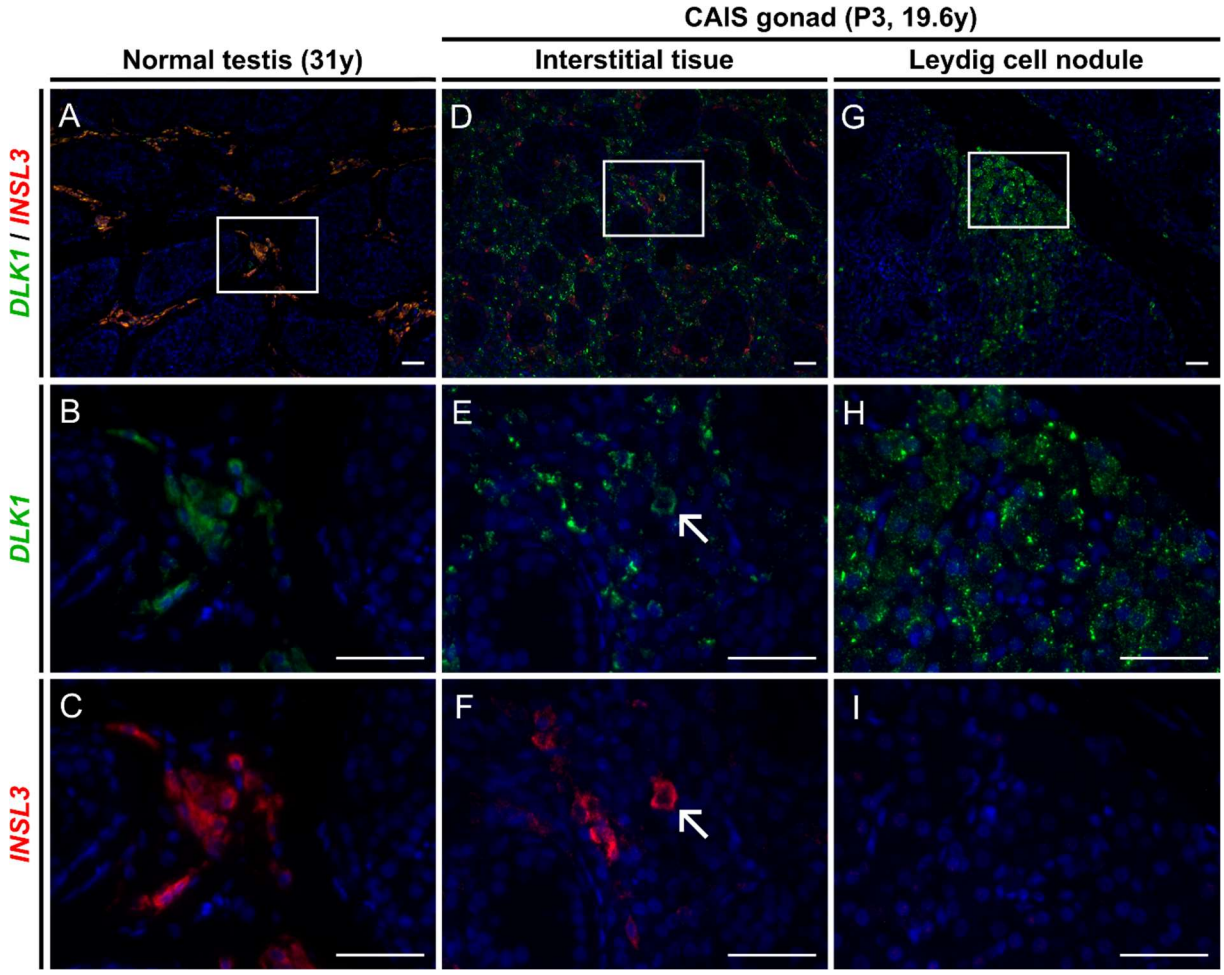

Figure 17. *DLK1* versus *INSL3* mRNA expression in gonadal tissue from a 19.6-year-old patient with CAIS (P3) compared to normal testicular tissue from a 31-year-old control. *DLK1* and *INSL3* are co-expressed in most LCs in the interstitial tissue in the control testis (A-C). *DLK1* is expressed in most Leydig cells in the interstitial tissue (D and E) and the Leydig cell nodule (G and H), while *INSL3* is expressed in fewer Leydig cells in the interstitial tissue (F) but not in the Leydig cell nodule (I). Very few Leydig cells co-express *DLK1* and *INSL3* in the interstitial tissue of the CAIS gonad (open arrows in E and F).

3.9 Further characterisation of the DLK1-overexpressing LC nodules

Overexpression of DLK1 in LC nodules in gonadal tissues from CAIS patients P1 and P3, along with polygonal shape of their LCs suggests that LCs in these nodules might be still in the foetal state. To further characterise these LC nodules, gonadal tissue sections from CAIS patients P1 and P3 were stained for steroidogenic markers CYP17A1, HSD17B3 and AKR1C3. The LC nodules strongly expressed CYP17A1 (Figure 19C and Supplementary materials Figure 35C) but barely expressed HSD17B3 (Figure 19F and Supplementary materials Figure 35F), like interstitial LCs in the same gonadal tissues (Figure 19B and E, and Supplementary materials Figure 35B and E). In contrast to the interstitial LCs (Figure 19H and Supplementary materials Figure 35H), the LC nodules barely expressed AKR1C3 (Figure 19I and Supplementary materials Figure 35I). Since the enzyme is proposed to be expressed in the adult but not foetal LCs, the LCs in the DLK1-overexpressing LC nodules might represent LCs with foetal characteristics (170).

The LC nodules bore some resemblance to testicular adrenal rest tumours (TARTs), a common complication in patients with congenital adrenal hyperplasia. Similar to the LC nodules reported in this study, TARTs express DLK1 but not INSL3. In addition, TARTs express other adrenal markers including CYP11A1, CYP21A2 and ACTH receptor/melanocortin two receptors (MC2R) (174). To exclude that the LC nodules in gonadal tissues form CAIS patient P1 and P3 are TARTs, gonadal tissue sections were stained for CYP21A2. Neither LCs in the interstitial tissues nor in the LC nodules expressed CYP21A2 (Figure 19K and L, and Supplementary materials Figure 35K and L). This excludes the possibility that these LC nodules represent TARTs in CAIS gonadal tissues (170).

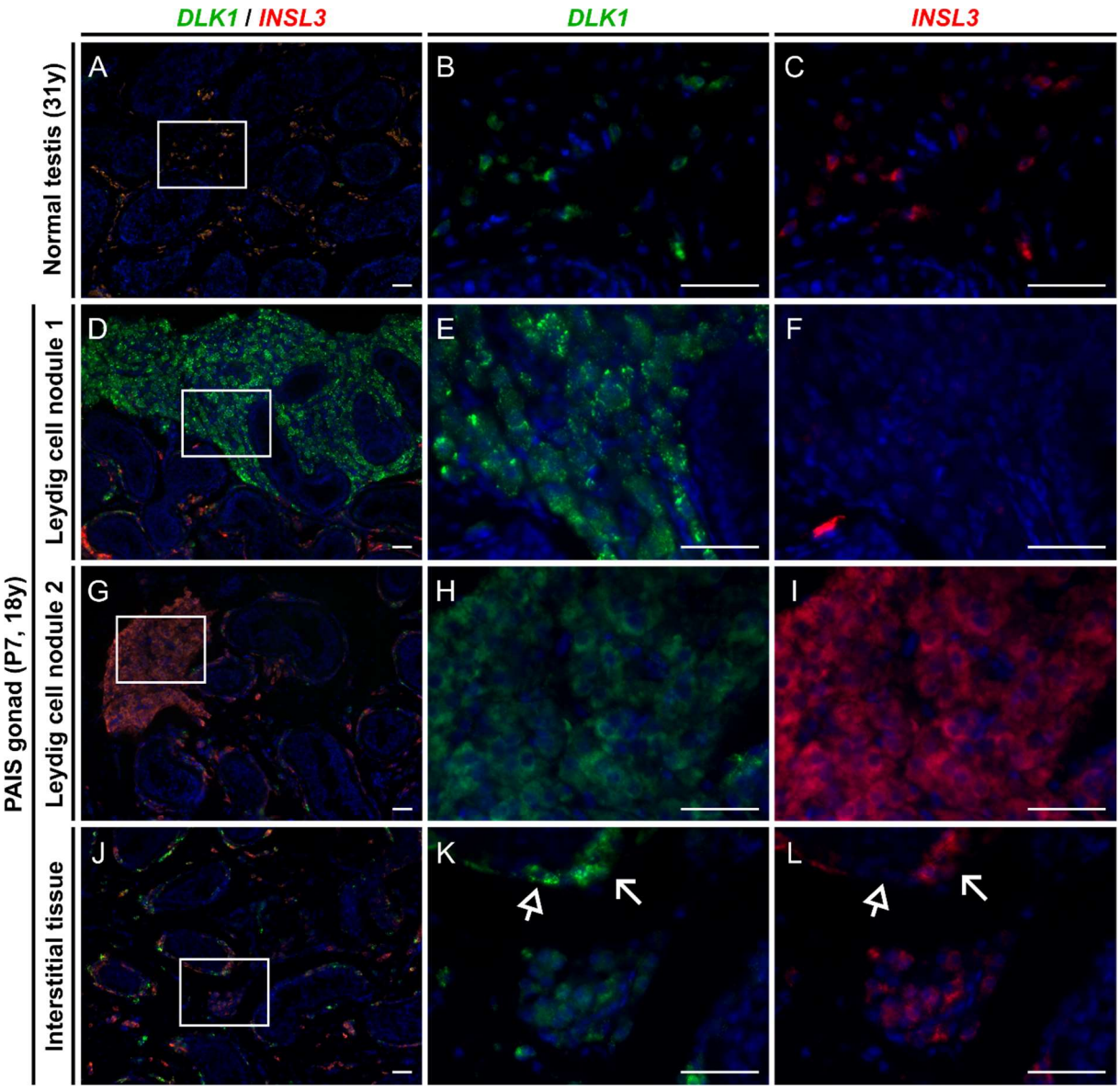

Figure 18. Expression of *DLK1* and *INSL3* mRNAs in in gonadal tissue from an 18-year-old patient with PAIS compared to normal testicular tissue from a 31-year-old control. *DLK1* and *INSL3* mRNAs are co-expressed in most Leydig cells in the control adult testis (A-C). *DLK1* mRNA is highly expressed in Leydig cell nodule 1 (D and E), while *INSL3* mRNA is not (D and F). Both *DLK1* and *INSL3* mRNAs are expressed in Leydig cell nodule 2 (G-I). Leydig cells in the interstitial tissue express *DLK1* mRNA either alone (closed arrows in K and L) or in conjunction with *INSL3* mRNA (open arrows in K and L). Scale bar, 50 µm.

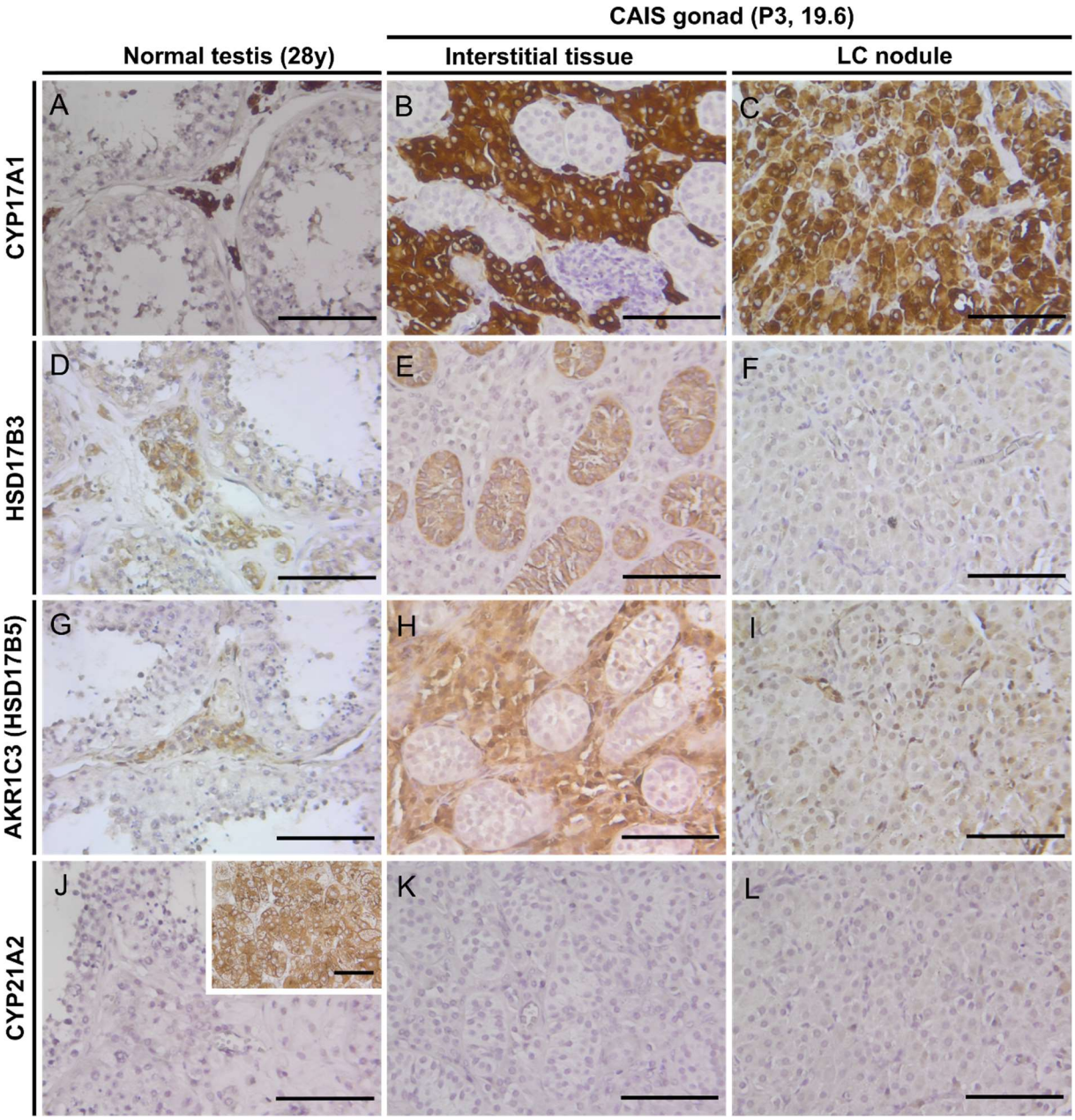

Figure 19. CYP17A1, HSD17B3, AKR1C3 and CYP21A2 protein expression in interstitial Leydig cells versus Leydig cell nodule in gonadal tissue form a 19.6-year-old patient with CAIS. CYP17A1 is expressed in Leydig cells in the normal adult testicular tissue (A) as well as Leydig cells in the interstitial tissue (B) and the Leydig cell nodule (C) in the young adult CAIS gonadal tissue. HSD17B3 is expressed in Leydig cells and to a lesser extent in Sertoli cells in the normal adult testicular tissue (D), but neither in Leydig cells in the interstitial tissue (E) nor in Leydig cells in the Leydig cell nodule (F). AKR1C3 (HSD17B5) is expressed in Leydig cells in the normal adult testicular tissue (G) and Leydig cells in the interstitial tissue (H) in the young adult CAIS gonadal tissue, but barely in the Leydig cell nodule (I). CYP21A2 is not expressed in Leydig cells in the normal adult testicular tissue (J), Leydig cells in the interstitial tissue (K) or Leydig cell nodule (L). Inner set in (J) represents CYP21A2 staining in normal adult adrenal cortical tissue as positive control in the experiment. Scale bar, 100 µm. Reproduced from (6) according to the terms of the creative Commons Attribution-NonComercial License (https://creativecommons.org/ licenses/by-nc/4.0/).

3.10 Proteins of the blood-testis barrier (BTB) are aberrantly expressed in SCs in gonadal tissues from CAIS and *CYP17A1* deficiency

As shown above, gonadal tissues from pubertal and young adult patients with CAIS and *CYP17A1* deficiency maintain the expression of *HSD17B3* in SCs, a feature that is known in foetal mouse testis and was shown recently in foetal human testis (107, 170, 175), suggesting that defective androgen signalling in CAIS and *CYP17A1* deficiency gonadal tissues is associated with defective differentiation of SCs. Since adult SCs play a central role in supporting germ cells, this defect in SC differentiation might be involved in germ cell loss shown above in these gonadal tissues, although the mechanism is not fully understood. A recent study investigated the role of androgen signalling on SC maturation and spermatogenesis and has shown that SCs in gonadal tissue from a young adult patient with CAIS does not express GJA1, also known as connexin 43 (CX43) (176), one of the gap junction proteins that take part in the formation of the blood-testis barrier in adult testis. The loss of expression of GJA1 (CX43) in this CAIS gonadal tissue suggests that the blood-testis barrier is deformed because of defective androgen signalling, making germ cells accessible to the immune system and possibly contributing to germ cell loss. To assess the integrity of the blood-testis barrier in gonadal tissues from adolescents and young adults with congenital defects of androgen signalling, the expression of *GJA1* (*CX43*), *CLDN11(Claudin 11)* and *TJP1* (*(Tight Junction Protein 1, also known as Zona occludens1, ZO-1*) was investigated in adolescents and young adults with CAIS and CYP17A1 deficiency.

3.10.1 GJA1 (CX43) expression is lost in SCs in gonadal tissues from adolescents and young adults with CAIS and *CYP17A1* deficiency

Recently, gonadal tissue from a young adult patient with CAIS were shown to express GJA1 (CX43) only in LCs and not in SCs (176), suggesting that defective androgen signalling might be implicated in blood-testis barrier formation and SC maturation. To test whether GJA1 (CX43) expression is lost in gonadal tissues of pubertal and young adults with congenital defects in androgen signalling, gonadal tissue sections from patients with CAIS (P1-P3) and a young adult patient with *CYP17A1*-deficiency (P5) were immunostained for GJA1 (CX43). Compared to testicular tissue from the normal adult control, GJA1 (CX43) localised only to the membranes of hyperplastic LCs in CAIS gonadal tissues (P1-P3) (Figure 20C and D, Supplementary materials Figure 38C-F) and the membranes of hypoplastic LCs in *CYP17A1*-deficincy gonadal tissue (P5) (Figure 20E and F), with no expression in seminiferous tubules in all gonadal tissues. Loss of GJA1 (CX43) expression in SCs in gonadal tissues form patients with CAIS and *CYP17A1*-deficiency patients suggests that androgen signalling might play a role regulation of GJA1 expression, although not directly, since GJA1 (CX43) expression is maintained in LCs in gonadal tissue from these patients.

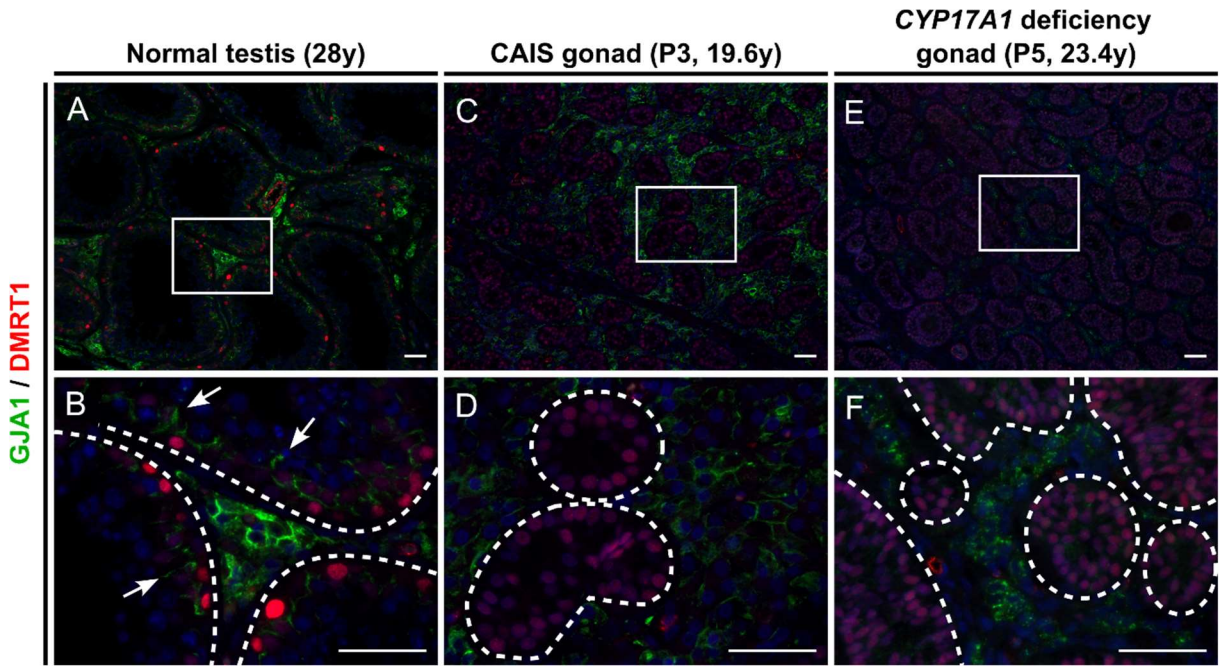

Figure 20. Loss of GJA1 protein expression at the blood-testis-barrier in Sertoli cells. Immunofluorescent detection of GJA1 protein was detected by TSA in gonadal tissues of a 19.6-year-old patient with CAIS (P3) and a 23.4-year-old patient with *CYP17A1* deficiency (P5) in comparison to normal testicular tissue of a 28-year-old control. GJA1 localises not only to membranes of Leydig cells, but also to the basal surfaces of the adjacent Sertoli cells at the site of blood-testis-barrier in the normal adult control (A and white arrows in B). In contrast, GJA1 localises only to the membranes of hyperplastic Leydig cells in the young adult patient with CAIS (C and D) and hypoplastic Leydig cells in the young adult patient with *CYP17A1* deficiency (E and F) and not in the seminiferous tubules (C-F). To identify seminiferous tubules (here shown inside the dashed white lines) from the surrounding interstitial tissue, DMRT1 was used to label Sertoli cells and spermatogonia in tissue sections. DMRT1 is moderately expressed in Sertoli cells and highly expressed in spermatogonia in seminiferous tubules from the normal adult testicular tissue (A and B). In contrast, all cells in seminiferous tubules in both gonadal tissues from patients with CAIS (C and D) and *CYP17A1* deficiency (E and F) moderately express DMRT1, being composed of Sertoli cells only, consistent with germ cell loss shown earlier in these tissues. Scale bar, 50 µm.

3.10.2 CLDN11 protein expression is lost although mRNA expression is maintained in SCs in gonadal tissues from adolescents and young adults with CAIS

Claudins are integral membrane proteins that form tight TJ fibrils to seal adjacent epithelial and endothelial cells and create cell polarity (118). In mouse testis, Cldn3 and Cldn11 contribute to TJs at the blood-testis barrier. *Cldn3* is regulated by androgens as SC-specific ArKO (SCArKO) downregulates *Cldn3*, but not *Cldn11*, and increases the permeability of BTB (128). Cldn11 knock out is associated with disruption of the BTB and germ cell apoptosis in adult mouse testis (120). In adult human testis, CLDN11 localises to the basal of seminiferous tubules, and its expression is disrupted under the effect of gonadotropin suppression, suggesting that CLDN11 might be regulated by follicle -stimulating hormone (FSH) and androgens (177, 178). To investigate whether the expression of CLDN11 is disrupted in gonadal tissues from pubertal and young adults with congenital resistance to androgen action, gonadal tissue sections from patients with CAIS (P1-P4) were immunostained for CLDN11. In testicular tissue from the normal adult control, CLDN11 was expressed in the

seminiferous tubules near the basal lamina (Figure 21A and Supplementary materials Figure 39A). In contrast, no CLDN11 protein could be detected in seminiferous tubules in gonadal tissues from patients with CAIS (Figure 21B, Supplementary materials Figure 39B-D). To further investigate *CLDN11* expression in CAIS gonadal tissues, accumulation of *CLDN11* mRNA was analysed in these tissues by fluorescent *in situ* hybridisation. Unexpectedly, *CLDN11* mRNA expression in seminiferous tubules of CAIS gonadal tissues (Figure 21E and F, Supplementary materials Figure 39G-L) was maintained to a level comparable to the normal adult testicular tissue (Figure 21C and D, Supplementary materials Figure 39E and F). Taken together, the results suggest that defective androgen signalling in CAIS gonadal tissues affects protein expression or accumulation but not the transcription of *CLDN11* and that androgen signalling may be implicated in regulation of *CLDN11* expression at a post-transcriptional level.

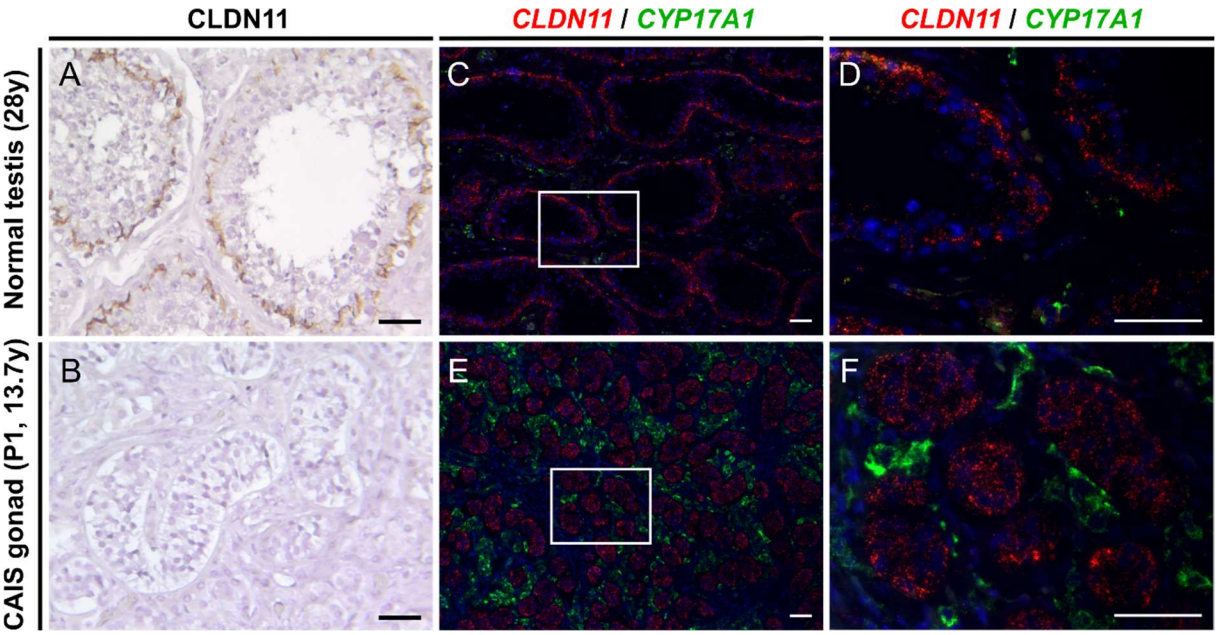

Figure 21. CLDN11 protein versus mRNA expression in gonadal tissue from a 13.7-year-old patient with CAIS (P1) compared to normal testicular tissue from a 28-year-old control. CLDN11 protein localises to the basal surfaces of the adjacent Sertoli cells in the normal adult testicular tissue (A) at the site of blood-testis barrier, but is undetectable in the seminiferous tubules of pubertal CAIS gonadal tissue (B). In contrast, *CLDN11* mRNA is expressed not only in the seminiferous tubules in the normal adult testicular tissue (C and D) but also in pubertal CAIS gonadal tissue (E and F). *CYP17A1* mRNA detection was used as an internal control in the multiplex fluorescent *in situ* hybridisation assay, being an abundantly expressed mRNA in both tissues, and labels normal and hyperplastic Leydig cells in the normal adult testicular tissue (C and D) and the pubertal CAIS gonadal tissue (E and F), respectively. Scale bar, 50 µm.

3.10.3 CLDN11 protein and mRNA expression is lost in gonadal tissue from the young adult with *CYP17A1* deficiency

To further investigate whether the expression of CLDN11 is disrupted in gonadal tissues from pubertal and young adults with congenital defects in androgen synthesis, *CLDN11* expression was assessed in gonadal tissue sections from a young adult with *CYP17A1* deficiency (P5) using

immunofluorescence and *in situ* hybridisation. Like CAIS gonadal tissues, CLDN11 protein is not expressed in SCs in the *CYP17A1* deficiency gonadal tissue (Figure 22B). Interestingly however, *CLDN11* mRNA was also undetectable in the *CYP17A1* deficiency gonadal tissue (Figure 22E and F). The downregulation of *CLDN11* at both the protein and the mRNA levels in the *CYP17A1* deficiency gonadal tissue suggests that other factors in addition to the androgen receptor (AR) play a role in *CLDN11* regulation, acting at the transcriptional level.

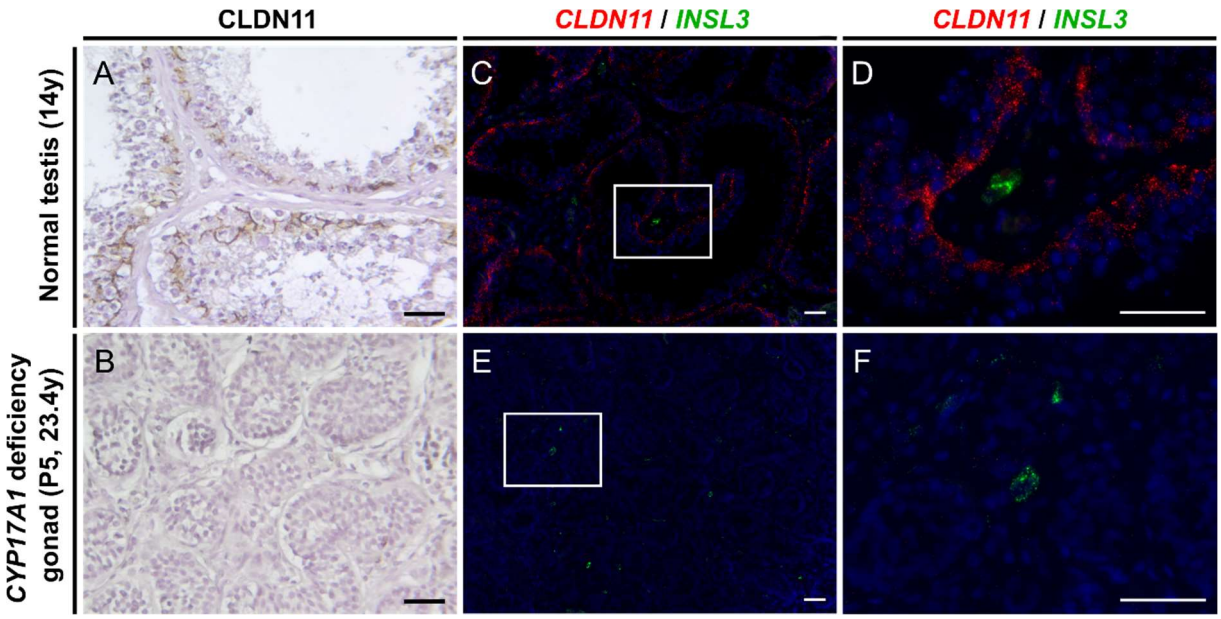

Figure 22. CLDN11 protein versus mRNA expression in gonadal tissue from a 23.4-year-old-patient with *CYP17A1* deficiency (P5) compared to normal testicular tissue from a 14-year-old control.
CLDN11 protein localises to the basal surfaces of the adjacent Sertoli cells in the pubertal testicular tissue (A) at the site of the blood-testis-barrier, but is not expressed in the seminiferous tubules in the young adult gonadal tissue with *CYP17A1* deficiency (B). *CLDN11* mRNA is expressed only in the seminiferous tubules in the normal adult testicular tissue (C and D) and not in the young adult *CYP17A1* deficiency gonadal tissue (E and F). *INSL3* mRNA detection was used as an internal control in the multiplex fluorescent *in situ* hybridisation assay, being expressed in both tissues, and labels Leydig cells in the pubertal control testicular tissue (C and D) and the young adult *CYP17A1* deficiency gonadal tissue (E and F). Scale bar, 50 µm.

3.10.4 *CLDN11* mRNA expressed in the pre-pubertal and maintained in the young adult PAIS gonadal tissue, while CLDN11 protein is not expressed in both gonadal tissues

To further investigate the expression of CLDN11 in partial resistance to androgen action, CLDN11 expression was investigated in one pre-pubertal and one pubertal PAIS gonadal tissue with immunofluorescence and *in situ* hybridisation. Like CAIS and *CYP17A1* deficiency gonadal tissues, CLDN11 protein is neither expressed in the pre-pubertal (Figure 23B) nor in the young adult (Figure 23C) PAIS gonadal tissue. Surprisingly, *CLDN11* mRNA is already expressed in the pre-pubertal PAIS gonadal tissue (Figure 23E and F) and likewise in the young adult PAIS gonadal tissue (Figure 23G and H). The results suggests that *CLDN11* expression in the pre-pubertal testis might be suppressed

post-transcriptionally and that the partial rescue of response to androgen stimulation specifically in this young adult PAIS gonadal tissue was not enough to rescue the accumulation of CLDN11 protein.

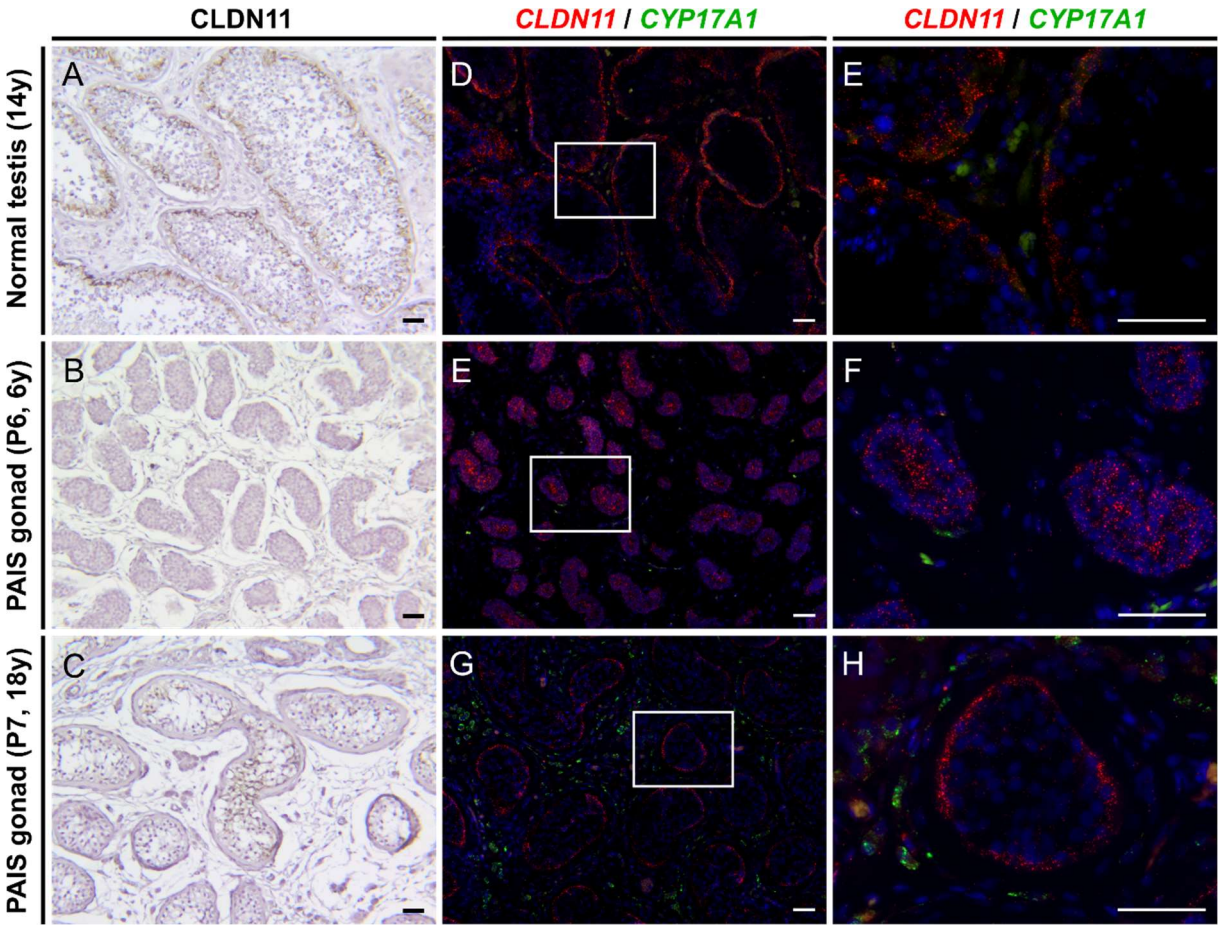

Figure 23. CLDN11 protein versus mRNA expression in gonadal tissues from 6- and 14-year-old patients with PAIS compared to testicular tissue from a 28-year-old control. CLDN11 protein localises to the basal surfaces of the adjacent Sertoli cells in the pubertal testicular tissue (A) at the site of the blood-testis-barrier, but is expressed neither in the pre-pubertal (B) nor in the young adult (C) PAIS gonadal tissues. In contrast, *CLDN11* mRNA is expressed not only in the seminiferous tubules in pubertal control testicular tissue (C and D) but also in the prepubertal (E and F) and the young adult (G and H) PAIS gonadal tissue. *CYP17A1* mRNA detection was used as an internal control in the multiplex fluorescent *in situ* hybridisation assay, being an expressed in both tissues, and labels Leydig cells in the pubertal control testicular tissue (D and E) and the pre-pubertal (E and F) and young adult (G and H) PAIS gonadal tissues, respectively. Scale bar, 50 µm.

3.10.5 TJP1 (ZO-1) expression in SCs in CAIS gonadal tissues show loss of cell polarity

The cytoplasmic plaque adjacent to the TJ are enriched in several scaffolding proteins, which bring integral membrane TJ proteins together and link them to the cytoskeletal elements (112). Zona occludens (ZO) proteins represent a category of these scaffolding (adaptor) proteins that are known to interact with connexins and claudins at the junctions between epithelial cells (112). They belong to the membrane-associated guanylate kinase (MAGUK) family and include ZO-1 (TJP1), ZO2 (TJP2) and ZO3 (TJP3) (112). ZO proteins have three PDZ domains, one SH3 domain and one GUK domain that mediate their interaction with other proteins supporting the TJs. Interestingly, Tjp1 (ZO-1) interacts with Gja1 (Cx43) in 42GPA9 SC lines not only at the membranes but more closely intracytoplasmic after drug-

induced gap junction endocytosis, suggesting that it plays a role in the internalisation of the gap junctional plaque (122) possibly by serving as a linker molecule between Gja1 (Cx43) and actin (123). Similarly, TJP1 (ZO-1) promote the polymerisation of claudins for assembly of TJs (124). Deletion of ZO-1 and suppression of ZO2 expression together, but not either of them, in mouse epithelial cell lines disrupts the TJs, and the ectopic expression of either ZO-1 or ZO2 can rescue Cldn3 localisation to TJs and the barrier function (124). The rescue of TJs by ectopic ZO-1 is mediated by its PZD, SH3 and GUK domains, since claudins did not polymerise by ectopic expression of the N-terminal ZO-1 lacking these domains (124). These data suggest that ZO-1 plays an important role in regulation of connexins and claudins and that its disruption might lead to mislocalisation of both proteins. To investigate whether the disruption of GJA1 (CX43) and CLDN11 proteins is associated with disruption of TJP1 (ZO-1) expression, TJP1 (ZO-1) was immune detected in gonadal tissues from pubertal and young adult patients with CAIS. TJP1 (ZO-1) was weakly expressed in the seminiferous tubules in CAIS gonadal tissues and localised to the whole membranes of SCs (Figure 24C and D, Supplementary materials Figure 40C-F) compared to the testicular tissue from the normal pubertal control, where the protein shows stronger expression and basolateral localisation in adjacent SCs in seminiferous tubules, the site of BTB (Figure 24A and B, Supplementary materials Figure 40A and B). These observations suggest that the loss of GJA1 and CLDN11 in these gonadal tissues is not the result of disruption of TJP1 expression but still shows the of polarity in the seminiferous epithelium is missing.

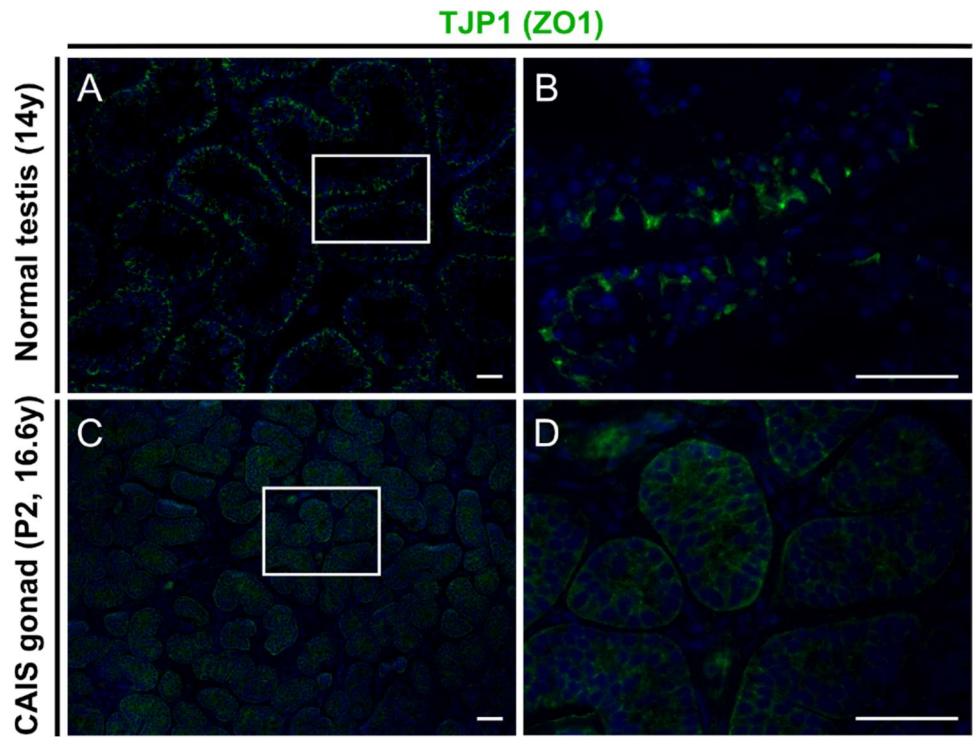

Figure 24. TJP1 (ZO-1) protein expression in gonadal tissue from a 16.6-year-old patient with CAIS (P2) compared to testicular tissue from a 31-year-old control. TJP1(ZO-1) protein localises to the basolateral surfaces of the adjacent Sertoli cells at the site of the blood-testis-barrier in the normal adult testicular tissue (A and B), but the whole membranes of Sertoli cells in young adult CAIS gonadal tissue (C and D). Scale bar, 50 µm.

3.11 Adult PTMCs protein markers ACTA2 and MYH11 are aberrantly expressed in CAIS gonadal tissues

To discriminate the interstitial and the tubular compartments in gonadal tissue from a pubertal patient with CAIS (P1) for spatial whole transcriptome analysis, several morphology/cell type markers were tested. Therefore, the tissue was stained with fluorescently labelled antibodies and scanned in the GeoMX DSP in a dry run without addition of the WTA probes to the hybridisation mixture. These marker proteins must be abundant, because the RNA probe hybridisation step requires a previous proteinase digestion that may fully degrade low abundant proteins. One of the tested markers was ACTA2 or α-smooth muscle actin which is expressed in normal adult testis in PTMCs surrounding the seminiferous tubules, separating them from the interstitial tissue. Unexpectedly, ACTA2 was found to be expressed only in the myoepithelial cells around blood vessels and not in PTMCs around the seminiferous tubules in gonadal tissue from P1, suggesting that PTMCs in gonadal tissues of patients with CAIS might not be fully differentiated. To investigate whether PTMCs in gonadal tissues of patients with CAIS are fully differentiated or not, gonadal tissues from P1-P3 were double immunostained with antibodies targeting two adult PTMCs protein markers ACTA2 and MYH11. Compared to the testicular tissue of the normal adult control, ACTA2 and MYH11 were not expressed around most of the seminiferous tubules in gonadal tissues from patients with CAIS (P1-P4) (Figure 25D and E, Supplementary materials Figure 41D-L). However, few seminiferous tubules from P1 and P3 were incompletely surrounded by cells expressing ACTA2 and MYH11 (Supplementary materials Figure 41D-L). The aberrant expression of adult PTMC markers ACTA2 and MYH11 suggests that PTMCs are not fully differentiated in gonadal tissues from pubertal and young adult patients with CAIS and that this differentiation defect might be attributed to defective androgen signalling in these patients.

3.12 Adult PTMCs protein markers ACTA2 and MYH11 are aberrantly expressed in *CYP17A1* gonadal tissues

To further investigate whether the defects in androgen synthesis would have a similar effect on the development of PTMCs, ACTA2 and MYH11 expression was investigated in the young adult *CYP17A1* deficiency gonadal tissue by immunofluorescence. As is the case in CAIS gonadal tissues, ACTA2 and MYH11 proteins were not expressed around most of the seminiferous tubules in the young adult *CYP17A1* deficiency gonadal tissue (Figure 26D-F) except for a single region with fibrous tissue, where MYH11 expression extends from the fibrosis to surround some of the seminiferous tubules (Figure 26G and I). The results corroborate the proposition that defective androgen signalling, either by lack of androgens or the resistance to their actions, affects the differentiation of PTMCs in pubertal and young adults with CAIS and *CYP17A1* deficiency and supports the proposed role of androgens in PTMCs development in human testis.

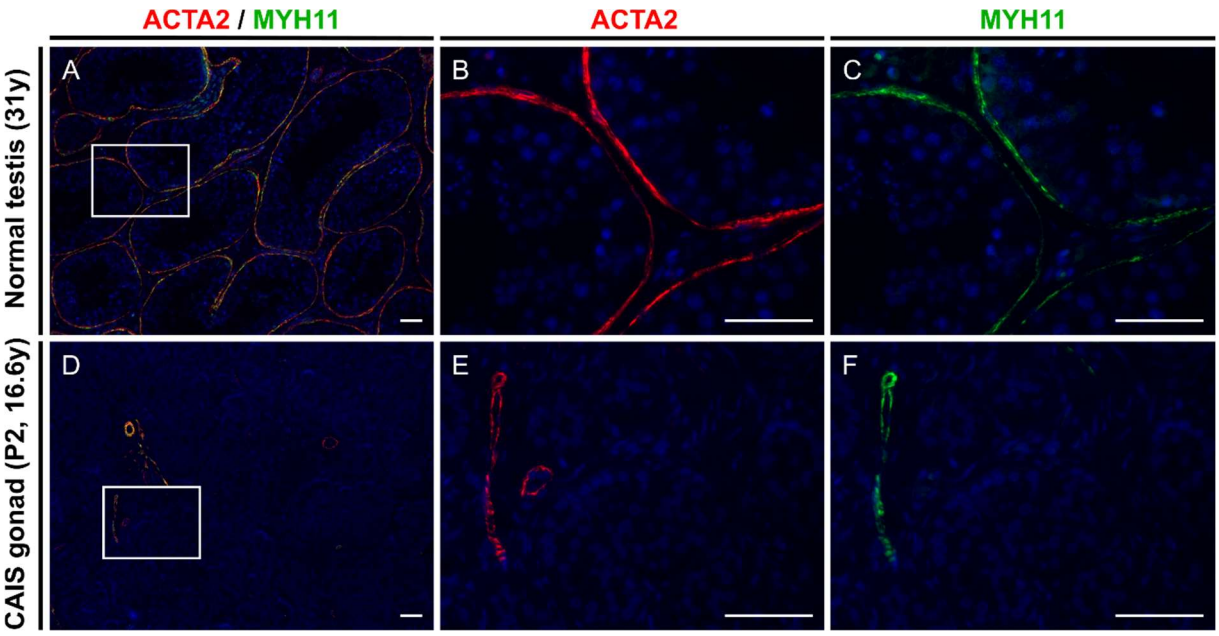

Figure 25. ACTA2 and MYH11 protein expression in gonadal tissue from a 16.6-year-old patient with CAIS (P2) compared to testicular tissue from a 31-year-old control. ACTA2 and MYH11 are expressed in PTMCs around the seminiferous tubules in the normal adult testicular tissue (A-C), but only in myoepithelial cells around blood vessels and not in PTMs around seminiferous tubules in the young adult CAIS gonadal tissue (D-E). Scale bar, 50 µm. Scale bar, 50 µm.

3.13 Adult PTMCs protein markers ACTA2 and MYH11 are normally expressed in young adult PAIS gonadal tissues

To further investigate whether PTMCs differentiation would be rescued in partial resistance to androgenic stimulation, ACTA2 and MYH11 expression was investigated in the young adult PAIS gonadal tissue by immunofluorescence. Compared to the pubertal control testicular tissue, ACTA2 and MYH11 were expressed in PTMCs around all the seminiferous tubules in the young adult PAIS gonadal tissue (Figure 27D-E), suggesting that the partial rescue of response to androgen stimulation in these patients was enough for proper differentiation of PTMCs in this young adult PAIS gonadal tissue.

3.14 Preliminary results of the GeoMx digital spatial whole transcriptome analysis of FFPE gonadal tissue of the 13.7-year-old CAIS individual

To further analyse LCs and SCs in conditions with congenital defects of androgen signalling, an uncontrolled spatial whole transcriptome analysis of a single FFPE gonadal tissue from the 13.7-year-old CAIS individual, being the most recent tissue acquired with higher probability of relatively more intact mRNAs. The spatial whole transcriptome analysis of this gonadal tissue was performed using the GeoMx DSP, which allows specific collection of photocleavable probes hybridised to the tissue sample guided by fluorescent-labelling of target cells. The inclusion of a control adult testicular tissue would not be informative for normal SCs, since they nurse relatively large number of GCs and it would be not possible to collect the hybridised probes form theses SCs with contamination form the GCs. However, it was possible in CAIS gonadal tissue since the seminiferous tubules feature GC loss. It was also possible to collect the hybridised probes from enough number of LCs, since the CAIS gonadal tissue show LC hyperplasia.

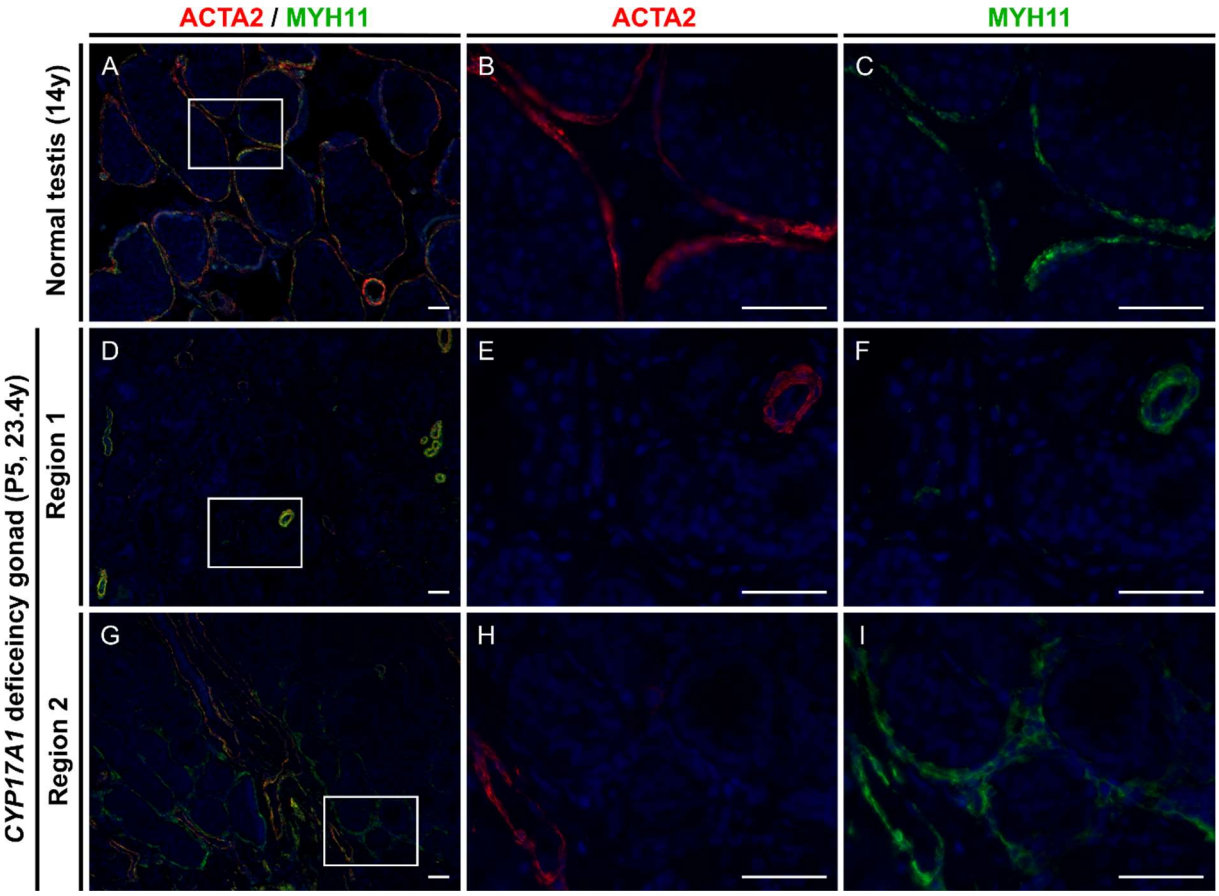

Figure 26. ACTA2 and MYH11 protein expression in gonadal tissue from a 23.4-year-old patient with CYP17A1 deficiency (P5) compared to testicular tissue from a 14-year-old control. ACTA2 and MYH11 are expressed in PTMCs and myoepithelial cells in pubertal control testicular tissue (A-C) but only in myoepithelial cells and not in PTMCs around most of the seminiferous tubules in gonadal tissue from the young adult with CYP17A1 deficiency (D-F). In one region, however, ACTA2 is expressed in fibrous tissue and myoepithelial cells (G and H), and MYH11 in myoepithelial cells and in PTMCs around some of the seminiferous tubules (G and I). Scale bar, 50 µm.

The whole transcriptome of 10 ROIs comprising SCs and 8 regions comprising LCs was first subjected to UMAP analyses using the umap package. ROIs with SCs clustered together and away from ROIs with LCs (Figure 28A), reflecting the differences in the transcriptomic signature of both cell types. Secondly, the transcriptomic data from the ROIs were subjected to differential gene expression using the LMM, retaining genes with more than one Log_2 fold change and adjusted *p*-value less than 0.05. More than 2000 genes were differentially expressed between ROIs comprising SCs and ROIs comprising LCs. Among the genes that are differentially expressed in ROIs comprising LCs are most of the genes involved in the steroidogenic pathway, including *STAR*, *FDX1*, *CYB5A*, *POR*, *CYP11A1* and *CYP17A1* (Figure 28B and C). The only exception was *HSD17B3* (Figure 28B and C) which showed higher expression in ROIs of (Log_2 fold change=1.98, adjusted *p*-value=2.5×10^{-9}) as shown in smFISH results (Figure 10). Other genes involved in steroid metabolism including *APOE*, *APOC1*, *SCARB1* and *MVD* as well as other LC-specific genes like *LHGCR* and *DLK1* were also enriched in these ROIs (Figure

28B and C). In contrast, ROIs comprising SCs were enriched in SC-specific genes including *AMH*, *INHBB*, *SOX9* and BEX1 among others (Figure 28B and C). Interestingly, *GJA1* and *CLDN11* were also among the genes enriched in ROIs with LCs and SCs, respectively. The full list of differentially expressed genes between ROIs with LCs and ROIs with SCs is provided in the supplementary materials (Table 21).

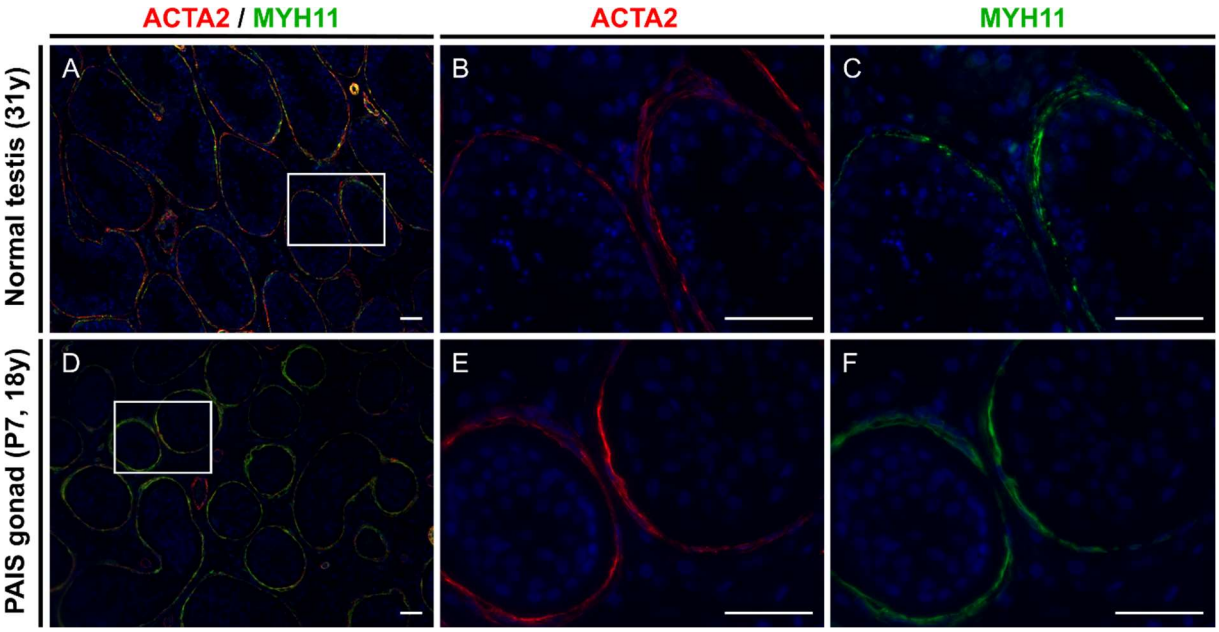

Figure 27. ACTA2 and MYH11 protein expression in gonadal tissue from an 18-year-old patient with PAIS (P7) compared to testicular tissue from a 31-year-old control. ACTA 2 and MYH11 are expressed in myoepithelial cells and in PTMCs around seminiferous tubules in the control adult testicular tissue (A-C) and the young adult PAIS gonadal tissue (D-F). Scale bar, 50 µm.

A

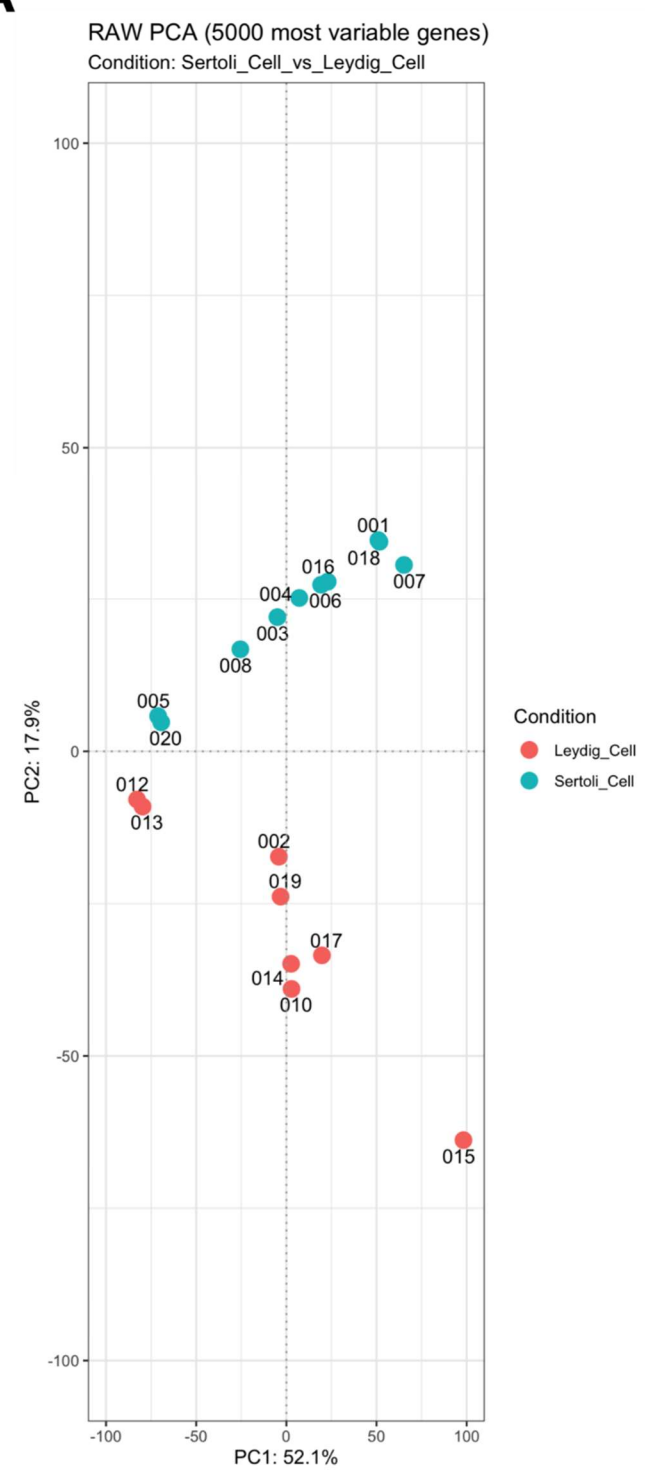
RAW PCA (5000 most variable genes)
Condition: Sertoli_Cell_vs_Leydig_Cell
PC2: 17.9%
PC1: 52.1%
100
50
0
-50
-100
-100
-50
0
50
100
001
018
007
016
004
006
003
008
005
020
012
013
002
019
017
014
010
015
Condition
Leydig_Cell
Sertoli_Cell

B

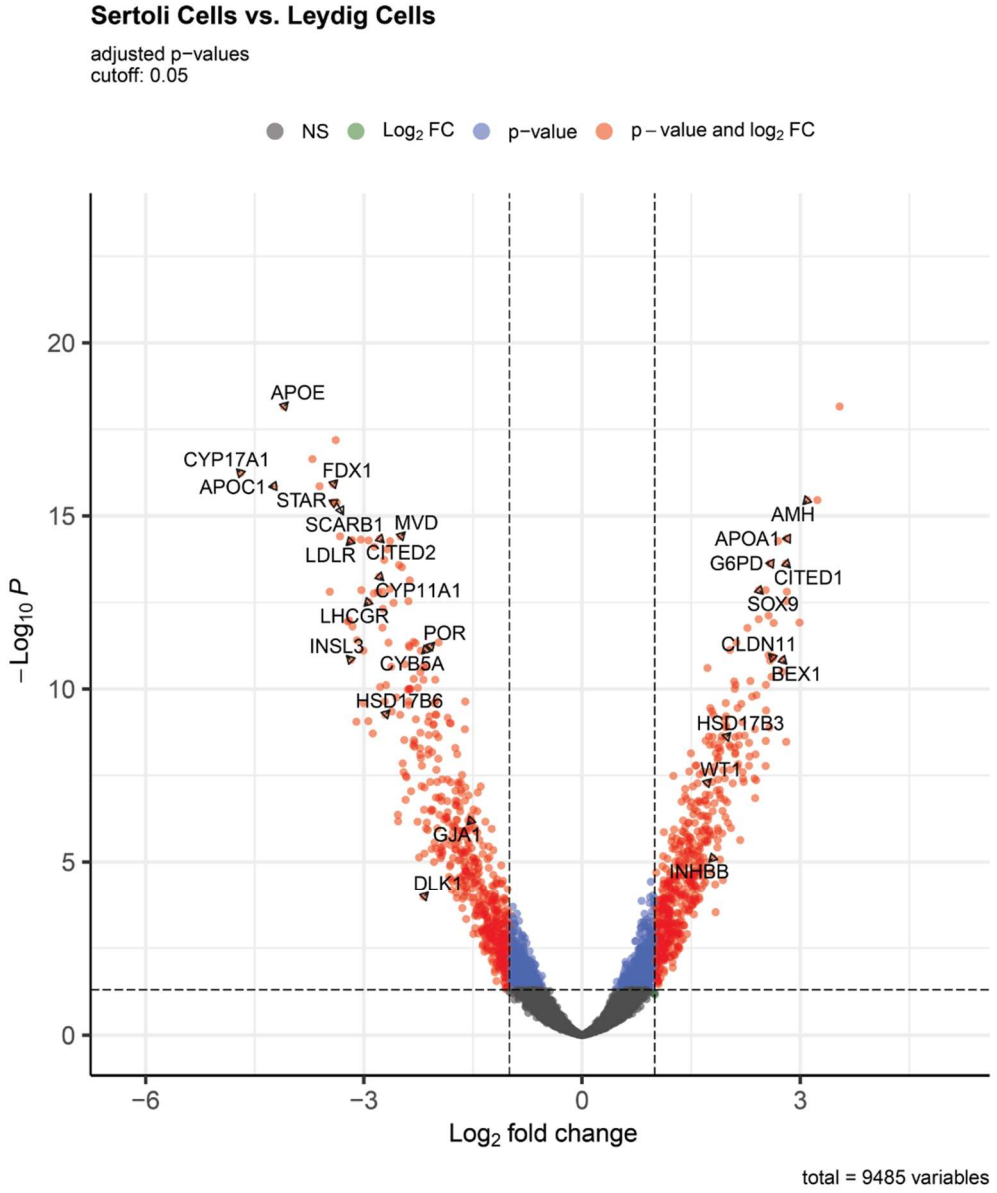
Sertoli Cells vs. Leydig Cells
adjusted p−values
cutoff: 0.05
NS
Log2 FC
p−value
p − value and log2 FC
−Log10 P
20
15
10
5
0
APOE
CYP17A1
FDX1
APOC1
STAR
SCARB1
MVD
LDLR
CITED2
CYP11A1
LHCGR
POR
INSL3
CYB5A
HSD17B6
GJA1
DLK1
AMH
APOA1
G6PD
CITED1
SOX9
CLDN11
BEX1
HSD17B3
WT1
INHBB
−6
−3
0
3
Log2 fold change
total = 9485 variables

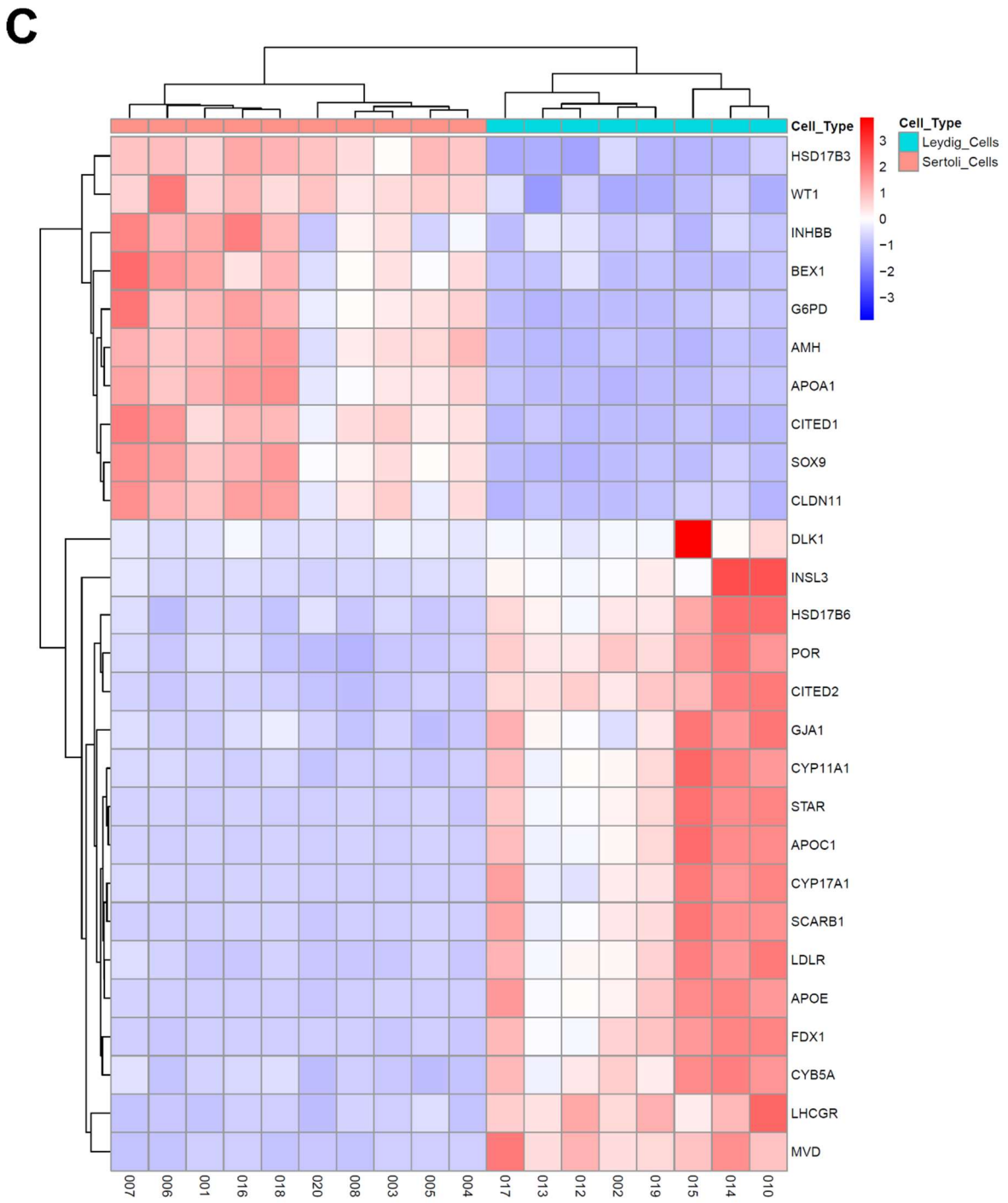

Figure 28. Preliminary analysis of spatial whole transcriptome data from 10 ROIs comprising Sertoli cells and 8 ROIs comprising LCs. (A) Dimension reduction representation of ROIs via UMAP. (B) Volcano plot representing the differentially expressed genes between ROIs with Sertoli cells and ROIs with Leydig cells. (C)Heat map of the top 30 differentially expressed genes ($P<0.05$, fold change>2.5) between regions comprising Leydig and regions comprising Sertoli cells in gonadal tissue from a 13.7-year-old CAIS patient. Blue colour depicts low expression and red high expression with white marking moderate levels of expression in between.

4 Discussion

This study shows that defective androgen signalling in adolescents and young adults with CAIS and *CYP17A1* deficiency is associated with defective differentiation and altered function of all somatic cell types in gonadal tissues. The data show that HSD17B3 is expressed in SCs and not in LCs in pubertal and adult gonadal tissues with congenital defects of androgen signalling, a pattern of expression that is known in foetal mouse (95, 96), and probably human (107, 170, 179) testis and suggests that androgen signalling is required for proper differentiation of LCs and SCs in adult human testis. Further characterisation of LC differentiation markers in these gonadal tissues identified two different populations of LCs: $DLK1^+$ foetal/immature and $INSL3^+$ adult/mature LCs, suggesting that defective androgen signalling in these tissues is associated with abnormal development of adult LCs or possible repopulation of foetal LCs (170). Reanalysis of scRNA-seq data from testicular tissue samples from the foetal to the adult stage (107, 153, 154, 180) shows a higher expression of *HSD17B3* mRNA in SCs than in LCs in foetal and neonatal samples, like in adult CAIS gonadal tissue, but also shows a decrease in the expression of *HSD17B3* afterwards and an increase in the expression of its isoenzyme *AKR1C3* (*HSD17B5*) beginning at puberty (Figure 15 and Supplementary materials Figures 36B and 37).

On the other hand, SCs in gonadal tissues of individuals with androgen signalling defects aberrantly express some of the proteins that contribute to the blood-testis barrier including GJA1 and CLDN11, which prevents an immune-privileged environment for spermatogenesis, and may contribute to germ cell loss observed in these patients. Although CLDN11 protein is lost in these gonadal tissues, *CLDN11* mRNA was still expressed in SCs, suggesting that androgen signalling regulates the expression of *CLDN11* at a post-transcriptional level. Furthermore, PTMCs aberrantly express adult markers ACTA2 and MYH11, suggesting that they are not fully differentiated. In addition, the study shows that partial gain of androgen signalling in individuals with PAIS is associated with switching of HSD17B3 expression from SCs in prepubertal to some LCs in pubertal gonadal tissues, suggesting a partially rescued LC differentiation in these PAIS gonadal tissues at puberty. CLDN11 protein accumulation is almost lost in SCs in pubertal PAIS gonadal tissues, suggesting that partial gain of androgen signalling did not rescue full differentiation of SCs in these gonadal tissues.

4.1 Differentiation of Leydig and Sertoli cells

Testosterone synthesis in foetal mouse testis is contributed by LCs and SCs (95, 96). Since foetal mouse LCs do not express *Hsd17b3*, they provide androgen precursors up to androstenedione, which is then reduced by *Hsd17b3* exclusively expressed in foetal mouse SCs. The exclusive expression of *Hsd17b3* in the tubular compartment of foetal and neonatal mouse testis was shown

in *in situ* hybridisation and northern blot assays (96). Moreover, when purified from foetal mouse testis, cultured in primary cell cultures and supplemented with androgen precursors, foetal LCs could only produce androgens up to androstenedione, whereas foetal SCs could reduce androstenedione to testosterone (95). The immunohistochemical characterisation of gonadal tissues form adolescents and young adults with CAIS and *CYP17A1* deficiency suggests that the foetal pattern of HSD17B3 expression observed in mice also exists in foetal humans and is corroborated by the reanalysis of scRNA-seq data (170). Similarly, adult *Cyp17a1* KO mice show the same expression pattern of *Hsd17b3* in the seminiferous tubules like foetal mouse testes, suggesting that the low testicular testosterone in these testicular tissues is also associated with LC and SC differentiation defects. Furthermore, immunohistochemical characterisation of PAIS gonadal tissues shows the switch of HSD17B3 expression form SCs in the prepubertal gonadal tissue to LCs in the pubertal gonadal tissue. These results suggest that defective androgen signalling in these gonadal tissues is associated and might be implicated in improper differentiation of both LCs and SCs.

The exclusive expression of HSD17B3 in SCs in CAIS gonadal tissues suggests that testicular reduction of androstenedione to testosterone is an exclusive function of SCs in these gonadal tissues; however, it was interesting to investigate whether LCs still contribute to testicular reduction of androstenedione to testosterone through the expression of AKR1C3 (HSD17B5), an isoenzyme of HSD17B3. The immunohistochemical staining shows the expression of AKR1C3 in LCs of pubertal and young adult CAIS gonadal tissues, suggesting that LCs might still contribute to testicular reduction of androstenedione to testosterone, although the extent of this contribution is still unknown. Although the observation might be irrelevant in functional terms, since androgen receptors are non-functional, it shows that LCs in these gonadal tissues could acquire some adult characteristics. The reanalysis scRNA-seq from testicular tissue from the foetal to adult stages in this study (Figure 15 and Supplementary materials Figures 36 and 37) showed an upregulation of *AKR1C3* and some downregulation of *HSD17B3* to lower level at puberty (170). A virilisation and increase of testosterone level in 46,XY individuals with *HSD17B3* deficiency at puberty together with an pubertal increase of AKR1C3 expression supports the role for AKR1C3 in testosterone biosynthesis (136).

The lack of HSD17B3 expression in LCs in CAIS and *CYP17A1* deficiency gonadal tissues could be interpreted in two different ways: Either LCs in these gonadal tissues represent a failure of maturation of adult LCs or a repopulation of foetal LCs (181). In line with the first proposition, scRNA-seq analysis of normal adult human testicular tissues shows that *HSD17B3* is expressed only in mature adult LCs but neither in progenitor nor in immature LCs. The role that androgens play in LC development in humans is not yet stablished but well studied in ArKO mouse model. LCs in adult ArKO mouse testes show reduced expression of *Hsd17b3* along with other adult LC-specific

transcripts, denoting that the lack of *Ar* expression in these cells leads to failure of adult LC maturation in adult mouse testes (102, 172, 182, 183). On the other hand, lineage tracing studies of foetal LCs show that they persist in testicular tissues from normal and ArKO mice while they still lack the *Hsd17b3* expression, suggesting they develop as androgen-independent LC population in mouse testis. In either case, the lack of HSD17B3 expression in LCs of CAIS and *CYP17A1* deficiency gonadal tissues shows that the development of LCs in both conditions is defective. To further characterise the development of LCs in these gonadal tissues, the expression of DLK1 and INSL3, two markers for foetal/immature LCs the adult/mature LCs, respectively. DLK1 is expressed in a large subset of the interstitial LCs in pubertal and young CAIS gonadal tissues, supporting the association of defective androgen signalling with defective LC differentiation in these gonadal tissues. DLK1 expression starts in human male and female gonads at week 7 post-conception and is maintained later on only in LCs in foetal testes and not in theca-like cells in foetal ovaries, suggesting that these *DLK1*+ cells might serve as progenitors for the steroidogenic cell lineage in human foetal testes (175). Similarly, the reanalysis of scRNA-seq shows that DLK1 is strongly expressed in LC clusters from embryonal and foetal samples (Supplementary material Figures 36C) (170).

INSL3 is expressed in subsets of LCs in gonadal tissues of all CAIS except for the oldest one, where the expression of INSL3 is completely lost. The lack of INSL3 expression in this gonadal tissue might be explained by the longer abdominal retention of gonads. The mutually exclusive expression of DLK1 and INSL3 was most evident in LC nodules that overexpress DLK1 but barely express INSL3 (Figures 16 and 17, and Supplementary materials Figure 34), suggesting that INSL3 expressing cells might represent adult LCs (170). The same pattern of DLK1 and INSL3 expression was reported in some adults with testicular pathologies in association with defective androgen signalling. In adults with subfertility and testicular germ cell tumours, DLK1 is expressed in subsets of hyperplastic LCs in the interstitial tissue and in LC nodules, with a positive correlation between the percentage of DLK1-expressing cells in the nodule and severity of the testicular dysfunction (173). Similarly, some large LC nodules in testicular tissues from adolescents and adults with Klinefelter syndrome exclusively express either DLK1 or INSL3 (173). However, DLK1 is also over expressed in TARTs, which also express other adrenal markers including CYP11B1, CYP21A2, MC2R (174) and HSD17B3 (184). Immunohistochemical characterisation of CAIS gonadal tissues shows lack of the expression of CYP21A2 and HSD17B3 in the LC nodules, excluding the possibility that they are TARTs (170).

It was interesting to investigate whether the switch of expression of *HSD17B3* from foetal SCs to adult LCs known in mouse testis takes place also in human testis. Reanalysis of scRNA-seq data from normal testicular tissues from foetal to adult stages shows higher expression of *HSD17B3* in SCs in foetal and neonatal testicular tissues as previously reported (107, 175), which recapitulates the

increase of *HSD17B3* expression represented from bulk RNA-seq data acquired from foetal testicular tissues (Supplementary materials Figure 37A). It was intriguing, however, that the reanalysis of scRNA-seq data did not reveal a significant switch in the expression of *HSD17B3* to LCs in pubertal and adult testicular tissues, instead it showed an increase of expression of its isoenzyme *AKR1C3* in LCs, challenging the convention of *HSD17B3* being the main steroidogenic enzyme involved in reduction of androstenedione to testosterone in puberty and adulthood in human. Therefore, it is speculated that the switch of testicular reduction of androstenedione to testosterone from SCs in foetal neonatal human testis to LCs in pubertal and adult human testis is not mediated by a simple switch of *HSD17B3* expression from the tubular to the interstitial compartments, but rather by downregulation of *HSD17B3* in the tubular compartment and upregulation of *AKR1C3* in the interstitial compartment (170). This might also explain the pubertal increase in testosterone production in 46,XY adolescents with *HSD17B3* deficiency, since these patients lack testosterone during the foetal stage and are often born with female appearing external genitalia but experience a surge of testosterone during puberty which leads to significant virilisation and in some cases changes in gender role (136). Nevertheless, the analysis of bulk RNA-seq from adult testicular tissues shows a higher expression of *HSD17B3* than *AKR1C3* (Supplementary materials Figure 37B), and immunohistochemical characterisation of HSD17B3 and AKR1C3 in the adult control testicular tissue shows the expression of both enzymes in LCs. The discrepancy between these results and the results of scRNA-seq reanalysis might be explained by differences between *HSD17B3* and *AKR1C3* in regards to the stability of their mRNAs during extraction, library preparation and transcriptomic analysis, or to discrepancies in post-transcriptional regulation as suggested in mouse (185), although this has not been shown in human, yet. Therefore, which of both enzymes is the main androstenedione-converting enzyme in adult human testis is still elusive (170).

4.2 Disruption of the blood-testis barrier

SCs orchestrate spermatogenesis not only by supporting foetal GCs specification and development, but also by maintaining spermatogonial stem cells (SSCs) and spermatogonia, supporting meiotic and post-meiotic GCs till the final release of sperms (186). For meiosis to proceed normally in the seminiferous epithelium at puberty, SCs modulate the microenvironment of meiotic and post-meiotic GCs by creating specialised junctions between the adjacent SCs that make up the BTB, sequestering the meiotic and post-meiotic GCs from blood and lymphatics systems, and hence creating an immune-privileged microenvironment for the completion of meiosis (187, 188). These junctions are formed at puberty and regulated by the action of FSH and testosterone on their corresponding receptors in SCs (189). The investigation of expression of different BTB proteins in this study has shown that GJA1 (CX43) and CLDN11 and TJP1 (ZO-1) are aberrantly expressed in gonadal

tissues from adolescents and young adults with CAIS, PAIS and *CYP17A1* deficiency, emphasising the role of androgens in regulating the BTB in human testis. In rat testis, Gja1 (Cx43) is expressed predominantly at the BTB and to a lesser extent near the apical ectoplasmic specialisations at SC-elongating spermatid interface, and its expression declines at both sites at late stage VIII onwards coinciding with restructuring of the BTB for the transit of preleptotene spermatocytes and disassembly of the apical ectoplasmic specialisations for spermiation (190). Its expression is lost by induction of GC loss in rat testis with adjudin treatment indicating that Gja1 (Cx43) contributes to adhesion junctions between GCs and the seminiferous epithelium (190). Although the knockdown of *Gja1* (*Cx43*) in SC primary cell culture neither affects the expression of integral membrane proteins or scaffold proteins of the BTB nor its permeability, the double knockout of *Gja1* (*Cx43*) and the desmosomal protein plakophilin 2 (*Pkp2*) significantly disrupts the expression and localisation of ZO-1 and occludin and affects the integrity of the BTB (190), indicating that Gja1 (Cx43) contributes to the integrity of the BTB by regulating the expression of other BTB structural proteins. In addition, disruption of TJ in SC primary cell culture by Ca^{2+} depletion or bisphenol A treatment was irreversible only with knock down of *Gja1* (*Cx43*), indicating its role in induction of reassembly of TJ proteins at the BTB (191). Interestingly, the SC-specific knockout of *Gja1* (*Cx43*) in mouse leads not only to arrest of spermatogenesis at the level of spermatogonia (192), but also to an increase in LC number with reduction of Gja1 (Cx43) expression in spite of apparently normal differentiation and steroidogenesis (193). Of note in this study is that *Hsd17b3* expression was investigated in whole testis homogenates, which does not identify whether *Hsd17b3* is expressed in LCs or SCs, and therefore the inference of normal LC development in SC-specific *Gja1* (*Cx43*) knockout testis is questionable and needs more investigation. In human testis, GJA1 (CX43) is expressed in the seminiferous epithelium, except at stages II and III coinciding with the transit of primary spermatocytes from the basal to the adluminal compartment and is lost in total GC loss in Sertoli-cell-only syndrome and seminiferous tubules with spermatogenic arrest at the level of spermatogonia (194). Similarly, GJA1 (CX43) expression is lost in seminiferous tubules infiltrated with carcinoma *in situ*, with re-expression of cytokeratin 18 (KRT18) in SCs denoting their dedifferentiation in the infiltrated tubules (195, 196). In Klinefelter syndrome, GJA1 (CX43) expression is reduced or completely lost in seminiferous tubules with a negative correlation between the severity of spermatogenic and GJA1 (CX43) expression (197). Intriguing, however, is that the expression of AR in Klinefelter testicular tissues is also reduced (198), suggesting that defective androgen signalling in Klinefelter syndrome might be involved in reduction of GJA1 (CX43) expression in these patients. In line with this proposition, immunofluorescent detection of GJA1 (CX43) in gonadal tissues from the adolescents and young adults with CAIS has shown the loss of its expression in seminiferous tubules but maintenance of its expression in LCs (Figure 20 and Supplementary materials Figure 38), confirming another observation that has been previously

reported in one adolescent with CAIS (176). The loss of GJA1 (CX43) is also seen in gonadal tissue of the young adult with *CYP17A1* deficiency where defective androgen signalling is caused rather by disrupted steroidogenesis (Figure 20). Taken together, these observations emphasise the role of androgens in regulating GJA1 (CX43) in SCs in pubertal and adult human testis; the mechanism is yet to be elucidated.

Further characterisation of the BTB in adolescents and young adults with CAIS, PAIS and *CYP17A1* deficiency has revealed the loss of expression of CLDN11 protein, another integral membrane protein that contributes to TJs at the BTB. In mouse testes, Cldn11 localises to the basal and the adluminal surfaces of preleptotene spermatocytes during migration (199). *Cldn11* knockout in mouse testes is associated with loss of polarity, sloughing and elimination of SCs through the lumina of the seminiferous tubules and failure of progression of spermatogenesis beyond meiosis (120), indicating the role of Cldn11 in TJ formation and spermatogenesis by sequestration of meiotic GCs from the immune system. The protein expression is not regulated by androgens in mouse testes (128). In rat testis, however, gonadotropin suppression leads to reduction of Cldn11 protein expression to levels undetectable in western blots, and the short-term hCG treatment (7 days) was not enough to recover the protein expression (with and without FSH) (200), suggesting androgenic regulation of Cldn11 protein expression in rat testis. Gonadotropin suppression in men disrupts the localization of CLDN11 (177). The same changes, however, have been also reported in patients with primary seminiferous tubule failure with meiotic arrest or Sertoli-cell-only syndrome, although the serum concentration of LH, and testosterone are comparable to the normal controls (178), suggesting that the changes in CLDN11 expression in these patients are a manifestation of altered differentiation state of SCs rather than a direct misregulation of protein expression in response to a pathogenic agent. In contrast, CLDN11 protein is not mislocalised but rather totally undetectable in gonadal tissues of adolescents and young adults with CAIS and *CYP17A1* deficiency, a more profound effect that might be explained by the total loss of androgen signalling in these gonadal tissues either due to complete androgen resistance or defective androgen synthesis. The loss of CLDN11 protein expression in the young adult PAIS gonadal tissue might be also explained by the possibility that androgen signalling in this tissue did not reach the threshold sufficient do drive the full differentiation of SCs, despite the partial rescue of AR transactivation function.

Intriguingly, the *in situ* hybridisation assays have shown the maintenance of *CLDN11* mRNA in SCs in adolescents and young adults with CAIS and PAIS to levels comparable to the adult control, in spite of loss of CLDN11 protein expression (Figures 21 and 23), suggesting that androgen signalling regulates *CLDN11* expression rather at a translational/posttranslational level. The discrepancy between mRNA and protein expression has been previously shown in mouse and rat testes. In

normal mouse testis, the expression of *Cldn11* mRNA lagged behind the protein (199). Since the proteins of the BTB are known to undergo endocytic internalisation and recycling, it was hypothesised that the protein expression lags due to posttranslational modulations. In rat testis, the gonadotropin suppression significantly reduces Cldn11 protein expression to undetectable levels in western blots, while the *Cldn11* mRNA expression was higher compared to the normal controls, and with the short-term treatment with hCG, the levels *Cldn11* mRNA decreased to levels still slightly higher than the normal control, but the protein was still not detectable (200). In human testis, gonadotropin suppression is associated with abnormal localisation of CLDN11 protein with no effect on mRNA expression (177). All these observations suggest that the transcription and translation of *CLDN11* gene are regulated and coordinated by different factors, and that androgens might regulate the translation/accumulation rather than the transcription of the *CLDN11* gene in human testes. Unexpectedly, the *in situ* hybridisation assays have shown the accumulation of *CLDN11* mRNA in SCs of the prepubertal PAIS gonadal tissue, at a developmental stage before active spermatogenesis or steroidogenesis, although the immunohistochemical assays show that CLDN11 protein was not expressed (Figure 23). The lack of active steroidogenesis in this gonadal tissue has been shown by CYP17A1 immunostaining, revealing the involution of LCs (Figure 12E). Although this observation supports the role that androgens play in regulation of CLDN11 protein accumulation rather than transcription, it poses other questions about how *CLDN11* is still transcribed and the role it plays in this pubertal gonadal tissue. The *in situ* hybridisation assays have also shown downregulation of *CLDN11* mRNA expression in the young adult *CYP17A1* deficiency gonadal tissue (Figure 22), suggesting that factors other than defective androgen signalling might contribute to loss of *CLDN11* gene expression acting at the transcriptional level.

Polymerisation of connexins and claudins is facilitated by zona occludens proteins that act as adaptors linking them to the cytoskeleton (122, 124). Immunofluorescent staining of TJP1 (ZO-1) in pubertal and young adult CAIS gonadal tissues has shown that the protein is still expressed and partially localises to the membranes of SCs, suggesting not only that the regulation of TJP1 (ZO-1) is different from GJA1 and CLDN11 but also that the loss of GJA1 and CLDN11 expression and localisation to SC membranes cannot be attributed solely to TJP1 (ZO-1). However, the TJP1 (ZO-1) did not localise to the basal surfaces of the adjacent SCs as in normal adult controls, but was distributed along the whole membranes indicating the loss of SC polarity in these gonadal tissues, which is another sign of differentiation defect of SCs in these individuals.

The connection of BTB disruption in gonadal tissues with congenital defects in androgen signalling to GC loss is still questionable. Although the disruption of BTB might give a reasonable explanation to the GC loss in these gonadal tissues at puberty and adulthood by making them accessible to the

immune system, it does not explain the early GC loss observed in CAIS gonadal tissues after the first year of life (147). At this age the BTB is not yet formed and the GCs are not sequestered from the immune system but meiosis is actively suppressed, possibly through mechanism including retinoic acid as well as by other molecules (201). However, residual GCs observed in gonadal tissues in this study, as well as others (147), fail to initiate spermatogenesis, suggesting that the disruption of BTB in these gonadal tissues still contributes to further loss of GCs at puberty and adulthood. This might also have implications on malignant transformation of GCs in these gonadal tissues. For instance, the seminiferous tubules infiltrated with carcinoma *in situ* or its invasive form seminoma, show reduction to complete loss of *GJA1* (*CX43*) transcription (195, 202), decreased expression and mislocalisation of TJP1 (ZO-1) and TJP1 (ZO-2) proteins (203), and mislocalisation of CLDN11 protein (204). Although the actual mechanism of malignant transformation is not completely resolved, it might be attributed to loss of inhibition of proliferation mediated by cell-cell contact as well as intercellular communication.

4.3 Defects in peritubular myoid cell development

The study of PTMC development has been always hampered by the lack of knowledge of specific PTMC markers. The immunofluorescence investigation of ACTA2 and MYH11 expression as markers of adult PTMC development has shown their aberrant expression with defective androgen signalling in gonadal tissues from adolescents and young adults with CAIS and *CYP17A1* deficiency but normal expression in gonadal tissue from the young adult with PAIS. The observation suggests that androgen signalling might be essential for PTMC development, differentiation and survival in human testicular tissues. ACTA2 expression has been reported in foetal human testis as early as 12 wpc and is maintained till the 20 wpc (69, 71, 72). In postnatal human testis, ACTA2 is no more detectable until before puberty (71) and is upregulated again throughout puberty and adulthood (153, 180). Intriguingly, the downregulation of ACTA2 in neonatal and prepubertal human testis coincides with downregulation of AR in PTMCs (71), and the gain of its expression in puberal testis is associated with initiation of steroidogenesis (153). The aberrant expression of ACTA2 in case of complete resistance to androgen action in CAIS and defective androgen production in *CYP17A1* deficiency, and the gain of its expression with partial rescue of AR function in PAIS, corroborate the previous observations and supports the proposition that androgens play an important role in PTMC differentiation and survival. It is unclear though; how defective androgen signalling contributes to PTMCs alterations in CAIS and *CYP17A1* deficiency patients. For instance, scRNA-seq analysis of testicular tissues from two adult transfemales shows indeed alteration of the transcriptomic signature of PTMCs in association with long term suppression of testosterone production, but with no clear indications of PTMC developmental regression (153). Partial loss of ACTA2 or MYH11 expression has been reported in

other disease models, including infertility, Klinefelter syndrome and testicular germ cell tumours. In human male infertility, impaired spermatogenesis is commonly associated with fibrotic remodelling of lamina propria formed by PTMCs, evidenced by MYH11 expression, which is maintained in seminiferous tubules with normal spermatogenesis, but restricted or absent in tubules with defective spermatogenesis or GC loss (205). This aberrant expression of MYH11 is associated with immune cell infiltration of the tubular walls, which is believed to modulate the microenvironment through prostaglandin signalling (205). Loss of ACTA2 expression is also reported in atrophic seminiferous tubules and tubules with total loss of GCs in Klinefelter syndrome and carcinoma in situ (173), suggesting that SC signalling plays additional role in differentiation and survival of PTMCs in adult human testes as previously shown in mouse testes (206). Therefore, androgen signalling might play a role not only directly on PTMCs, but also indirectly by affecting the different cell types in testes, modulating the microenvironment around PTMCs for proper development and survival.

Defective PTMC differentiation in human gonadal tissues with congenital defective androgen signalling might contribute to GC loss in these conditions. Compared to wild-type, mice with PTMC-specific ArKO show GC reduction, azoospermia and infertility in adulthood (207). One proposed mechanism is that PTMCs maintain GCs in the adult testes by release of trophic factors in an androgen dependent manner. The glial cell line-derived neurotrophic factor (Gdnf), a known paracrine factor required for self-renewal of spermatogonial stem cells (SSCs) both *in vivo* and *in vitro*, was shown to be induced in adult mouse PTMCs in primary cell culture in response to testosterone stimulation, maintaining co-cultured SSC population and enhancing its proliferation (208). Moreover, when Thy1-positive spermatogonia are cocultured with testosterone-treated PTMCs and then transplanted into germ-cell-depleted mouse testis, more SSCs could colonise the recipient testis (208). Furthermore, PTMC-specific knockout of *Gdnf* is associated with loss of spermatogonia and disruption of spermatogenesis (209). However, the ArKO in PTMC is associated with defective SC function evidenced by reduction of seminal fluid production and downregulation of some SC-specific androgen-dependent genes (207), and is also associated with defective adult LC differentiation and function evidenced by downregulation of steroidogenic enzymes and developmental markers (210), suggesting that ArKO in PTMCs might induce GC loss indirectly by affecting SCs and LCs development. Taken together, androgen signalling in PTMCs is proposed to serve the development of GCs directly by PTMCs-GC signalling as well as indirectly through PTMC-SC and PTMC-LCs signalling.

4.4 Spatial transcriptomic profiling

The preliminary data from GeoMx digital spatial profiling of FFPE gonadal tissue of the 13.7-year-old CAIS patient, archived for more than three years, show the potential that spatial transcriptomics offer

in the investigation of such conditions. First, the analysis of 8 ROIs with LCs and 10 ROIs with SCs could identify the specific gene markers of each cell type. ROIs with LCs show higher expression of steroidogenic markers and *LHCGR*, which are known LC markers. On the other hand, ROIs with SCs show higher expression of *SOX9*, *WT1* and *INHBB*, which are specific SC markers. Interestingly, AMH was among the highly enriched genes expressed in SCs, which is known to be upregulated in CAIS gonadal tissues (176, 211), that might be mediated by estrogens (212) and resistance to androgen actions (213). The analysis could recapitulate many of the results acquired by IHC, IF and smFISH. For instance, *HSD17B3* expression was higher in ROIs with SCs than in ROIs with LCs (Figure 28) as shown with IHC (Figures 8 and 9 and Supplementary materials Figures 29 and 30) and smFISH (Figure 10). *GJA1* expression was higher in ROIs with LCs than ROIs with SCs which matches the protein expression shown in IF (Figure 20 and Supplementary materials Figure 38). In addition, *CLDN11* was also enriched in ROIs with SCs which matches the mRNA expression shown in smFISH (Figure 21 and Supplementary materials Figure 39). In the spatial transcriptomic analysis, SCs were shown to express some genes related to lipid and cholesterol metabolism including *MVD*. The enzyme was shown to be downregulated among other genes related to lipid metabolism in mouse XX *Sry* SCs compared to XY SCs (214). Given that that XX Sry SCs are incapable of supporting GCs, it might be interesting to compare the expression of this enzyme as well as other genes of lipid metabolism between SCs in CAIS gonadal tissues and normal testicular tissues.

In conclusion, the current study shows the influence of congenital defective androgen signalling on the development of LCs, SCs and PTMCs in gonadal tissues of children, adolescents and young adults with CAIS, PAIS and *CYP17A1* deficiency. How these changes would be involved in germ cell loss and cancer development is yet to be investigated.

5 Conclusion and Outlook

This study shows for the first time the influence of congenital defects of androgen signalling on the differentiation of the different somatic cell types in testicular tissues of patients with complete and partial AIS as well as patients with *CYP17A1* deficiency and emphasises the role of androgens in normal testicular development in human. However, more investigation is needed to understand the underlying pathology of GC loss and cancer development. The lack of biological materials from such rare conditions, as in other DSDs, and the lack of the appropriate methodology has always limited the biological information that could be extracted from such materials to better understand the underlying pathology in such conditions. As shown in this study, the recent advancements in spatial transcriptomic analysis techniques have the potential to reveal more information about such pathological conditions from FFPE gonadal tissues, archived for long periods that might extend to years. The first expression profiles of ROIs with SCs or LCs generated by GeoMx digital spatial profiling of one archived CAIS gonadal tissue has recapitulated many of the observations acquired by IHC, IF and smFISH in the cohort of individuals with this condition. However, the technique has its limitations. As the collection of the whole transcriptome from the different ROIs is guided by fluorescent labelling of cells in these ROIs for a single protein or RNA marker, it does not consider the heterogeneity among the cells in the single ROI, even if they are of the same type. Therefore, the resulting transcriptomic data represent rather a pseudobulk RNA data of ROIs enriched in certain cell type, although encompassing different subclasses or differentiation states of the same cell type. Secondly, the structural and cellular complexity of tissues might make the collection transcriptome of a single, fluorescently-labelled cell type impossible without contamination from the adjacent non-labelled cells, as is the case of normal seminiferous tubules in which a large number of different GC types intercalate between the adjacent SCs. Therefore, profiling the whole transcriptome of such archived FFPE tissues at near single-cell or single-cell needs more advanced techniques. One possibility is a more recent spatial whole transcriptomic analysis available from 10× Genomics under the name Visium HD, in which the whole transcriptome probes hybridised to the FFPE section is captured on a capture area with continuous lawn of capture oligos, barcoded to identify the coordinates of the captured transcripts to assign it back to its location in the FFPE section (215). This method of collection the probes allow for a near single-cell resolution transcriptomic analysis of the FFPE tissues. Another method is the based on the isolation of single nuclei from FFPE tissues with subsequent single-nuclei capture in microfluidic droplets for barcoding and reverse transcription of RNAs and amplification followed sequencing (216), which also allows the whole transcriptomic analysis at single-cell resolution, although with a smaller number of captured transcripts. Such advancements would make possible the transcriptomic profiling of single cells, even the rare ones,

allow for inferring the developmental relationships between the different cells, and in the case of the spatial transcriptomics characterise the microenvironment of different cells which would ultimately give more information about pathological conditions like GC loss and cancer development in DSDs.

6 References

1. Svingen T, Koopman P. Building the mammalian testis: origins, differentiation, and assembly of the component cell populations. Genes Dev. 2013;27(22):2409-26.
2. Hiort O, Werner R. Sex Determination and Differentiation: Physiology Leading to Male and Female Development. In: Wass JAH, Arlt W, Semple RK, Wass J, Arlt W, Semple R, editors. Oxford Textbook of Endocrinology and Diabetes 3e: Oxford University Press; 2022. p. 0.
3. Achermann JC, Hughes IA. Pediatric disorders of sex development. Williams Textbook of Endocrinology2016. p. 893-963.
4. Kreidberg JA, Sariola H, Loring JM, Maeda M, Pelletier J, Housman D, et al. WT-1 is required for early kidney development. Cell. 1993;74(4):679-91.
5. Luo X, Ikeda Y, Parker KL. A cell-specific nuclear receptor is essential for adrenal and gonadal development and sexual differentiation. Cell. 1994;77(4):481-90.
6. Birk OS, Casiano DE, Wassif CA, Cogliati T, Zhao L, Zhao Y, et al. The LIM homeobox gene Lhx9 is essential for mouse gonad formation. Nature. 2000;403(6772):909-13.
7. Katoh-Fukui Y, Tsuchiya R, Shiroishi T, Nakahara Y, Hashimoto N, Noguchi K, et al. Male-to-female sex reversal in M33 mutant mice. Nature. 1998;393(6686):688-92.
8. Miyamoto N, Yoshida M, Kuratani S, Matsuo I, Aizawa S. Defects of urogenital development in mice lacking Emx2. Development. 1997;124(9):1653-64.
9. Koopman P, Gubbay J, Vivian N, Goodfellow P, Lovell-Badge R. Male development of chromosomally female mice transgenic for Sry. Nature. 1991;351(6322):117-21.
10. Foster JW, Dominguez-Steglich MA, Guioli S, Kwok C, Weller PA, Stevanović M, et al. Campomelic dysplasia and autosomal sex reversal caused by mutations in an SRY-related gene. Nature. 1994;372(6506):525-30.
11. Wagner T, Wirth J, Meyer J, Zabel B, Held M, Zimmer J, et al. Autosomal sex reversal and campomelic dysplasia are caused by mutations in and around the SRY-related gene SOX9. Cell. 1994;79(6):1111-20.
12. Huang B, Wang S, Ning Y, Lamb AN, Bartley J. Autosomal XX sex reversal caused by duplication of SOX9. Am J Med Genet. 1999;87(4):349-53.
13. Vidal VPI, Chaboissier M-C, de Rooij DG, Schedl A. Sox9 induces testis development in XX transgenic mice. Nat Genet. 2001;28(3):216-7.
14. Chaboissier MC, Kobayashi A, Vidal VI, Lutzkendorf S, van de Kant HJ, Wegner M, et al. Functional analysis of Sox8 and Sox9 during sex determination in the mouse. Development. 2004;131(9):1891-901.
15. Barrionuevo F, Bagheri-Fam S, Klattig J, Kist R, Taketo MM, Englert C, et al. Homozygous inactivation of Sox9 causes complete XY sex reversal in mice. Biol Reprod. 2006;74(1):195-201.
16. Nef S, Schaad O, Stallings NR, Cederroth CR, Pitetti JL, Schaer G, et al. Gene expression during sex determination reveals a robust female genetic program at the onset of ovarian development. Dev Biol. 2005;287(2):361-77.
17. Kim Y, Kobayashi A, Sekido R, DiNapoli L, Brennan J, Chaboissier MC, et al. Fgf9 and Wnt4 act as antagonistic signals to regulate mammalian sex determination. PLoS Biol. 2006;4(6):e187.
18. Ottolenghi C, Pelosi E, Tran J, Colombino M, Douglass E, Nedorezov T, et al. Loss of Wnt4 and Foxl2 leads to female-to-male sex reversal extending to germ cells. Hum Mol Genet. 2007;16(23):2795-804.
19. Jameson SA, Natarajan A, Cool J, DeFalco T, Maatouk DM, Mork L, et al. Temporal transcriptional profiling of somatic and germ cells reveals biased lineage priming of sexual fate in the fetal mouse gonad. PLoS Genet. 2012;8(3):e1002575.
20. Ying Y, Zhao GQ. Cooperation of endoderm-derived BMP2 and extraembryonic ectoderm-derived BMP4 in primordial germ cell generation in the mouse. Dev Biol. 2001;232(2):484-92.

21. Ying Y, Liu X-M, Marble A, Lawson KA, Zhao G-Q. Requirement of Bmp8b for the generation of primordial germ cells in the mouse. Mol Endocrinol. 2000;14(7):1053-63.

22. Lawson KA, Dunn NR, Roelen BA, Zeinstra LM, Davis AM, Wright CV, et al. Bmp4 is required for the generation of primordial germ cells in the mouse embryo. Genes Dev. 1999;13(4):424-36.

23. Makela JA, Koskenniemi JJ, Virtanen HE, Toppari J. Testis Development. Endocr Rev. 2019;40(4):857-905.

24. Arnold SJ, Maretto S, Islam A, Bikoff EK, Robertson EJ. Dose-dependent Smad1, Smad5 and Smad8 signaling in the early mouse embryo. Dev Biol. 2006;296(1):104-18.

25. Chu GC, Dunn NR, Anderson DC, Oxburgh L, Robertson EJ. Differential requirements for Smad4 in TGFbeta-dependent patterning of the early mouse embryo. Development. 2004;131(15):3501-12.

26. Hayashi K, Kobayashi T, Umino T, Goitsuka R, Matsui Y, Kitamura D. SMAD1 signaling is critical for initial commitment of germ cell lineage from mouse epiblast. Mech Dev. 2002;118(1-2):99-109.

27. Chang H, Matzuk MM. Smad5 is required for mouse primordial germ cell development. Mech Dev. 2001;104(1-2):61-7.

28. Aramaki S, Hayashi K, Kurimoto K, Ohta H, Yabuta Y, Iwanari H, et al. A mesodermal factor, T, specifies mouse germ cell fate by directly activating germline determinants. Dev Cell. 2013;27(5):516-29.

29. Magnusdottir E, Dietmann S, Murakami K, Gunesdogan U, Tang F, Bao S, et al. A tripartite transcription factor network regulates primordial germ cell specification in mice. Nat Cell Biol. 2013;15(8):905-15.

30. Yamaji M, Seki Y, Kurimoto K, Yabuta Y, Yuasa M, Shigeta M, et al. Critical function of Prdm14 for the establishment of the germ cell lineage in mice. Nat Genet. 2008;40(8):1016-22.

31. Weber S, Eckert D, Nettersheim D, Gillis AJ, Schafer S, Kuckenberg P, et al. Critical function of AP-2 gamma/TCFAP2C in mouse embryonic germ cell maintenance. Biol Reprod. 2010;82(1):214-23.

32. Kurimoto K, Yabuta Y, Ohinata Y, Shigeta M, Yamanaka K, Saitou M. Complex genome-wide transcription dynamics orchestrated by Blimp1 for the specification of the germ cell lineage in mice. Genes Dev. 2008;22(12):1617-35.

33. Cochard LR. Netter's atlas of human embryology: updated edition: Elsevier Health Sciences; 2012.

34. Mamsen LS, Brochner CB, Byskov AG, Mollgard K. The migration and loss of human primordial germ stem cells from the hind gut epithelium towards the gonadal ridge. Int J Dev Biol. 2012;56(10-12):771-8.

35. Kerr CL, Hill CM, Blumenthal PD, Gearhart JD. Expression of pluripotent stem cell markers in the human fetal ovary. Hum Reprod. 2008;23(3):589-99.

36. Hoyer PE, Byskov AG, Mollgard K. Stem cell factor and c-Kit in human primordial germ cells and fetal ovaries. Mol Cell Endocrinol. 2005;234(1-2):1-10.

37. Molyneaux KA, Zinszner H, Kunwar PS, Schaible K, Stebler J, Sunshine MJ, et al. The chemokine SDF1/CXCL12 and its receptor CXCR4 regulate mouse germ cell migration and survival. Development. 2003;130(18):4279-86.

38. Ara T, Nakamura Y, Egawa T, Sugiyama T, Abe K, Kishimoto T, et al. Impaired colonization of the gonads by primordial germ cells in mice lacking a chemokine, stromal cell-derived factor-1 (SDF-1). Proceedings of the National Academy of Sciences. 2003;100(9):5319-23.

39. Gu Y, Runyan C, Shoemaker A, Surani MA, Wylie C. Membrane-bound steel factor maintains a high local concentration for mouse primordial germ cell motility, and defines the region of their migration. PLoS One. 2011;6(10):e25984.

40. Laird DJ, Altshuler-Keylin S, Kissner MD, Zhou X, Anderson KV. Ror2 enhances polarity and directional migration of primordial germ cells. PLoS Genet. 2011;7(12):e1002428.

41. Di Carlo A, De Felici M. A role for E-cadherin in mouse primordial germ cell development. Dev Biol. 2000;226(2):209-19.

42. Bendel-Stenzel MR, Gomperts M, Anderson R, Heasman J, Wylie C. The role of cadherins during primordial germ cell migration and early gonad formation in the mouse. Mech Dev. 2000;91(1-2):143-52.

43. Anderson R, Fassler R, Georges-Labouesse E, Hynes RO, Bader BL, Kreidberg JA, et al. Mouse primordial germ cells lacking beta1 integrins enter the germline but fail to migrate normally to the gonads. Development. 1999;126(8):1655-64.

44. Karl J, Capel B. Sertoli cells of the mouse testis originate from the coelomic epithelium. Dev Biol. 1998;203(2):323-33.

45. Albrecht KH, Eicher EM. Evidence that Sry is expressed in pre-Sertoli cells and Sertoli and granulosa cells have a common precursor. Dev Biol. 2001;240(1):92-107.

46. Bullejos M, Koopman P. Spatially dynamic expression of Sry in mouse genital ridges. Dev Dyn. 2001;221(2):201-5.

47. Lardenois A, Suglia A, Moore C, Evrard B, Noël L, Rivaud P, et al. Single-cell transcriptome landscape of developing fetal gonads defines somatic cell lineage specification in humans. bioRxiv. 2023:2023.08.07.552336.

48. Bullejos M, Koopman P. Delayed Sry and Sox9 expression in developing mouse gonads underlies B6-Y(DOM) sex reversal. Dev Biol. 2005;278(2):473-81.

49. Wilhelm D, Washburn LL, Truong V, Fellous M, Eicher EM, Koopman P. Antagonism of the testis- and ovary-determining pathways during ovotestis development in mice. Mech Dev. 2009;126(5-6):324-36.

50. Palmer SJ, Burgoyne PS. In situ analysis of fetal, prepuberal and adult XX----XY chimaeric mouse testes: Sertoli cells are predominantly, but not exclusively, XY. Development. 1991;112(1):265-8.

51. Wilhelm D, Martinson F, Bradford S, Wilson MJ, Combes AN, Beverdam A, et al. Sertoli cell differentiation is induced both cell-autonomously and through prostaglandin signaling during mammalian sex determination. Dev Biol. 2005;287(1):111-24.

52. Hadley MA, Byers SW, Suarez-Quian CA, Kleinman HK, Dym M. Extracellular matrix regulates Sertoli cell differentiation, testicular cord formation, and germ cell development in vitro. J Cell Biol. 1985;101(4):1511-22.

53. Cupp AS, Tessarollo L, Skinner MK. Testis developmental phenotypes in neurotropin receptor trkA and trkC null mutations: role in formation of seminiferous cords and germ cell survival. Biol Reprod. 2002;66(6):1838-45.

54. Hiramatsu R, Harikae K, Tsunekawa N, Kurohmaru M, Matsuo I, Kanai Y. FGF signaling directs a center-to-pole expansion of tubulogenesis in mouse testis differentiation. Development. 2010;137(2):303-12.

55. Jameson SA, Lin YT, Capel B. Testis development requires the repression of Wnt4 by Fgf signaling. Dev Biol. 2012;370(1):24-32.

56. Matson CK, Murphy MW, Sarver AL, Griswold MD, Bardwell VJ, Zarkower D. DMRT1 prevents female reprogramming in the postnatal mammalian testis. Nature. 2011;476(7358):101-4.

57. Uhlenhaut NH, Jakob S, Anlag K, Eisenberger T, Sekido R, Kress J, et al. Somatic sex reprogramming of adult ovaries to testes by FOXL2 ablation. Cell. 2009;139(6):1130-42.

58. Combes AN, Wilhelm D, Davidson T, Dejana E, Harley V, Sinclair A, et al. Endothelial cell migration directs testis cord formation. Dev Biol. 2009;326(1):112-20.

59. Escalante-Alcalde D, Merchant-Larios H. Somatic and germ cell interactions during histogenetic aggregation of mouse fetal testes. Exp Cell Res. 1992;198(1):150-8.

60. McCoshen JA. Quantitation of sex chromosomal influence(s) on the somatic growth of fetal gonads in vivo. Am J Obstet Gynecol. 1983;145(4):469-73.

61. McCoshen JA. In vivo sex differentiation of congeneic germinal cell aplastic gonads. Am J Obstet Gynecol. 1982;142(1):83-8.

62. Merchant H. Rat gonadal and ovarioan organogenesis with and without germ cells. An ultrastructural study. Dev Biol. 1975;44(1):1-21.

63. Koubova J, Menke DB, Zhou Q, Capel B, Griswold MD, Page DC. Retinoic acid regulates sex-specific timing of meiotic initiation in mice. Proc Natl Acad Sci U S A. 2006;103(8):2474-9.

64. Bowles J, Knight D, Smith C, Wilhelm D, Richman J, Mamiya S, et al. Retinoid signaling determines germ cell fate in mice. Science. 2006;312(5773):596-600.

65. Mendis SH, Meachem SJ, Sarraj MA, Loveland KL. Activin A balances Sertoli and germ cell proliferation in the fetal mouse testis. Biol Reprod. 2011;84(2):379-91.

66. Moreno SG, Attali M, Allemand I, Messiaen S, Fouchet P, Coffigny H, et al. TGFbeta signaling in male germ cells regulates gonocyte quiescence and fertility in mice. Dev Biol. 2010;342(1):74-84.

67. Thuillier R, Wang Y, Culty M. Prenatal exposure to estrogenic compounds alters the expression pattern of platelet-derived growth factor receptors alpha and beta in neonatal rat testis: identification of gonocytes as targets of estrogen exposure. Biol Reprod. 2003;68(3):867-80.

68. Bustos-Obregon E, Holstein AF. On structural patterns of the lamina propria of human seminiferous tubules. Z Zellforsch Mikrosk Anat. 1973;141(3):413-25.

69. Cunha GR, Cao M, Aksel S, Derpinghaus A, Baskin LS. Mouse-human species differences in early testicular development and its implications. Differentiation. 2023;129:79-95.

70. Jeanes A, Wilhelm D, Wilson MJ, Bowles J, McClive PJ, Sinclair AH, et al. Evaluation of candidate markers for the peritubular myoid cell lineage in the developing mouse testis. Reproduction. 2005;130(4):509-16.

71. Li Y, Overland M, Derpinghaus A, Aksel S, Cao M, Ladwig N, et al. Development of the human fetal testis: Morphology and expression of cellular differentiation markers. Differentiation. 2023;129:17-36.

72. Ostrer H, Huang HY, Masch RJ, Shapiro E. A cellular study of human testis development. Sex Dev. 2007;1(5):286-92.

73. Merchant-Larios H, Moreno-Mendoza N, Buehr M. The role of the mesonephros in cell differentiation and morphogenesis of the mouse fetal testis. The International Journal of Developmental Biology. 1993;37(3):407-15.

74. Buehr M, Gu S, McLaren A. Mesonephric contribution to testis differentiation in the fetal mouse. Development. 1993;117(1):273-81.

75. Cool J, Carmona FD, Szucsik JC, Capel B. Peritubular myoid cells are not the migrating population required for testis cord formation in the XY gonad. Sex Dev. 2008;2(3):128-33.

76. Park SY, Tong M, Jameson JL. Distinct roles for steroidogenic factor 1 and desert hedgehog pathways in fetal and adult Leydig cell development. Endocrinology. 2007;148(8):3704-10.

77. Bitgood MJ, Shen L, McMahon AP. Sertoli cell signaling by Desert hedgehog regulates the male germline. Curr Biol. 1996;6(3):298-304.

78. Yao HH, Whoriskey W, Capel B. Desert Hedgehog/Patched 1 signaling specifies fetal Leydig cell fate in testis organogenesis. Genes Dev. 2002;16(11):1433-40.

79. Pierucci-Alves F, Clark AM, Russell LD. A developmental study of the Desert hedgehog-null mouse testis. Biol Reprod. 2001;65(5):1392-402.

80. Clark AM, Garland KK, Russell LD. Desert hedgehog (Dhh) gene is required in the mouse testis for formation of adult-type Leydig cells and normal development of peritubular cells and seminiferous tubules. Biol Reprod. 2000;63(6):1825-38.

81. Barsoum IB, Bingham NC, Parker KL, Jorgensen JS, Yao HH. Activation of the Hedgehog pathway in the mouse fetal ovary leads to ectopic appearance of fetal Leydig cells and female pseudohermaphroditism. Dev Biol. 2009;329(1):96-103.

82. Meeks JJ, Crawford SE, Russell TA, Morohashi K, Weiss J, Jameson JL. Dax1 regulates testis cord organization during gonadal differentiation. Development. 2003;130(5):1029-36.

83. Shima Y. Development of fetal and adult Leydig cells. Reprod Med Biol. 2019;18(4):323-30.

84. Griswold SL, Behringer RR. Fetal Leydig cell origin and development. Sex Dev. 2009;3(1):1-15.

85. DeFalco T, Takahashi S, Capel B. Two distinct origins for Leydig cell progenitors in the fetal testis. Dev Biol. 2011;352(1):14-26.

86. Davidoff MS, Schulze W, Middendorff R, Holstein AF. The Leydig cell of the human testis —A new member of the diffuse neuroendocrine system. Cell Tissue Res. 1993;271(3):429-39.

87. Garcia-Alonso L, Lorenzi V, Mazzeo CI, Alves-Lopes JP, Roberts K, Sancho-Serra C, et al. Single-cell roadmap of human gonadal development. Nature. 2022;607(7919):540-7.

88. Stevant I, Neirijnck Y, Borel C, Escoffier J, Smith LB, Antonarakis SE, et al. Deciphering Cell Lineage Specification during Male Sex Determination with Single-Cell RNA Sequencing. Cell Rep. 2018;22(6):1589-99.

89. Park SY, Meeks JJ, Raverot G, Pfaff LE, Weiss J, Hammer GD, et al. Nuclear receptors Sf1 and Dax1 function cooperatively to mediate somatic cell differentiation during testis development. Development. 2005;132(10):2415-23.

90. Karpova T, Ravichandiran K, Insisienmay L, Rice D, Agbor V, Heckert LL. Steroidogenic factor 1 differentially regulates fetal and adult leydig cell development in male mice. Biol Reprod. 2015;93(4):83.

91. Tang H, Brennan J, Karl J, Hamada Y, Raetzman L, Capel B. Notch signaling maintains Leydig progenitor cells in the mouse testis. Development. 2008;135(22):3745-53.

92. O'Shaughnessy PJ, Baker P, Sohnius U, Haavisto AM, Charlton HM, Huhtaniemi I. Fetal development of Leydig cell activity in the mouse is independent of pituitary gonadotroph function. Endocrinology. 1998;139(3):1141-6.

93. Zhang FP, Pakarainen T, Zhu F, Poutanen M, Huhtaniemi I. Molecular characterization of postnatal development of testicular steroidogenesis in luteinizing hormone receptor knockout mice. Endocrinology. 2004;145(3):1453-63.

94. Themmen APN, Huhtaniemi IT. Mutations of gonadotropins and gonadotropin receptors: elucidating the physiology and pathophysiology of pituitary-gonadal function. Endocr Rev. 2000;21(5):551-83.

95. Shima Y, Miyabayashi K, Haraguchi S, Arakawa T, Otake H, Baba T, et al. Contribution of Leydig and Sertoli cells to testosterone production in mouse fetal testes. Mol Endocrinol. 2013;27(1):63-73.

96. O'Shaughnessy PJ, Baker PJ, Heikkilä M, Vainio S, McMahon AP. Localization of 17β-Hydroxysteroid Dehydrogenase/17Ketosteroid Reductase Isoform Expression in the Developing Mouse Testis—Androstenedione Is the Major Androgen Secreted by Fetal/Neonatal Leydig Cells. Endocrinology. 2000;141(7):2631-7.

97. Ivell R, Wade JD, Anand-Ivell R. INSL3 as a biomarker of Leydig cell functionality. Biol Reprod. 2013;88(6):147.

98. Gorlov IP, Kamat A, Bogatcheva NV, Jones E, Lamb DJ, Truong A, et al. Mutations of the GREAT gene cause cryptorchidism. Hum Mol Genet. 2002;11(19):2309-18.

99. Overbeek PA, Gorlov IP, Sutherland RW, Houston JB, Harrison WR, Boettger-Tong HL, et al. A transgenic insertion causing cryptorchidism in mice. Genesis. 2001;30(1):26-35.

100. Nef S, Parada LF. Cryptorchidism in mice mutant for Insl3. Nat Genet. 1999;22(3):295-9.

101. Zimmermann S, Schöttler P, Engel W, Adham IM. Mouse Leydig insulin-like (Ley I-L) gene: Structure and expression during testis and ovary development. Mol Reprod Dev. 1997;47(1):30-8.

102. Shima Y, Matsuzaki S, Miyabayashi K, Otake H, Baba T, Kato S, et al. Fetal Leydig Cells Persist as an Androgen-Independent Subpopulation in the Postnatal Testis. Mol Endocrinol. 2015;29(11):1581-93.

103. Kaftanovskaya EM, Lopez C, Ferguson L, Myhr C, Agoulnik AI. Genetic ablation of androgen receptor signaling in fetal Leydig cell lineage affects Leydig cell functions in adult testis. FASEB J. 2015;29(6):2327-37.

104. Zhang FP, Poutanen M, Wilbertz J, Huhtaniemi I. Normal prenatal but arrested postnatal sexual development of luteinizing hormone receptor knockout (LuRKO) mice. Mol Endocrinol. 2001;15(1):172-83.

105. O'Shaughnessy PJ, Fleming LM, Jackson G, Hochgeschwender U, Reed P, Baker PJ. Adrenocorticotropic hormone directly stimulates testosterone production by the fetal and neonatal mouse testis. Endocrinology. 2003;144(8):3279-84.

106. Barsoum IB, Kaur J, Ge RS, Cooke PS, Yao HH. Dynamic changes in fetal Leydig cell populations influence adult Leydig cell populations in mice. FASEB J. 2013;27(7):2657-66.

107. Guo J, Sosa E, Chitiashvili T, Nie X, Rojas EJ, Oliver E, et al. Single-cell analysis of the developing human testis reveals somatic niche cell specification and fetal germline stem cell establishment. Cell Stem Cell. 2021;28(4):764-78 e4.

108. Shima Y, Miyabayashi K, Sato T, Suyama M, Ohkawa Y, Doi M, et al. Fetal Leydig cells dedifferentiate and serve as adult Leydig stem cells. Development. 2018;145(23).

109. Gnessi L, Basciani S, Mariani S, Arizzi M, Spera G, Wang C, et al. Leydig cell loss and spermatogenic arrest in platelet-derived growth factor (PDGF)-A-deficient mice. J Cell Biol. 2000;149(5):1019-26.

110. Kilcoyne KR, Smith LB, Atanassova N, Macpherson S, McKinnell C, van den Driesche S, et al. Fetal programming of adult Leydig cell function by androgenic effects on stem/progenitor cells. Proc Natl Acad Sci U S A. 2014;111(18):E1924-32.

111. Hess RA, Renato de Franca L. Spermatogenesis and cycle of the seminiferous epithelium. Adv Exp Med Biol. 2008;636:1-15.

112. Mruk DD, Cheng CY. The Mammalian Blood-Testis Barrier: Its Biology and Regulation. Endocr Rev. 2015;36(5):564-91.

113. Amann RP. The cycle of the seminiferous epithelium in humans: a need to revisit? J Androl. 2008;29(5):469-87.

114. Feldman GJ, Mullin JM, Ryan MP. Occludin: structure, function and regulation. Adv Drug Deliv Rev. 2005;57(6):883-917.

115. Moroi S, Saitou M, Fujimoto K, Sakakibara A, Furuse M, Yoshida O, et al. Occludin is concentrated at tight junctions of mouse/rat but not human/guinea pig Sertoli cells in testes. Am J Physiol. 1998;274(6):C1708-17.

116. Balda MS, Whitney JA, Flores C, Gonzalez S, Cereijido M, Matter K. Functional dissociation of paracellular permeability and transepithelial electrical resistance and disruption of the apical-basolateral intramembrane diffusion barrier by expression of a mutant tight junction membrane protein. J Cell Biol. 1996;134(4):1031-49.

117. Du D, Xu F, Yu L, Zhang C, Lu X, Yuan H, et al. The tight junction protein, occludin, regulates the directional migration of epithelial cells. Dev Cell. 2010;18(1):52-63.

118. Furuse M, Sasaki H, Fujimoto K, Tsukita S. A Single Gene Product, Claudin-1 or -2, Reconstitutes Tight Junction Strands and Recruits Occludin in Fibroblasts. J Cell Biol. 1998;143(2):391-401.

119. Smith BE, Braun RE. Germ cell migration across Sertoli cell tight junctions. Science. 2012;338(6108):798-802.

120. Mazaud-Guittot S, Meugnier E, Pesenti S, Wu X, Vidal H, Gow A, et al. Claudin 11 deficiency in mice results in loss of the Sertoli cell epithelial phenotype in the testis. Biol Reprod. 2010;82(1):202-13.

121. Gow A, Southwood CM, Li JS, Pariali M, Riordan GP, Brodie SE, et al. CNS myelin and sertoli cell tight junction strands are absent in Osp/claudin-11 null mice. Cell. 1999;99(6):649-59.

122. Segretain D, Fiorini C, Decrouy X, Defamie N, Prat JR, Pointis G. A proposed role for ZO-1 in targeting connexin 43 gap junctions to the endocytic pathway. Biochimie. 2004;86(4-5):241-4.

123. Toyofuku T, Yabuki M, Otsu K, Kuzuya T, Hori M, Tada M. Direct association of the gap junction protein connexin-43 with ZO-1 in cardiac myocytes. J Biol Chem. 1998;273(21):12725-31.

124. Umeda K, Ikenouchi J, Katahira-Tayama S, Furuse K, Sasaki H, Nakayama M, et al. ZO-1 and ZO-2 independently determine where claudins are polymerized in tight-junction strand formation. Cell. 2006;126(4):741-54.

125. Lie PP, Cheng CY, Mruk DD. Signalling pathways regulating the blood-testis barrier. Int J Biochem Cell Biol. 2013;45(3):621-5.

126. Lydka M, Bilinska B, Cheng CY, Mruk DD. Tumor necrosis factor alpha-mediated restructuring of the Sertoli cell barrier in vitro involves matrix metalloprotease 9 (MMP9), membrane-bound intercellular adhesion molecule-1 (ICAM-1) and the actin cytoskeleton. Spermatogenesis. 2012;2(4):294-303.

127. Siu MK, Lee WM, Cheng CY. The interplay of collagen IV, tumor necrosis factor-alpha, gelatinase B (matrix metalloprotease-9), and tissue inhibitor of metalloproteases-1 in the basal lamina regulates Sertoli cell-tight junction dynamics in the rat testis. Endocrinology. 2003;144(1):371-87.

128. Meng J, Holdcraft RW, Shima JE, Griswold MD, Braun RE. Androgens regulate the permeability of the blood-testis barrier. Proc Natl Acad Sci U S A. 2005;102(46):16696-700.

129. Xia W, Wong EW, Mruk DD, Cheng CY. TGF-beta3 and TNFalpha perturb blood-testis barrier (BTB) dynamics by accelerating the clathrin-mediated endocytosis of integral membrane proteins: a new concept of BTB regulation during spermatogenesis. Dev Biol. 2009;327(1):48-61.

130. Su L, Mruk DD, Lee WM, Cheng CY. Differential effects of testosterone and TGF-beta3 on endocytic vesicle-mediated protein trafficking events at the blood-testis barrier. Exp Cell Res. 2010;316(17):2945-60.

131. Lie PP, Cheng CY, Mruk DD. Interleukin-1alpha is a regulator of the blood-testis barrier. FASEB J. 2011;25(4):1244-53.

132. Lie PP, Mruk DD, Lee WM, Cheng CY. Epidermal growth factor receptor pathway substrate 8 (Eps8) is a novel regulator of cell adhesion and the blood-testis barrier integrity in the seminiferous epithelium. FASEB J. 2009;23(8):2555-67.

133. Thyen U, Hampel E, Hiort O. [Disorders of sex development]. Bundesgesundheitsblatt Gesundheitsforschung Gesundheitsschutz. 2007;50(12):1569-77.

134. Flück CE, Pandey AV. In: Simoni M, Huhtaniemi IT, editors. Endocrinology of the testis and male reproduction. Endocrinology 1. 1: Springer International Publishing AG; 2017. p. 343.

135. Hiort O, Holterhus PM, Werner R, Marschke C, Hoppe U, Partsch CJ, et al. Homozygous disruption of P450 side-chain cleavage (CYP11A1) is associated with prematurity, complete 46,XY sex reversal, and severe adrenal failure. J Clin Endocrinol Metab. 2005;90(1):538-41.

136. Werner R, Kulle A, Sommerfeld I, Riepe FG, Wudy S, Hartmann MF, et al. Testosterone synthesis in patients with 17beta-hydroxysteroid dehydrogenase 3 deficiency. Sex Dev. 2012;6(4):161-8.

137. Hochberg Z, Chayen R, Reiss N, Falik Z, Makler A, Munichor M, et al. Clinical, biochemical, and genetic findings in a large pedigree of male and female patients with 5 alpha-reductase 2 deficiency. J Clin Endocrinol Metab. 1996;81(8):2821-7.

138. Hornig NC, Holterhus PM. Molecular basis of androgen insensitivity syndromes. Mol Cell Endocrinol. 2021;523:111146.

139. Hughes IA, Davies JD, Bunch TI, Pasterski V, Mastroyannopoulou K, MacDougall J. Androgen insensitivity syndrome. The Lancet. 2012;380(9851):1419-28.

140. Hughes IA, Werner R, Bunch T, Hiort O. Androgen insensitivity syndrome. Semin Reprod Med. 2012;30(5):432-42.

141. Hiort O, Sinnecker GH, Holterhus PM, Nitsche EM, Kruse K. Inherited and de novo androgen receptor gene mutations: investigation of single-case families. J Pediatr. 1998;132(6):939-43.

142. Hiort O, Sinnecker GH, Holterhus PM, Nitsche EM, Kruse K. The clinical and molecular spectrum of androgen insensitivity syndromes. Am J Med Genet. 1996;63(1):218-22.

143. Hiort O. Clinical and molecular aspects of androgen insensitivity. Endocr Dev. 2013;24:33-40.

144. Massanyi EZ, Dicarlo HN, Migeon CJ, Gearhart JP. Review and management of 46,XY disorders of sex development. J Pediatr Urol. 2013;9(3):368-79.

145. Burckhardt MA, Udhane SS, Marti N, Schnyder I, Tapia C, Nielsen JE, et al. Human 3beta-hydroxysteroid dehydrogenase deficiency seems to affect fertility but may not harbor a tumor risk: lesson from an experiment of nature. European Journal of Endocrinology. 2015;173(5):K1-K12.

146. Cools M, van Aerde K, Kersemaekers AM, Boter M, Drop SLS, Wolffenbuttel KP, et al. Morphological and immunohistochemical differences between gonadal maturation delay and early germ cell neoplasia in patients with undervirilization syndromes. J Clin Endocrinol Metab. 2005;90(9):5295-303.

147. Hannema SE, Scott IS, Rajpert-De Meyts E, Skakkebaek NE, Coleman N, Hughes IA. Testicular development in the complete androgen insensitivity syndrome. J Pathol. 2006;208(4):518-27.

148. Kaprova-Pleskacova J, Stoop H, Bruggenwirth H, Cools M, Wolffenbuttel KP, Drop SL, et al. Complete androgen insensitivity syndrome: factors influencing gonadal histology including germ cell pathology. Mod Pathol. 2014;27(5):721-30.

149. Aliberti P, Perez Garrido N, Marino R, Ramirez P, Solari AJ, Sciurano R, et al. Androgen Insensitivity Syndrome at Prepuberty: Marked Loss of Spermatogonial Cells at Early Childhood and Presence of Gonocytes up to Puberty. Sex Dev. 2017;11(5-6):225-37.

150. Jarzabek K, Koda M, Chrusciel M, Kanczuga-Koda L, Sobczynska-Tomaszewska A, Rahman NA, et al. Features of the fetal gonad in androgen synthesis in the postpubertal testis are preserved in complete androgen insensitivity syndrome due to a novel genetic splice site donor variant in androgen receptor gene intron 1. J Steroid Biochem Mol Biol. 2019;193:105420.

151. Aherrahrou R, Kulle AE, Alenina N, Werner R, Vens-Cappell S, Bader M, et al. CYP17A1 deficient XY mice display susceptibility to atherosclerosis, altered lipidomic profile and atypical sex development. Sci Rep. 2020;10(1):8792.

152. RNAscope™ Multiplex Fluorescent Reagent Kit v2 User Manual: Advanced Cell Diagnostics, Inc. ; 2022. Available from: https://acdbio.com/sites/default/files/UM%20323100%20Multiplex%20Fluorescent%20v2_RevB.pdf.

153. Guo J, Nie X, Giebler M, Mlcochova H, Wang Y, Grow EJ, et al. The Dynamic Transcriptional Cell Atlas of Testis Development during Human Puberty. Cell Stem Cell. 2020;26(2):262-76 e4.

154. Sohni A, Tan K, Song HW, Burow D, de Rooij DG, Laurent L, et al. The Neonatal and Adult Human Testis Defined at the Single-Cell Level. Cell Rep. 2019;26(6):1501-17 e4.

155. Chen S, Zhou Y, Chen Y, Gu J. fastp: an ultra-fast all-in-one FASTQ preprocessor. Bioinformatics. 2018;34(17):i884-i90.

156. Melsted P, Booeshaghi AS, Liu L, Gao F, Lu L, Min KHJ, et al. Modular, efficient and constant-memory single-cell RNA-seq preprocessing. Nat Biotechnol. 2021;39(7):813-8.

157. Zhou H, Ji J, Chen X, Bi Y, Li J, Wang Q, et al. Identification of novel bat coronaviruses sheds light on the evolutionary origins of SARS-CoV-2 and related viruses. Cell. 2021;184(17):4380-91 e14.

158. Rudat C, Grieskamp T, Rohr C, Airik R, Wrede C, Hegermann J, et al. Upk3b is dispensable for development and integrity of urothelium and mesothelium. PLoS One. 2014;9(11):e112112.

159. Roselli S, Gribouval O, Boute N, Sich M, Benessy F, Attie T, et al. Podocin localizes in the kidney to the slit diaphragm area. Am J Pathol. 2002;160(1):131-9.

160. Wickham H. Data Analysis. ggplot2: Elegant Graphics for Data Analysis. Cham: Springer International Publishing; 2016. p. 189-201.

161. Dawson C. Ggprism: A'Ggplot2'Extension Inspired by'GraphPad Prism'. 2021.

162. R Core Team. R: A language and environment for statistical computing. R Foundation for Statistical Computing, Vienna, Austria. http://wwwR-projectorg/. 2021.

163. Merritt CR, Ong GT, Church SE, Barker K, Danaher P, Geiss G, et al. Multiplex digital spatial profiling of proteins and RNA in fixed tissue. Nat Biotechnol. 2020;38(5):586-99.

164. GeoMx® DSP Manual Slide Preparation User Manual: NanoString Technologies, Inc.; 2023. Available from: https://university.nanostring.com/geomx-dsp-manual-slide-preparation-user-manual.

165. GeoMx® DSP Instrument User Manual: NanoString Technologies, Inc.; 2023. Available from: https://university.nanostring.com/geomx-dsp-instrument-user-manual.

166. GeoMx® DSP NGS Readout User Manual: NanoString Technologies, Inc.; 2023. Available from: https://university.nanostring.com/geomx-dsp-ngs-readout-user-manual/1193408.

167. GeoMx® DSP Data Analysis User Manual: NanoString Technologies, Inc.; 2023. Available from: https://university.nanostring.com/geomx-dsp-data-analysis-user-manual/1163670.

168. Inoue M, Shima Y, Miyabayashi K, Tokunaga K, Sato T, Baba T, et al. Isolation and Characterization of Fetal Leydig Progenitor Cells of Male Mice. Endocrinology. 2016;157(3):1222-33.

169. Rebourcet D, Mackay R, Darbey A, Curley MK, Jorgensen A, Frederiksen H, et al. Ablation of the canonical testosterone production pathway via knockout of the steroidogenic enzyme HSD17B3, reveals a novel mechanism of testicular testosterone production. FASEB J. 2020;34(8):10373-86.

170. Al-Sharkawi M, Calonga-Solis V, Dressler FF, Busch H, Hiort O, Werner R. Persistence of foetal testicular features in patients with defective androgen signalling. Eur J Endocrinol. 2023;188(1).

171. Schiffer L, Barnard L, Baranowski ES, Gilligan LC, Taylor AE, Arlt W, et al. Human steroid biosynthesis, metabolism and excretion are differentially reflected by serum and urine steroid metabolomes: A comprehensive review. J Steroid Biochem Mol Biol. 2019;194:105439.

172. O'Shaughnessy PJ, Johnston H, Willerton L, Baker PJ. Failure of normal adult Leydig cell development in androgen-receptor-deficient mice. J Cell Sci. 2002;115(Pt 17):3491-6.

173. Lottrup G, Nielsen JE, Maroun LL, Moller LM, Yassin M, Leffers H, et al. Expression patterns of DLK1 and INSL3 identify stages of Leydig cell differentiation during normal development and in testicular pathologies, including testicular cancer and Klinefelter syndrome. Hum Reprod. 2014;29(8):1637-50.

174. Lottrup G, Nielsen JE, Skakkebaek NE, Juul A, Rajpert-De Meyts E. Abundance of DLK1, differential expression of CYP11B1, CYP21A2 and MC2R, and lack of INSL3 distinguish testicular adrenal rest tumours from Leydig cell tumours. European Journal of Endocrinology. 2015;172(4):491-9.

175. Wang Y, Liu B, Zhao G, Lee Y, Buzdin A, Mu X, et al. Spatial transcriptomics: Technologies, applications and experimental considerations. Genomics. 2023;115(5):110671.

176. Lapoirie M, Dijoud F, Lejeune H, Plotton I. Effect of androgens on Sertoli cell maturation in human testis from birth to puberty. Basic Clin Androl. 2021;31(1):31.

177. McCabe MJ, Tarulli GA, Laven-Law G, Matthiesson KL, Meachem SJ, McLachlan RI, et al. Gonadotropin suppression in men leads to a reduction in claudin-11 at the Sertoli cell tight junction. Hum Reprod. 2016;31(4):875-86.

178. Haverfield JT, Meachem SJ, O'Bryan MK, McLachlan RI, Stanton PG. Claudin-11 and connexin-43 display altered spatial patterns of organization in men with primary seminiferous tubule failure compared with controls. Fertil Steril. 2013;100(3):658-66.

179. Wang R, Liu X, Li L, Yang M, Yong J, Zhai F, et al. Dissecting Human Gonadal Cell Lineage Specification and Sex Determination Using A Single-cell RNA-seq Approach. Genomics Proteomics Bioinformatics. 2022;20(2):223-45.

180. Guo J, Grow EJ, Mlcochova H, Maher GJ, Lindskog C, Nie X, et al. The adult human testis transcriptional cell atlas. Cell Res. 2018;28(12):1141-57.

181. Mahyari E, Guo J, Lima AC, Lewinsohn DP, Stendahl AM, Vigh-Conrad KA, et al. Comparative single-cell analysis of biopsies clarifies pathogenic mechanisms in Klinefelter syndrome. The American Journal of Human Genetics. 2021;108(10):1924-45.

182. O'Shaughnessy PJ, Mitchell RT, Monteiro A, O'Hara L, Cruickshanks L, der Grinten HC, et al. Androgen receptor expression is required to ensure development of adult Leydig cells and to prevent development of steroidogenic cells with adrenal characteristics in the mouse testis. BMC Dev Biol. 2019;19(1):8.

183. O'Hara L, McInnes K, Simitsidellis I, Morgan S, Atanassova N, Slowikowska-Hilczer J, et al. Autocrine androgen action is essential for Leydig cell maturation and function, and protects against late-onset Leydig cell apoptosis in both mice and men. FASEB J. 2015;29(3):894-910.

184. Schroder MAM, Sweep F, van Herwaarden AE, Mitchell RT, Eliveld J, van Pelt AMM, et al. Transcriptional comparison of testicular adrenal rest tumors with fetal and adult tissues. Eur J Endocrinol. 2022;187(5):607-15.

185. O'Shaughnessy PJ, Willerton L, Baker PJ. Changes in Leydig cell gene expression during development in the mouse. Biol Reprod. 2002;66(4):966-75.

186. O'Donnell L, Smith LB, Rebourcet D. Sertoli cells as key drivers of testis function. Semin Cell Dev Biol. 2022;121:2-9.

187. Hedger MP. The Immunophysiology of Male Reproduction. Knobil and Neill's Physiology of Reproduction2015. p. 805-92.

188. Fijak M, Meinhardt A. The testis in immune privilege. Immunol Rev. 2006;213:66-81.

189. Sluka P, O'Donnell L, Bartles JR, Stanton PG. FSH regulates the formation of adherens junctions and ectoplasmic specialisations between rat Sertoli cells in vitro and in vivo. J Endocrinol. 2006;189(2):381-95.

190. Li MWM, Mruk DD, Lee WM, Cheng CY. Connexin 43 and plakophilin-2 as a protein complex that regulates blood–testis barrier dynamics. Proceedings of the National Academy of Sciences. 2009;106(25):10213-8.

191. Li MWM, Mruk DD, Lee WM, Cheng CY. Connexin 43 is critical to maintain the homeostasis of the blood–testis barrier via its effects on tight junction reassembly. Proceedings of the National Academy of Sciences. 2010;107(42):17998-8003.

192. Brehm R, Zeiler M, Ruttinger C, Herde K, Kibschull M, Winterhager E, et al. A sertoli cell-specific knockout of connexin43 prevents initiation of spermatogenesis. Am J Pathol. 2007;171(1):19-31.

193. Noelke J, Wistuba J, Damm OS, Fietz D, Gerber J, Gaehle M, et al. A Sertoli cell-specific connexin43 knockout leads to altered interstitial connexin expression and increased Leydig cell numbers. Cell Tissue Res. 2015;361(2):633-44.

194. Steger K, Tetens F, Bergmann M. Expression of connexin 43 in human testis. Histochem Cell Biol. 1999;112(3):215-20.

195. Brehm R, Marks A, Rey R, Kliesch S, Bergmann M, Steger K. Altered expression of connexins 26 and 43 in Sertoli cells in seminiferous tubules infiltrated with carcinoma-in-situ or seminoma. J Pathol. 2002;197(5):647-53.

196. Fink C, Baal N, Wilhelm J, Sarode P, Weigel R, Schumacher V, et al. On the origin of germ cell neoplasia in situ: Dedifferentiation of human adult Sertoli cells in cross talk with seminoma cells in vitro. Neoplasia. 2021;23(7):731-42.

197. Kotula-Balak M, Hejmej A, Sadowska J, Bilinska B. Connexin 43 expression in human and mouse testes with impaired spermatogenesis. Eur J Histochem. 2007;51(4):261-8.

198. Giudice MG, Vermeulen M, Wyns C. Blood Testis Barrier and Somatic Cells Impairment in a Series of 35 Adult Klinefelter Syndrome Patients. Int J Mol Sci. 2019;20(22).

199. Chihara M, Otsuka S, Ichii O, Hashimoto Y, Kon Y. Molecular dynamics of the blood-testis barrier components during murine spermatogenesis. Mol Reprod Dev. 2010;77(7):630-9.

200. McCabe MJ, Tarulli GA, Meachem SJ, Robertson DM, Smooker PM, Stanton PG. Gonadotropins regulate rat testicular tight junctions in vivo. Endocrinology. 2010;151(6):2911-22.

201. Griswold MD, Hogarth CA, Bowles J, Koopman P. Initiating meiosis: the case for retinoic acid. Biol Reprod. 2012;86(2):35.

202. Brehm R, Ruttinger C, Fischer P, Gashaw I, Winterhager E, Kliesch S, et al. Transition from preinvasive carcinoma in situ to seminoma is accompanied by a reduction of connexin 43 expression in Sertoli cells and germ cells. Neoplasia. 2006;8(6):499-509.

203. Fink C, Weigel R, Hembes T, Lauke-Wettwer H, Kliesch S, Bergmann M, et al. Altered expression of ZO-1 and ZO-2 in Sertoli cells and loss of blood-testis barrier integrity in testicular carcinoma in situ. Neoplasia. 2006;8(12):1019-27.

204. Fink C, Weigel R, Fink L, Wilhelm J, Kliesch S, Zeiler M, et al. Claudin-11 is over-expressed and dislocated from the blood-testis barrier in Sertoli cells associated with testicular intraepithelial neoplasia in men. Histochem Cell Biol. 2009;131(6):755-64.

205. Welter H, Kampfer C, Lauf S, Feil R, Schwarzer JU, Kohn FM, et al. Partial loss of contractile marker proteins in human testicular peritubular cells in infertility patients. Andrology. 2013;1(2):318-24.

206. Rebourcet D, O'Shaughnessy PJ, Monteiro A, Milne L, Cruickshanks L, Jeffrey N, et al. Sertoli cells maintain Leydig cell number and peritubular myoid cell activity in the adult mouse testis. PLoS One. 2014;9(8):e105687.

207. Welsh M, Saunders PT, Atanassova N, Sharpe RM, Smith LB. Androgen action via testicular peritubular myoid cells is essential for male fertility. FASEB J. 2009;23(12):4218-30.

208. Chen LY, Brown PR, Willis WB, Eddy EM. Peritubular myoid cells participate in male mouse spermatogonial stem cell maintenance. Endocrinology. 2014;155(12):4964-74.

209. Chen LY, Willis WD, Eddy EM. Targeting the Gdnf Gene in peritubular myoid cells disrupts undifferentiated spermatogonial cell development. Proc Natl Acad Sci U S A. 2016;113(7):1829-34.

210. Welsh M, Moffat L, Belling K, de Franca LR, Segatelli TM, Saunders PT, et al. Androgen receptor signalling in peritubular myoid cells is essential for normal differentiation and function of adult Leydig cells. Int J Androl. 2012;35(1):25-40.

211. Boukari K, Meduri G, Brailly-Tabard S, Guibourdenche J, Ciampi ML, Massin N, et al. Lack of androgen receptor expression in Sertoli cells accounts for the absence of anti-Mullerian hormone repression during early human testis development. J Clin Endocrinol Metab. 2009;94(5):1818-25.

212. Valeri C, Lovaisa MM, Racine C, Edelsztein NY, Riggio M, Giulianelli S, et al. Molecular mechanisms underlying AMH elevation in hyperoestrogenic states in males. Sci Rep. 2020;10(1):15062.

213. Edelsztein NY, Racine C, di Clemente N, Schteingart HF, Rey RA. Androgens downregulate anti-Mullerian hormone promoter activity in the Sertoli cell through the androgen receptor and intact steroidogenic factor 1 sites. Biol Reprod. 2018;99(6):1303-12.

214. Shishido Y, Baba T, Sato T, Shima Y, Miyabayashi K, Inoue M, et al. Differential lactate and cholesterol synthetic activities in XY and XX Sertoli cells. Sci Rep. 2017;7:41912.

215. Oliveira MF, Romero JP, Chung M, Williams S, Gottscho AD, Gupta A, et al. Characterization of immune cell populations in the tumor microenvironment of colorectal cancer using high definition spatial profiling. bioRxiv. 2024:2024.06. 04.597233.

216. Vallejo AF, Harvey K, Wang T, Wise K, Butler LM, Polo J, et al. snPATHO-seq: unlocking the FFPE archives for single nucleus RNA profiling. bioRxiv. 2022:2022.08. 23.505054.

217. Chitiashvili T, Dror I, Kim R, Hsu FM, Chaudhari R, Pandolfi E, et al. Female human primordial germ cells display X-chromosome dosage compensation despite the absence of X-inactivation. Nat Cell Biol. 2020;22(12):1436-46.

218. Athar A, Fullgrabe A, George N, Iqbal H, Huerta L, Ali A, et al. ArrayExpress update - from bulk to single-cell expression data. Nucleic acids research. 2019;47(D1):D711-D5.

219. Carithers LJ, Ardlie K, Barcus M, Branton PA, Britton A, Buia SA, et al. A Novel Approach to High-Quality Postmortem Tissue Procurement: The GTEx Project. Biopreserv Biobank. 2015;13(5):311-9.

Appendix

Supplementary Materials

Table 19. List of single cell RNA data of testicular samples reanalysed in this study derived from previous publications and deposited in the Gene Expression Omnibus database (GEO).

GEO Sample	GEO Series	Sample description	Group	Reference
GSM4257562	GSE143356	Week 6 post-fertilization	Embryo	(217)
GSM4257563		Week 7 post-fertilization		
GSM4257564		Week 8 post-fertilization		
GSM4485991		Week 12 post-fertilization	Foetus	
GSM4257566		Week 15 post-fertilization		
GSM4257567		Week 16 post-fertilization		
GSM3526583	GSE124263	2 days old (ITGA6 enriched)	Neonate	(154)
GSM3526584		2 days old (unfractionated)		
GSM3526585		7 days old (ITGA6 enriched)		
GSM3526586		7 days old (unfractionated)		
GSM4910868	GSE161617	5 months old (repetition 1)	Mini puberty	(107)
GSM4910869		5 months old (repetition 2)		
GSM3937918	GSE134144	7 years old (repetition 1)	Prepuberty	(153)
GSM3937919		7 years old (repetition 2)		
GSM3937920		11 years old (repetition 1)		
GSM3937921		11 years old (repetition 2)		
GSM3937922		13 years old (repetition 1)	Peripuberty	
GSM3937923		13 years old (repetition 2)		
GSM3937924		14 years old (repetition 1)		
GSM3937925		14 years old (repetition 2)		
GSM3526587	GSE124263	37 years olds (ITGA6 enriched)	Adult	(154)
GSM3526588		37 years olds (unfractionated)		
GSM3526589		42 years olds (ITGA6 enriched)		
GSM3526590		42 years olds (unfractionated)		

Table 20. List of bulk RNA data of testicular tissue obtained from public datasets reanalysed in this study.

Accession	Dataset	Sample description	Group	Reference
E-MTAB-6814	ArrayExpress	18 human testis samples from 8 to 19 weeks post fertilization	Embryo and Foetus	(218)
phs000424.v7.p2	GTEx Analysis V7	259 human testis samples from adults	Adults	(219)

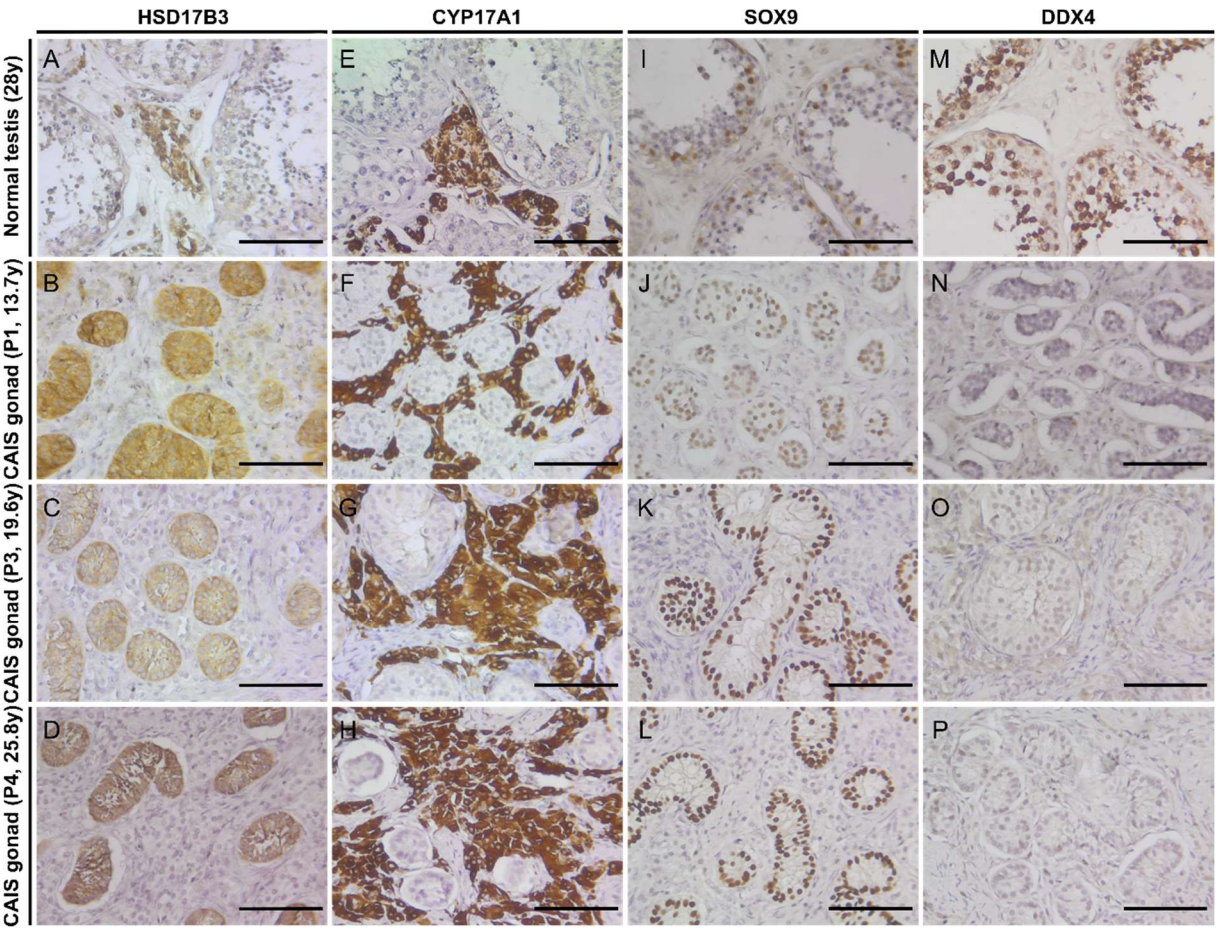

Figure 29. HSD17B3, CYP17A1, SOX9 and DDX4 protein expression in gonadal tissues from CAIS patients P1, P3 and P4 compared to testicular tissue from a normal adult. HSD17B3 is expressed in Leydig cells and to a lesser extent in seminiferous tubules in normal adult testicular tissue (A) but exclusively in seminiferous tubules in CAIS gonadal tissues (B-D). CYP17A1 labels normal Leydig cells in the normal adult testicular tissue (E) and hyperplastic Leydig cells in CAIS gonadal tissues (F-H). SOX9 labels Sertoli cells in the normal adult testicular tissue (I) and CAIS gonadal tissues (J-K). DDX4 is expressed only in germ cells in the normal adult testicular tissue (M) but not in most seminiferous tubules in CAIS gonadal tissues (N-P). Scale bar, 100 µm. Reproduced from (170) according to the terms of the creative Commons Attribution-NonComercial License (https://creativecommons.org/ licenses/by-nc/4.0/).

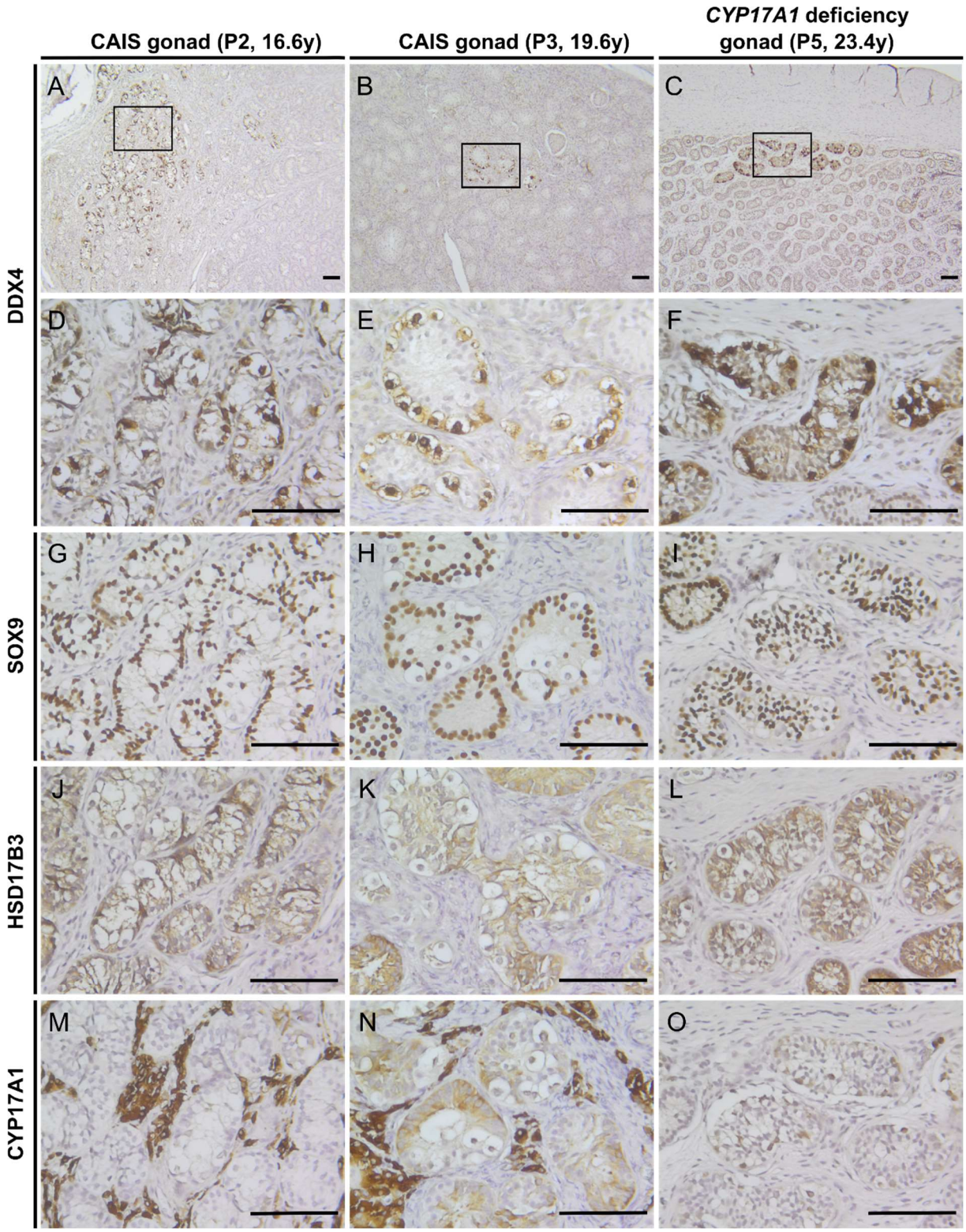

Figure 30. DDX4, SOX9, HSD17B3 and CYP17A1 protein expression in regions with residual germ cells in gonadal tissues from CAIS patients P2 and P3, and CYP17A1 deficiency patient P5. DDX4 is expressed in residual germ cells in some seminiferous tubules in CAIS gonadal tissues and CYP17A1 deficiency gonadal tissue (A-F). Sertoli cells in these seminiferous tubules express SOX9 (G-I) and HSD17B3 (J-L). CYP17A1 is expressed in neighbouring Leydig cells in CAIS gonadal tissues (M and N) but not in the neighbouring interstitial tissue in CYP17A1-deficiency gonadal tissue (O). Scale bar, 100 µm. Reproduced from (170) according to the terms of the creative Commons Attribution-NonComercial License (https://creativecommons.org/ licenses/by-nc/4.0/).

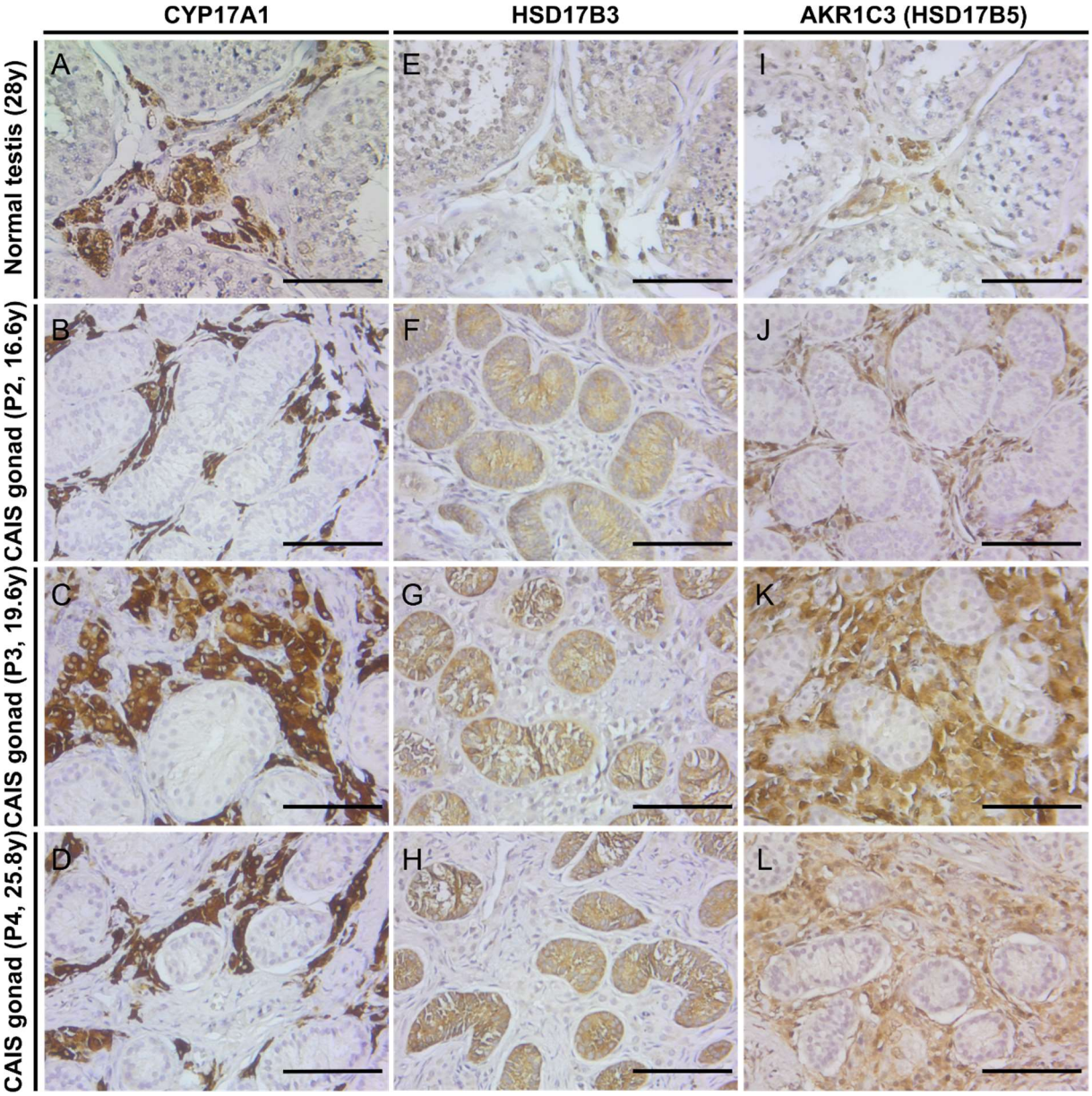

Figure 31. CYP17A1, HSD17B3, AKR1C3 (HSD17B5) protein expression in gonadal tissues from CAIS patients P2, P3 and P4 compared to testicular tissue from normal adult control. CYP17A1 labels normal (A) and hyperplastic (B-D) Leydig cells in normal adult testicular tissues and CAIS gonadal tissues, respectively. HSD17B3 is expressed in Leydig cells and to a lesser extent in seminiferous tubules in normal adult testicular tissue (E) but exclusively in seminiferous tubule sin CAIS gonadal tissues (F-H). In contrast, AKR1C3 (HSD17B5) is expressed in normal (I) and hyperplastic Leydig cells (J-L) in normal adult testicular tissue and CAIS gonadal tissues, respectively. Scale bar, 100 µm. Scale bar, 100 µm. Reproduced from (170) according to the terms of the creative Commons Attribution-NonComercial License (https://creativecommons.org/ licenses/by-nc/4.0/).

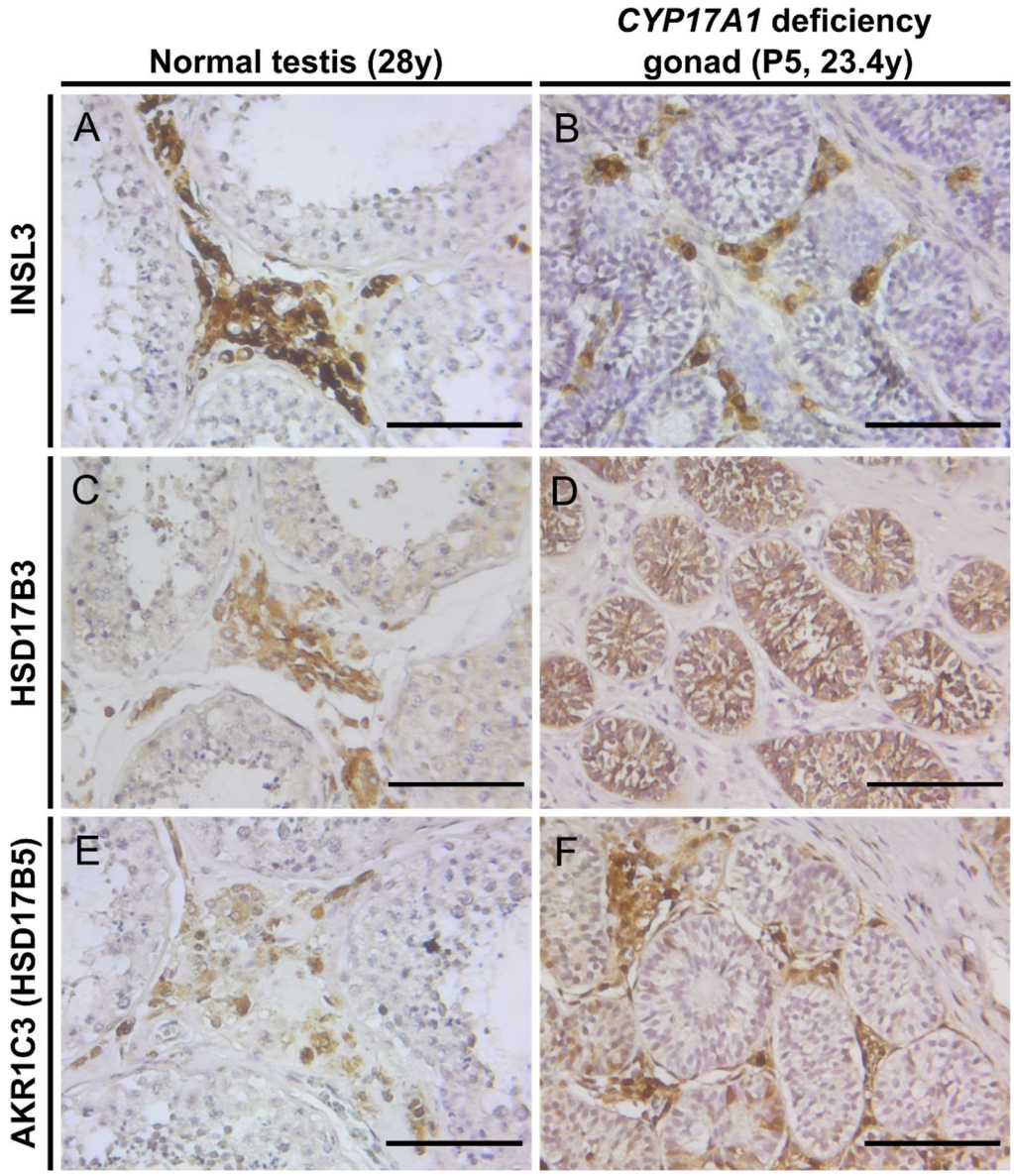

Figure 32. INSL3, HSD17B3 and AKR1C3 protein expression in gonadal tissue form a 23.4-year-old patient with CYP17A1 deficiency compared to normal testicular tissue from a 28-year-old control. INSL3 labels normal (A) and hypoplastic (B) Leydig cells in normal adult testicular tissue and CYP17A1 deficiency gonadal tissue, respectively. HSD17B3 is expressed in Leydig cells and to a lesser extent in seminiferous tubules in the normal adult testicular tissue (C) but exclusively in seminiferous tubules in the CYP17A1 deficiency gonadal tissue (D). In contrast, AKR1C3 (HSD17B5) is expressed normal (E) and hypoplastic (F) Leydig cells in normal adult testicular tissue and CYP17A1 deficiency gonadal tissue, respectively. Scale bar, 100 µm. Scale bar, 100 µm. Reproduced from (170) according to the terms of the creative Commons Attribution-NonComercial License (https://creativecommons.org/ licenses/by-nc/4.0/).

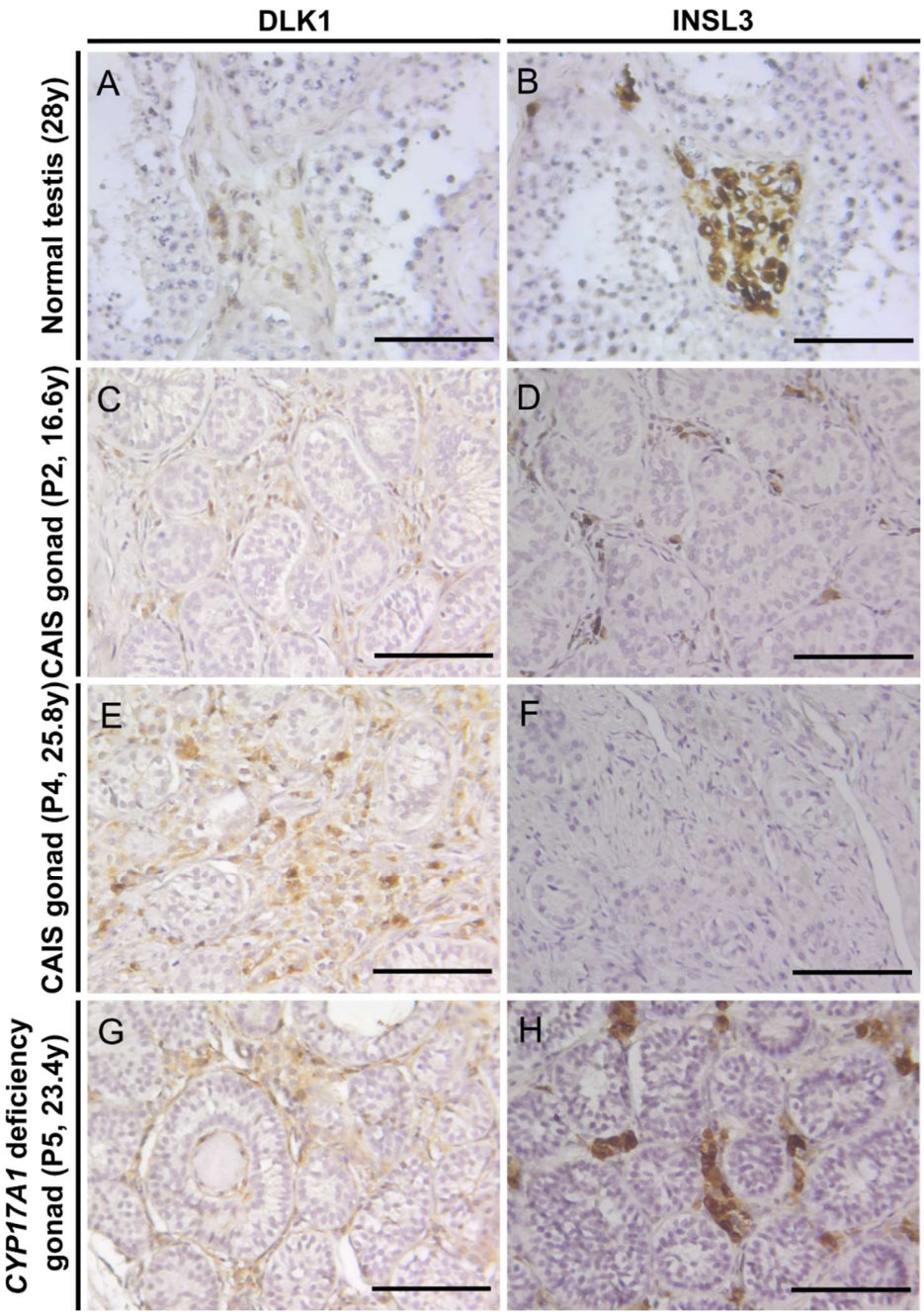

Figure 33. INSL3 and DLK1 protein expression in gonadal tissues from patients with CAIS (P2 and P4) and CYP17A1 deficiency (P5) compared to testicular tissue from a normal adult control. In normal adult testicular tissue, INSL3 is expressed in most Leydig cells (A) and DLK1 in a few Leydig cells (B). In CAIS gonadal tissue from P2, INSL3 (C) and DLK1 (D) are expressed in subsets of Leydig cells. In CAIS gonadal tissue from P3, INSL3 is not expressed (E) but DLK1 is highly expressed in subsets of Leydig cells (F). In CYP17A1 deficiency gonadal tissue, INSL3 is expressed in most of the hypoplastic Leydig cells (G) and DLK1 is expressed in some of them (H). Scale bar, 100 µm. Scale bar, 100 µm. Reproduced from (170) according to the terms of the creative Commons Attribution-NonComercial License (https://creativecommons.org/ licenses/by-nc/4.0/).

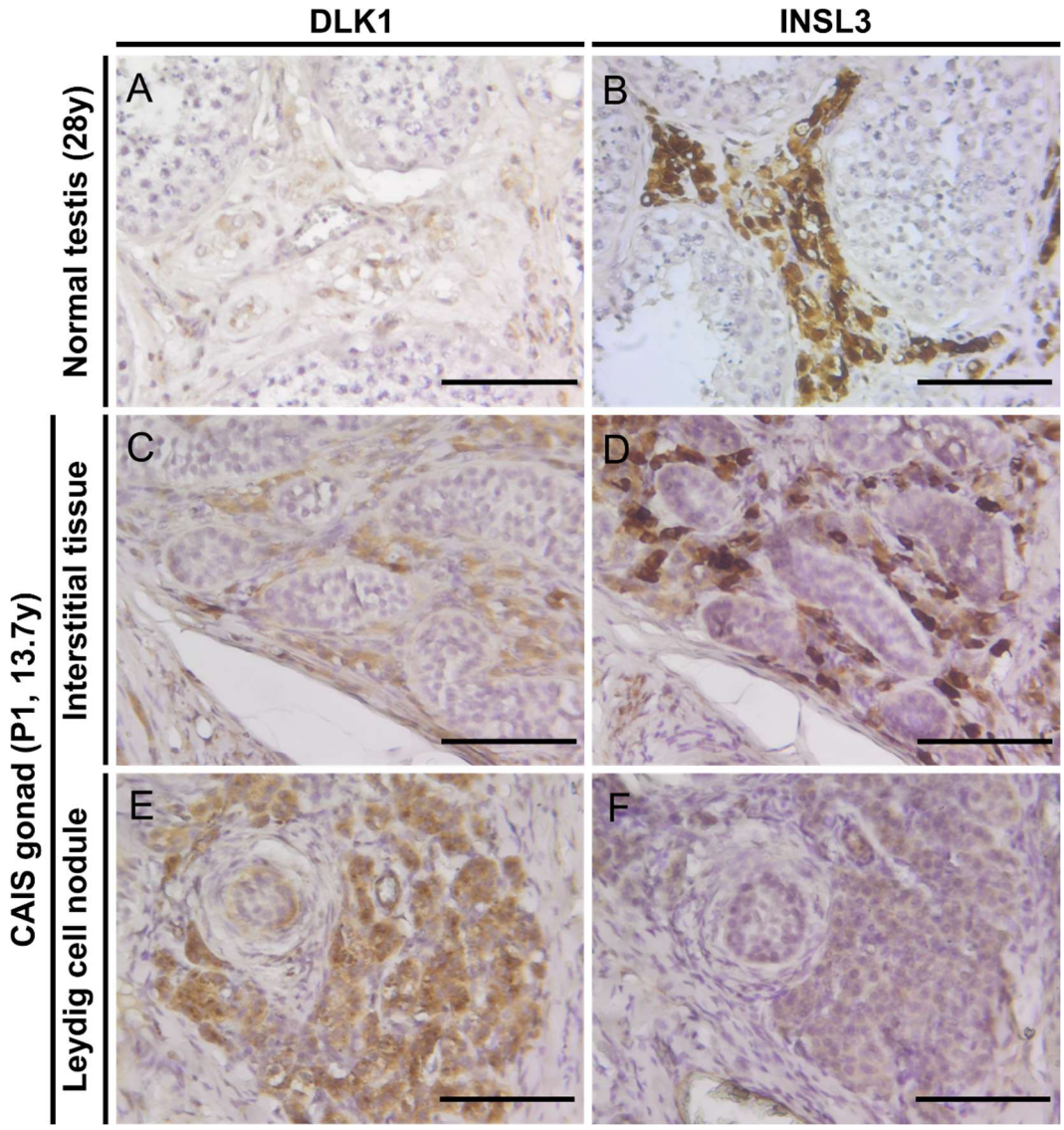

Figure 34. INSL3 and DLK1 expression in interstitial Leydig cells versus Leydig cell nodule in gonadal tissue from a 13.7-year-old patient with CAIS compared to normal testicular tissue from a 28-year-old control. INSL3 is expressed in most of Leydig cells in the normal adult testicular tissue (A) while DLK1 is expressed in some of them (B). INSL3 and DLK1 are expressed in subsets of Leydig cells in the young adult CAIS gonadal tissue (C and D). A Leydig cell nodule in the CAIS gonadal tissue barely express INSL3 (E) but highly express DLK1 (F). Scale bar, 100 µm. Scale bar, 100 µm. Reproduced from (170) according to the terms of the creative Commons Attribution-NonComercial License (https://creativecommons.org/ licenses/by-nc/4.0/).

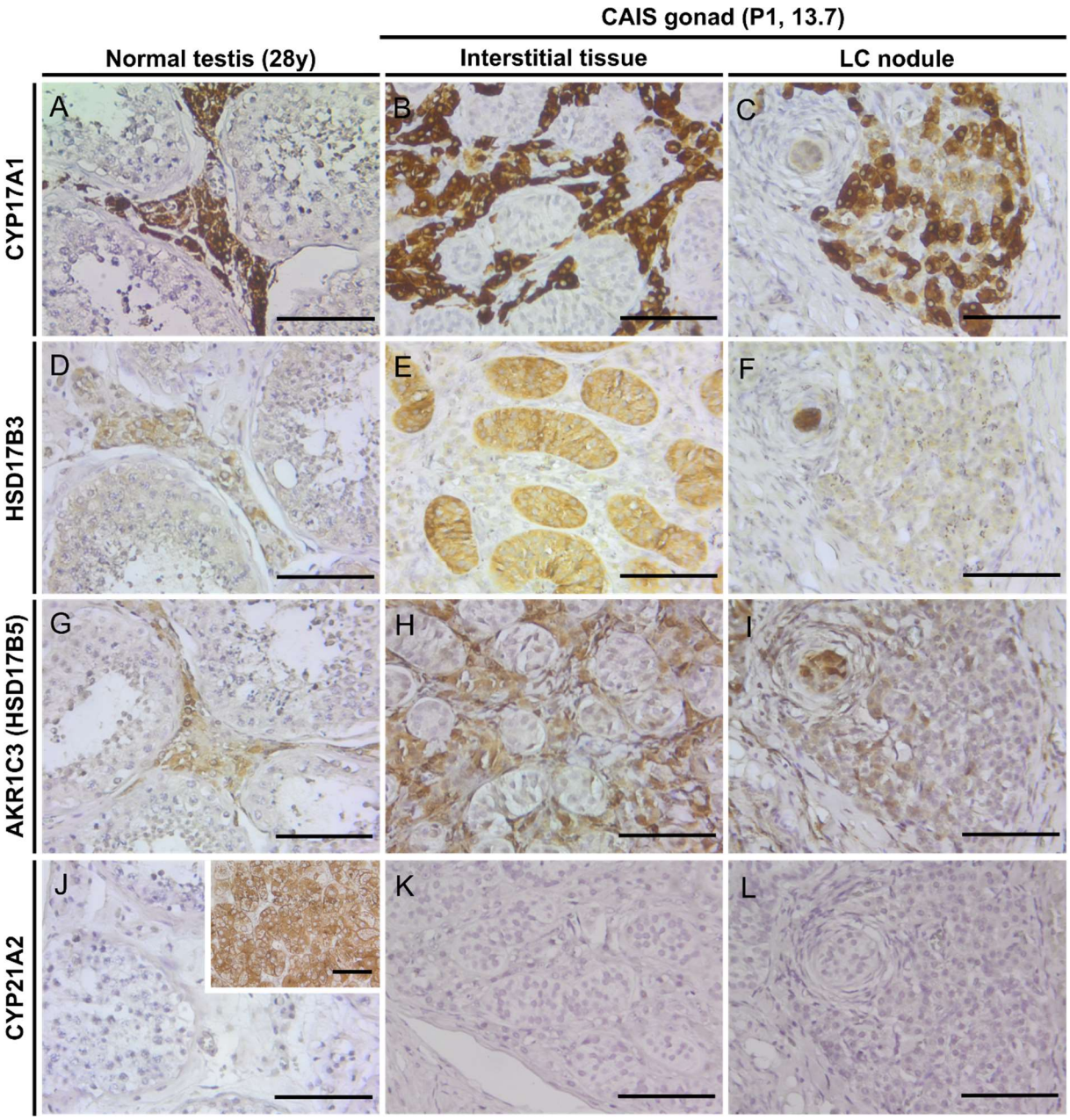

Figure 35. CYP17A1, HSD17B3, AKR1C3 and CYP21A2 protein expression in interstitial Leydig cells versus Leydig cell nodule in gonadal tissue form a 13.7-year-old patient with CAIS. CYP17A1 is expressed in Leydig cells in the normal adult testicular tissue (A) as well as Leydig cells in the interstitial tissue (B) and the Leydig cell nodule (C) in the young adult CAIS gonadal tissue. HSD17B3 is expressed in Leydig cells and to a lesser extent in Sertoli cells in the normal adult testicular tissue (D), but neither in Leydig cells in the interstitial tissue (E) nor in Leydig cells in the Leydig cell nodule (F). AKR1C3 (HSD17B5) is expressed in Leydig cells in the normal adult testicular tissue (G) and Leydig cells in the interstitial tissue (H) in the young adult CAIS gonadal tissue, but not in the Leydig cell nodule (I). CYP21A2 is not expressed in Leydig cells in the normal adult testicular tissue (J), Leydig cells in the interstitial tissue (K) or Leydig cell nodule (L). Inner set in (J) represents CYP21A2 staining in normal adult adrenal cortical tissue as positive control in the experiment. Scale bar, 100 µm. Scale bar, 100 µm. Reproduced from (170) according to the terms of the creative Commons Attribution-NonComercial License (https://creativecommons.org/ licenses/by-nc/4.0/).

A

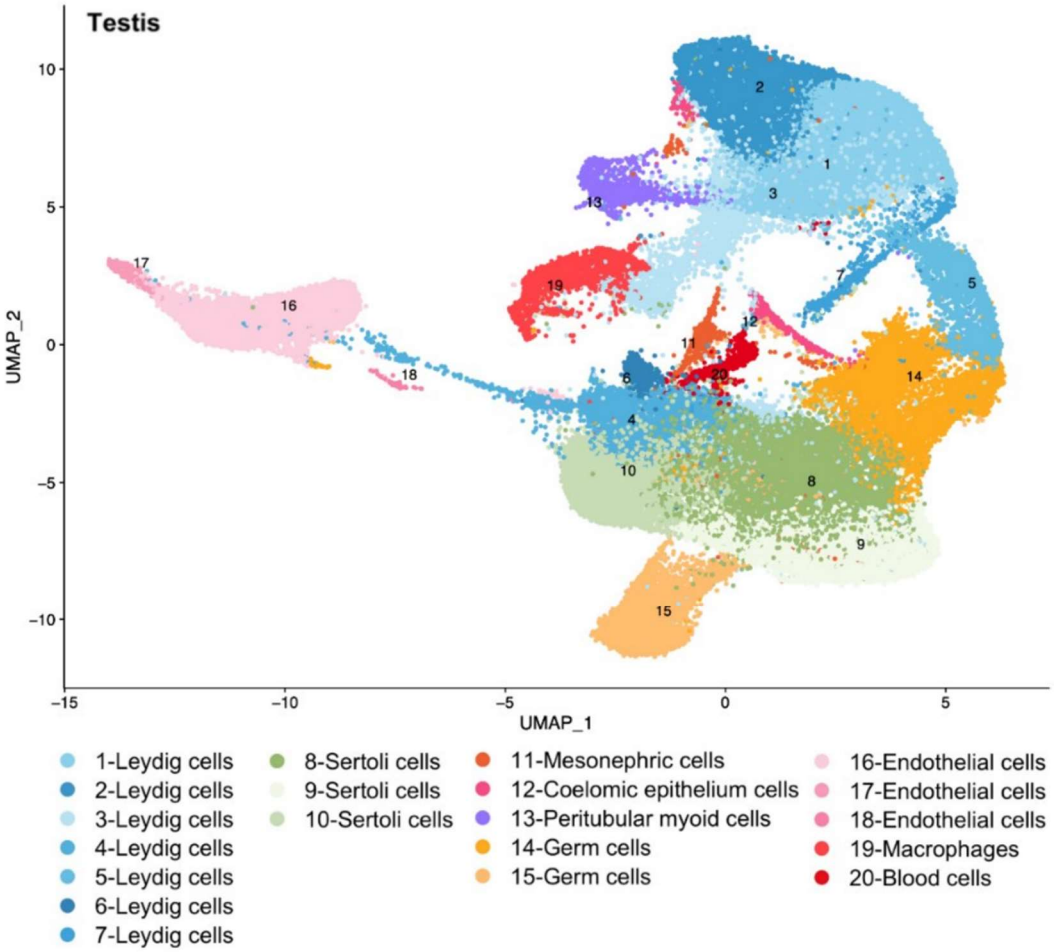
Testis
UMAP_2
UMAP_1
10
5
0
−5
−10
−15
−10
−5
0
5
1-Leydig cells
2-Leydig cells
3-Leydig cells
4-Leydig cells
5-Leydig cells
6-Leydig cells
7-Leydig cells
8-Sertoli cells
9-Sertoli cells
10-Sertoli cells
11-Mesonephric cells
12-Coelomic epithelium cells
13-Peritubular myoid cells
14-Germ cells
15-Germ cells
16-Endothelial cells
17-Endothelial cells
18-Endothelial cells
19-Macrophages
20-Blood cells

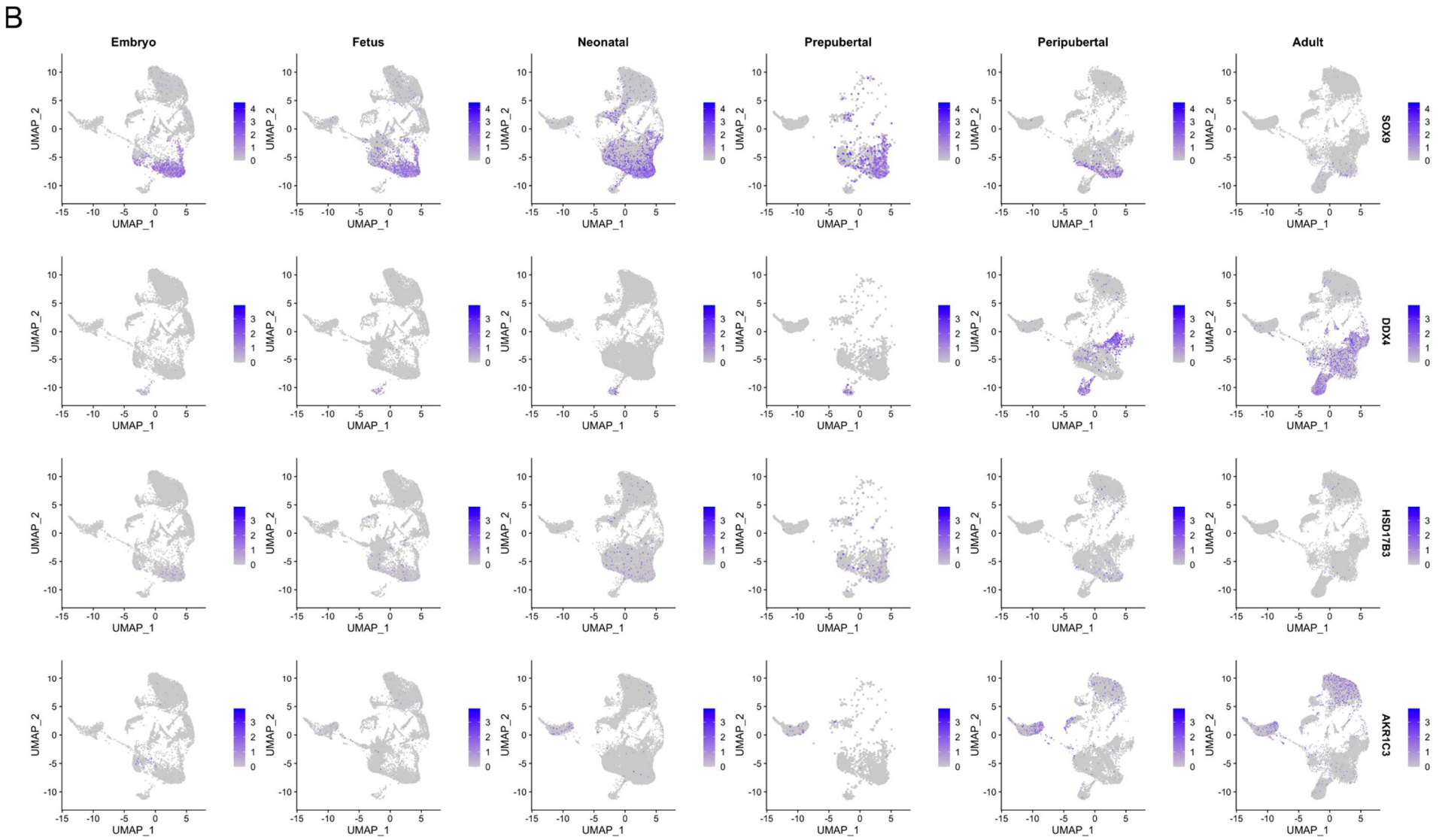
B
Embryo
Fetus
Neonatal
Prepubertal
Peripubertal
Adult
SOX9
DDX4
HSD17B3
AKR1C3
UMAP_1
UMAP_2

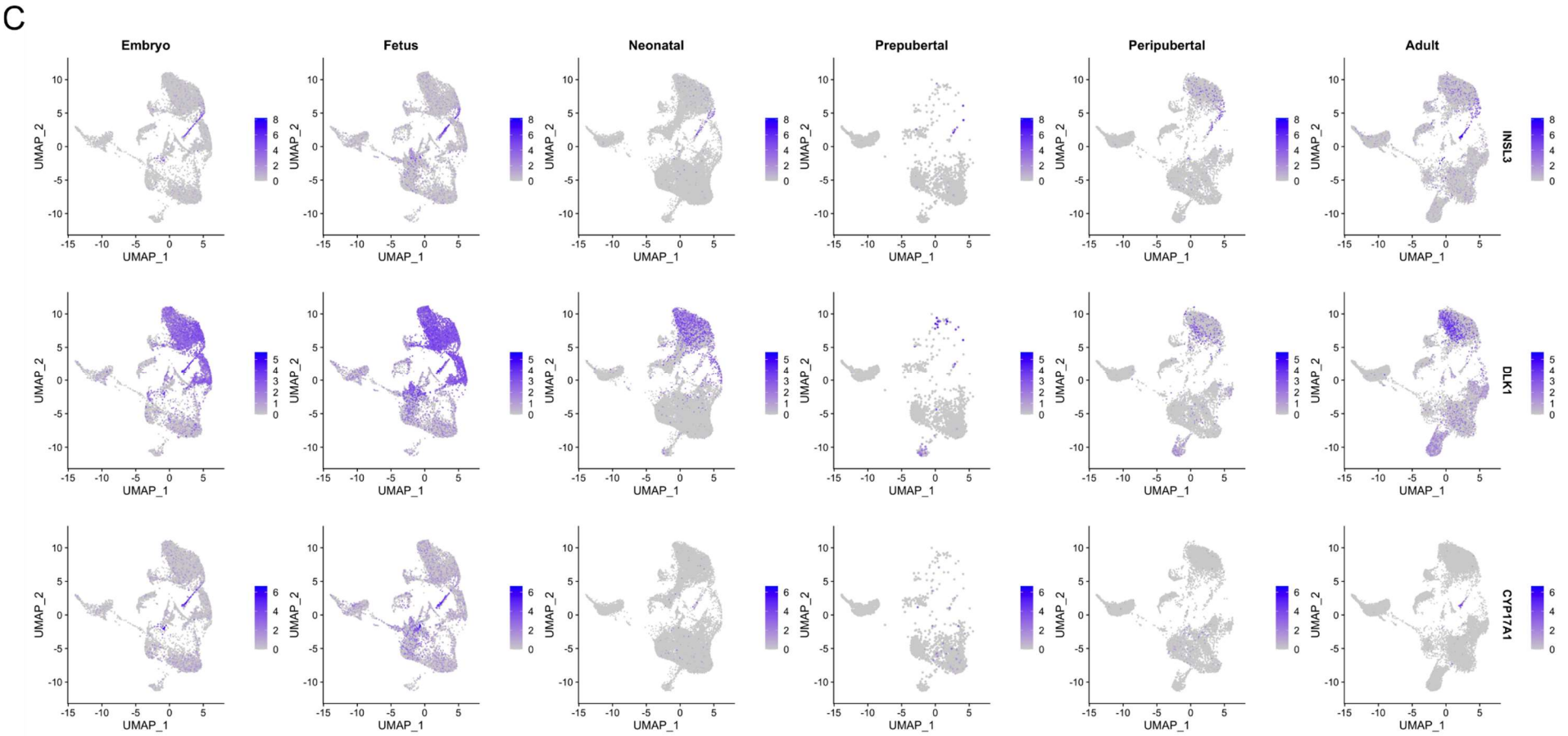

Figure 36. Reanalysis of publicly available single-cell RNA sequencing data from testicular tissue collected from embryonal, foetal, neonatal, prepubertal, pubertal and adult stages. (A) UMAP representation of testicular cells coloured by cluster and annotated based on known cell type markers. (B and C) UMAP visualisation of expression of some of cell type markers and developmental markers in each developmental stage. The data are extracted from publicly available single-cell RNA sequencing data from the studies listed in Table S1. Scale bar, 100 µm. Reproduced from (170) according to the terms of the creative Commons Attribution-NonComercial License (https://creativecommons.org/ licenses/by-nc/4.0/).

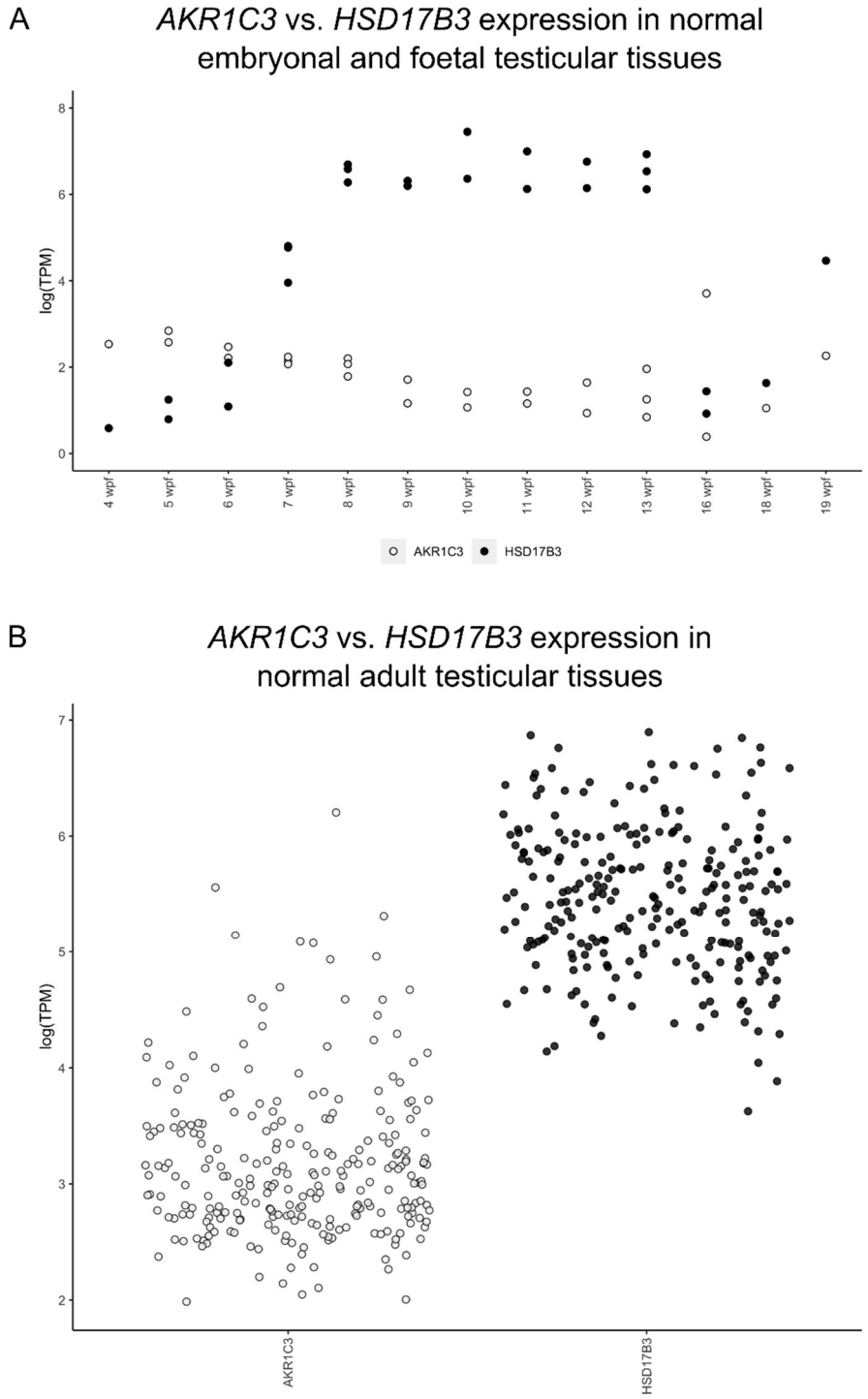

Figure 37. Representation AKR1C3 and HSD17B3 expression in embryonal, foetal and adult testicular tissues from publicly available bulk RNA sequencing data. (A) Dot plot comparing the expression of AKR1C3 and HSD17B3 in whole testicular tissues from normal human embryos and foetuses between 4-19 weeks post fertilisation. (B) Dot plots comparing the expression of AKR1C3 and HSD17B3 in whole testicular tissues from normal adults. The data were extracted from data sets listed in Table S2. Scale bar, 100 µm. Reproduced from (170) according to the terms of the creative Commons Attribution-NonComercial License (https://creativecommons.org/ licenses/by-nc/4.0/).

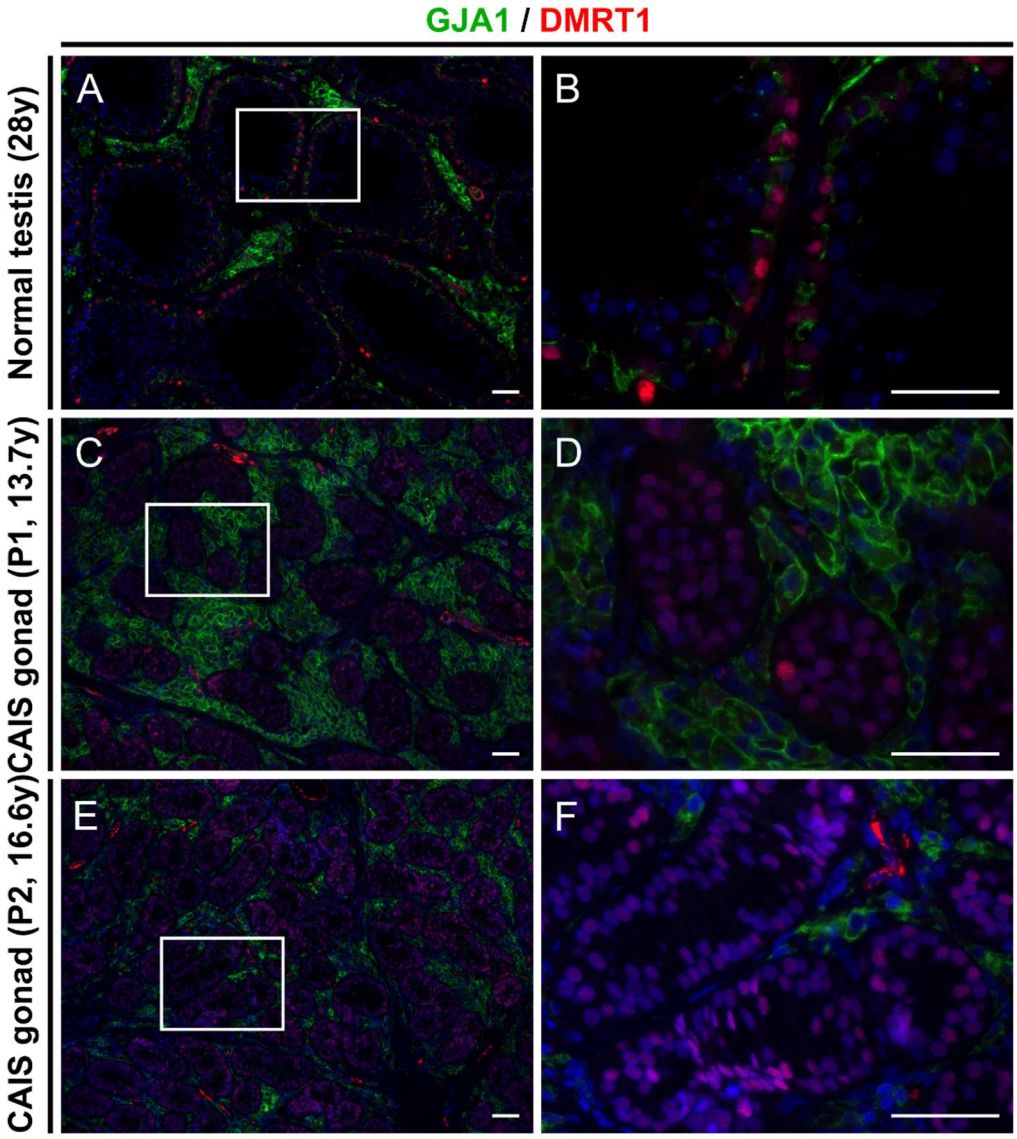

Figure 38. GJA1 protein expression in gonadal tissues from patients with CAIS (P1 and P2) compared to testicular tissue from a normal adult control. GJA1 localises not only to membranes of Leydig cells, but also to the basal surfaces of the adjacent Sertoli cells at the site of blood-testis-barrier in the normal adult control (A and B). In contrast, GJA1 localises only to the membranes of hyperplastic Leydig cells in the pubertal and the young adult patients with CAIS (C-F). DMRT1 is moderately expressed in Sertoli cells and highly expressed in spermatogonia in seminiferous tubules from the normal adult testicular tissue (A and B). In contrast, all cells in seminiferous tubules in both gonadal tissues from patients with CAIS (C-F) moderately express DMRT1, being composed of Sertoli cells only, consistent with germ cell loss shown earlier in these tissues. Scale bar, 50 µm.

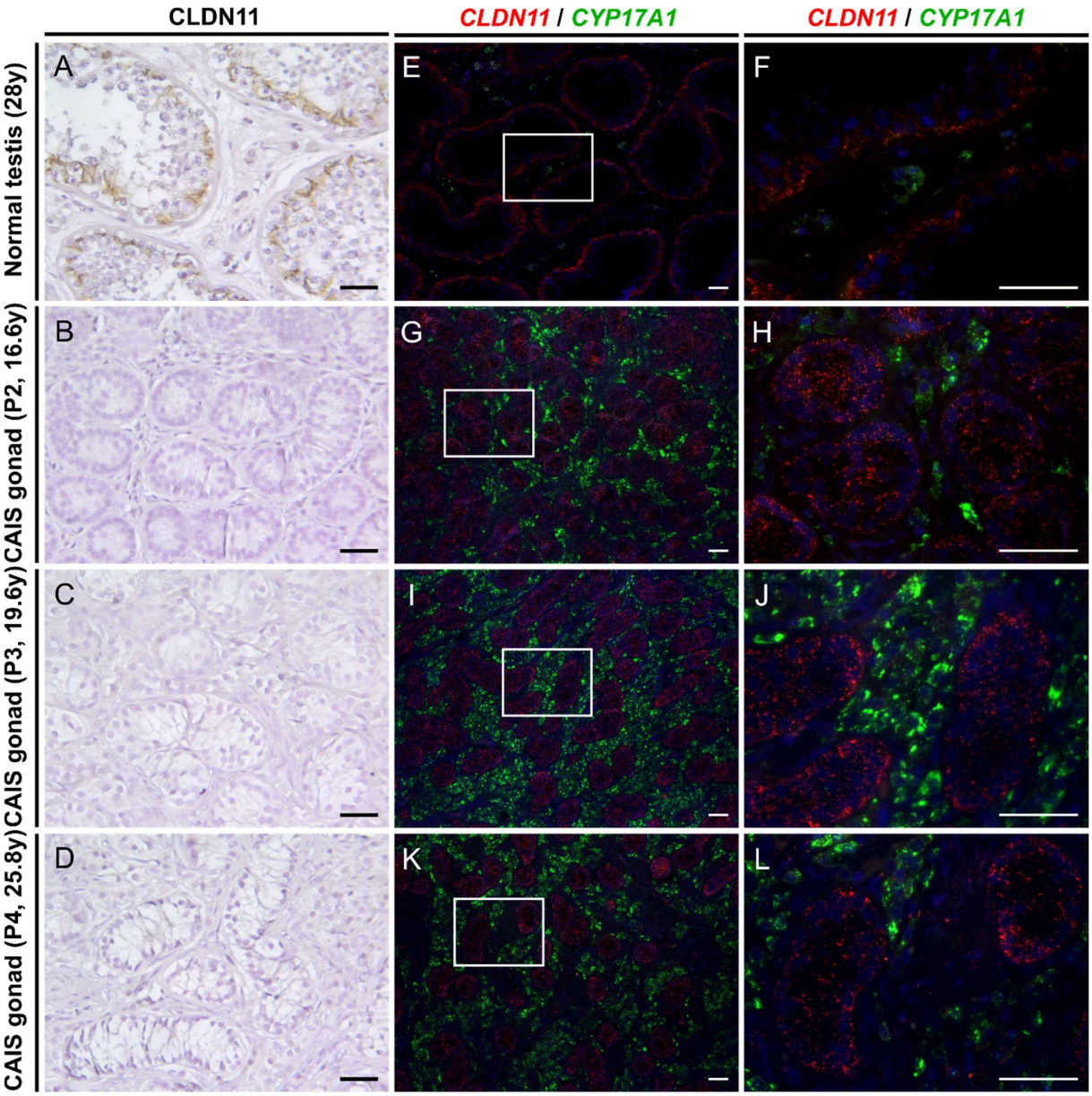

Figure 39. CLDN11 protein versus mRNA expression in gonadal tissue from patients with CAIS (P2-P4) compared to testicular tissue from normal adult control. CLDN11 protein localises to the basal surfaces of the adjacent Sertoli cells in the normal adult testicular tissue (A) at the site of blood-testis barrier, but is not expressed in the seminiferous tubules in pubertal CAIS gonadal tissues (B-D). In contrast, CLDN11 mRNA is expressed not only in the seminiferous tubules in the normal adult testicular tissue (E and F) but also in CAIS gonadal tissue (G-L). CYP17A1 mRNA detection was used as an internal control in the multiplex fluorescent in situ hybridisation assay, being an abundantly expressed mRNA in both tissues, and labels normal (E and F) and hyperplastic (G-L) Leydig cells in the normal adult testicular tissue and the pubertal CAIS gonadal tissue, respectively. Scale bar, 50 µm.

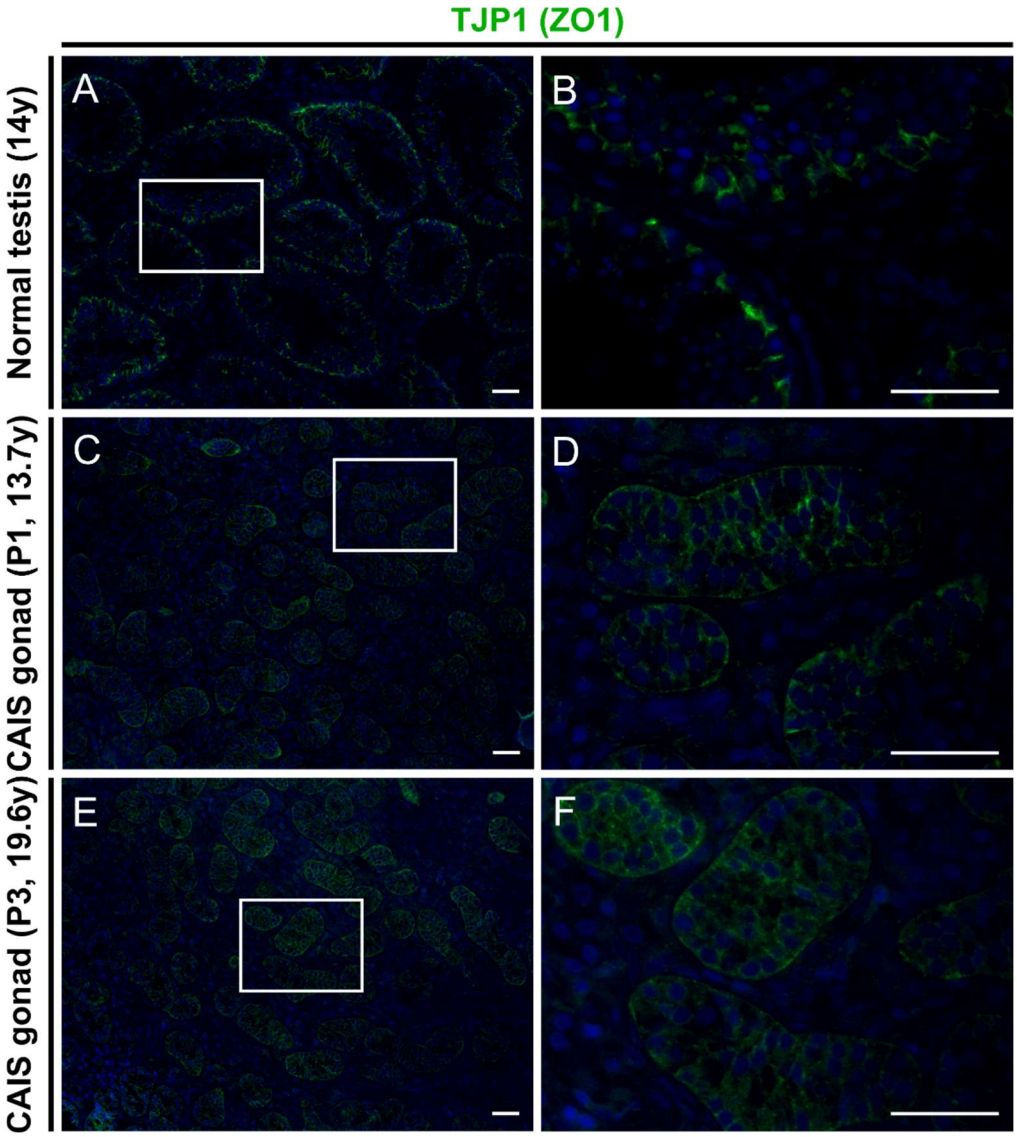

Figure 40. TJP1 (ZO-1) protein expression in gonadal tissues from patients with CAIS (P1 and P3) compared to testicular tissue from a testicular tissue from a normal adult control. TJP1(ZO-1) protein localises to the basal surfaces of the adjacent Sertoli cells at the site of the blood-testis-barrier in the normal adult testicular tissue (A and B), but the whole membranes of Sertoli cells in young adult CAIS gonadal tissue (C-F). Scale bar, 50 µm.

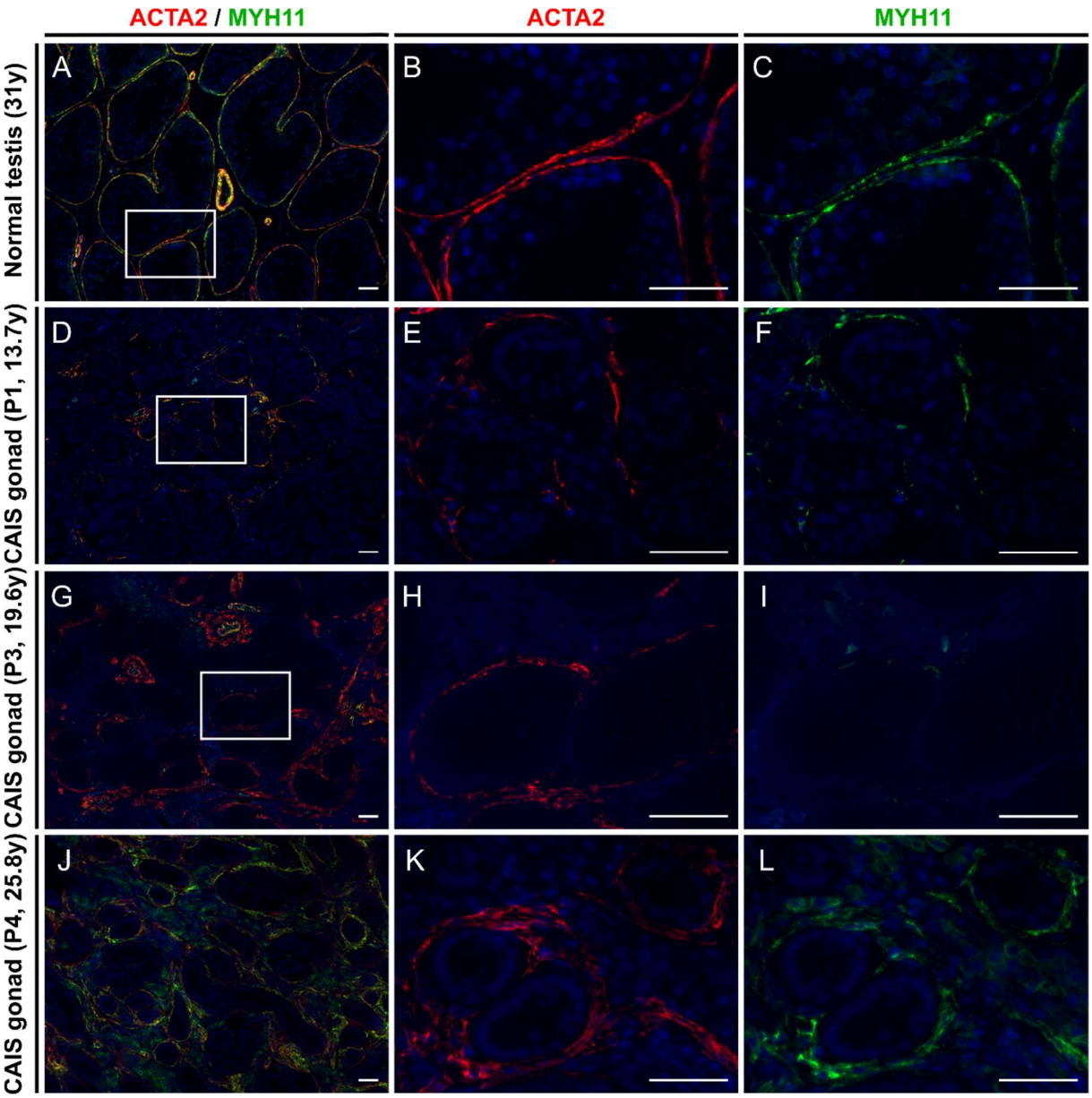

Figure 41. ACTA2 and MYH11 protein expression in gonadal tissues from patients with CAIS (P1 and P3) compared to testicular tissue from a normal adult control. ACTA2 and MYH11 are expressed in PTMCs around the seminiferous tubules in the normal adult testicular tissue (A-C). In contrast, ACTA2 is expressed in myoepithelial cells surrounding blood vessels, fibrous tissues dividing CAIS gonadal tissue into lobules and in few PTMs incompletely surrounding seminiferous tubules in CAIS gonadal tissues (D-I). Scale bar, 50 µm

Table 21. List of the first 100 genes that are differentially expressed between ROIs with Sertoli cells and ROIs with Leydig cells profiled by GeoMx digital spatial profiler

Gene	logFC	AveExpr	t Val	adj.P.Val	B Val
NXF3	3,5	8,4	17,7	6,9E-19	41,5
APOE	-4,1	8,6	-17,4	6,9E-19	41,1
IGFBP2	-3,4	7,8	-16,4	6,5E-18	38,4
S100A6	-3,7	8,6	-15,7	2,3E-17	37,0
CYP17A1	-4,7	10,3	-15,3	5,8E-17	35,9
FDX1	-3,4	7,9	-15,0	1,2E-16	34,9
LSP1	-3,6	7,4	-14,8	1,4E-16	34,5
APOC1	-4,2	7,8	-14,8	1,4E-16	34,5
NTNG2	3,2	7,8	14,4	3,5E-16	33,3
AMH	3,1	9,0	14,4	3,5E-16	33,4
SCARB1	-3,4	9,0	-14,3	4,0E-16	33,2
STAR	-3,4	8,2	-14,3	4,1E-16	33,1
MVD	-2,5	8,4	-13,4	3,9E-15	30,8
SLC16A9	-3,3	6,9	-13,4	3,9E-15	30,6
APOA1	2,8	10,5	13,3	4,6E-15	30,5
CITED2	-2,8	8,6	-13,3	4,6E-15	30,4
PDK4	-3,0	7,1	-13,3	4,9E-15	30,2
TM7SF2	-3,2	7,3	-13,2	5,0E-15	30,2
NR2F2	-2,9	7,2	-13,2	5,1E-15	30,1
LDLR	-3,2	8,2	-13,2	5,4E-15	30,0
GATM	2,7	8,6	13,2	5,4E-15	30,0
HMGCS1	-2,6	9,3	-13,1	5,4E-15	29,9
FHL2	-2,9	7,4	-13,0	7,9E-15	29,5
DUSP1	-2,7	7,9	-12,9	9,2E-15	29,3
MYL9	-2,7	10,2	-12,7	1,9E-14	28,6
G6PD	2,6	9,2	12,6	2,4E-14	28,3
CITED1	2,8	7,7	12,6	2,4E-14	28,3
TMSB4X	-2,5	8,6	-12,5	2,6E-14	28,1
FDPS	-2,5	8,6	-12,5	3,0E-14	28,0
CYP11A1	-2,8	9,4	-12,2	5,6E-14	27,3
PEG3	-2,4	8,7	-12,1	7,3E-14	27,0
SCUBE1	-2,6	7,4	-11,9	1,3E-13	26,4
SOX9	2,4	8,5	11,9	1,4E-13	26,3
CLEC18C	2,5	7,9	11,9	1,4E-13	26,3
DHCR24	-3,0	9,8	-11,9	1,4E-13	26,3
C7	-2,8	7,8	-11,8	1,6E-13	26,1
NUPR1	-2,7	8,1	-11,8	1,6E-13	26,1
IGSF9B	2,8	7,5	11,8	1,6E-13	26,1
HSPB6	-3,5	7,0	-11,8	1,6E-13	26,0
ALAS1	-2,9	7,5	-11,8	1,7E-13	25,9
FOS	-2,4	8,6	-11,6	2,9E-13	25,4

Gene	logFC	AveExpr	t Val	adj.P.Val	B Val
CAMSAP3	2,8	7,2	11,6	2,9E-13	25,3
LHCGR	-2,9	6,8	-11,6	3,0E-13	25,3
COL6A2	-2,6	7,6	-11,5	3,3E-13	25,2
IGFBP7	-2,7	7,5	-11,4	4,8E-13	24,8
CLU	2,6	9,0	11,3	7,6E-13	24,3
HERC5	2,4	7,8	11,2	9,7E-13	24,1
PAPSS2	-3,2	6,5	-11,1	1,0E-12	23,9
KLF4	-3,2	6,5	-11,1	1,1E-12	23,8
ASTN2	3,0	7,7	11,1	1,2E-12	23,8
SEMA6C	2,6	7,3	11,1	1,2E-12	23,7
EPHX1	-3,2	9,2	-11,0	1,6E-12	23,5
FABP3	-2,7	7,2	-11,0	1,7E-12	23,4
CKB	2,3	8,5	11,0	1,7E-12	23,4
CDH11	-3,1	6,7	-10,7	3,9E-12	22,5
NR4A1	-2,3	8,0	-10,7	4,4E-12	22,4
LSS	-2,0	8,3	-10,6	4,6E-12	22,3
GPRC5B	2,1	7,9	10,6	4,6E-12	22,3
CYB561A3	-2,7	7,2	-10,6	4,6E-12	22,3
HSPE1	-2,3	8,6	-10,6	4,7E-12	22,2
OAT	-2,4	7,7	-10,5	5,6E-12	22,1
POR	-2,1	8,3	-10,5	6,0E-12	22,0
ENG	-2,4	7,3	-10,5	6,2E-12	22,0
CYB5A	-2,1	8,9	-10,4	7,3E-12	21,7
ZYX	2,0	8,7	10,4	7,5E-12	21,7
ZFP36	-3,0	8,3	-10,4	7,8E-12	21,7
SNED1	-2,2	7,4	-10,4	7,8E-12	21,7
FBXL19	2,6	7,7	10,3	1,1E-11	21,4
CTSV	2,6	7,8	10,3	1,2E-11	21,2
CLDN11	2,6	7,9	10,3	1,3E-11	21,1
BEX1	2,8	7,3	10,2	1,5E-11	21,0
INSL3	-3,2	7,8	-10,2	1,5E-11	21,0
MMP15	2,6	7,0	10,2	1,5E-11	20,9
SLC6A6	-2,4	6,5	-10,1	1,9E-11	20,7
TPM1	-2,1	7,2	-10,1	2,3E-11	20,5
TSC22D3	-2,6	6,7	-10,0	2,3E-11	20,5
LBHD1	-2,2	7,4	-10,0	2,3E-11	20,4
TSPYL2	1,7	9,4	10,0	2,5E-11	20,3
SERPINA5	2,8	8,6	9,9	3,2E-11	20,1
METTL7A	-2,2	7,3	-9,9	3,3E-11	20,1
MTCL1	2,6	7,0	9,8	4,5E-11	19,8
GSTA1	-2,3	10,1	-9,8	5,2E-11	19,5

Gene	logFC	AveExpr	t Val	adj.P.Val	B Val
GSTP1	-2,2	7,9	-9,8	5,4E-11	19,5
EGR1	-2,0	8,9	-9,8	5,4E-11	19,5
ADGRG1	2,3	7,2	9,7	5,9E-11	19,5
FHOD3	2,1	7,8	9,7	6,1E-11	19,4
PLXNC1	2,5	7,6	9,6	7,6E-11	19,2
CCND2	2,1	7,8	9,6	7,6E-11	19,1
C2CD2	-2,7	6,1	-9,6	7,8E-11	19,1
ADCY3	-2,8	6,1	-9,6	8,8E-11	19,0

Gene	logFC	AveExpr	t Val	adj.P.Val	B Val
LAMB1	-2,3	6,8	-9,6	9,3E-11	18,9
CALB2	-2,4	8,3	-9,6	9,9E-11	18,8
JAM2	2,1	7,6	9,5	9,9E-11	18,8
AK1	-2,4	7,7	-9,5	9,9E-11	18,8
TOB1	-2,4	7,3	-9,5	1,0E-10	18,8
PBX1	-2,4	6,6	-9,5	1,1E-10	18,8
LRP8	2,4	6,8	9,4	1,5E-10	18,4
SCRG1	2,3	7,0	9,4	1,7E-10	18,3
MT2A	-2,6	7,0	-9,4	1,8E-10	18,2
FOXO4	-2,0	7,4	-9,3	2,2E-10	18,0

Acknowledgments

I would like to express my deepest gratitude to my supervisor, Prof. Dr. med. Olaf Hiort and my mentor Dr. rer. nat. Ralf Werner, for their invaluable guidance, unwavering support, and insightful feedback throughout the course of my dissertation. Their expertise and dedication have been instrumental in shaping my research and helping me navigate the challenges of this project. I am immensely grateful for their patience, encouragement, and the countless hours they have invested in mentoring me. Beyond their scientific guidance, their personal support has been equally invaluable. They have been a source of motivation, offering kind words and understanding during times of difficulty and uncertainty. This work would not have been possible without their continuous support and belief in my abilities.

I would like to extend my sincere appreciation to Prof. Dr. med. Verena-Wilbeth Sailer, Dr. med. Franz F. Dressler and Dr. med. Florian Lenz from the Institute of Pathology, University of Lübeck and Dr. Helena Fabbri-Scallet, Center for Molecular Biology and Genetic Engineering, State University of Campinas, São Paulo, Brazil who have generously provided the tissue sections used in this study. Their contributions have been vital to the success of my research, and their willingness to collaborate and share resources is greatly appreciated. Without their assistance, this project would not have been possible.

I am also deeply grateful to Prof. Dr. rer. nat. Hauke Busch, Dr. Verónica Calonga-Solís, Dr. rer. nat. Anke Fähnrich, Yamil Maluje and Svenja Denker who performed the bioinformatic analysis of data. Their expertise, collaboration, and dedication have been crucial in processing and interpreting the complex data involved in this research. Their support and contributions have greatly enhanced the quality and depth of my work.

I would like to acknowledge the generous contribution of Prof. Dr. med. Malte Spielmann the head of Institute of Human Genetics, University of Lübeck and Kiel for performing the Next-Generation Sequencing (NGS). I am deeply grateful for his support and collaboration.

My heartfelt thanks also go to Mrs. Karen Rieck, Mrs. Jutta Leutelt, Mrs. Kübra Kösem who provided kind assistance throughout this project. Their technical expertise, meticulous attention to detail, and willingness to help with various aspects of the research have been invaluable. Their support has ensured the smooth progress of my experiments and data collection.

I am sincerely thankful to Prof. Dr. Inas Mazen who made this whole work possible by establishing the contacts to Prof. Dr. med. Olaf Hiort and supporting my scholarship applications, which lasted for more than two years until I was awarded the German Egyptian Research Long-term Scholarship (GERLS) from the German Academic Exchange Service (DAAD) in 2019.

I am deeply indebted to Prof. Dr. Amr Gouda, Prof. Dr. Ekram Fateen at my home institute for their guidance in my scientific career, for their invaluable encouragement throughout the scholarship applications, and for their belief in my potential provided me with the confidence to pursue this opportunity.

I would also like to extend my heartfelt thanks to the DAAD for financing my scholarship. Their financial support has provided me with the opportunity to pursue my academic and research goals. The scholarship has been a crucial factor in enabling me to focus entirely on my studies and research, and I am deeply appreciative of this opportunity.